

NAC3-272

143 pages

Experimental and Theoretical Study of Propeller

Spinner / Shank Interference

A Thesis

by

CARL CLAYTON CORNELL

(NASA-CR-176954) EXPERIMENTAL AND
THEORETICAL STUDY OF PROPELLER SPINNER/SHANK
INTERFERENCE M.S. Thesis (Texas A&M Univ.)
143 p

CSCL 01A

N86-29773

Unclas

G3/02 43517

MAY 1986

EXPERIMENTAL AND THEORETICAL STUDY OF PROPELLER
SPINNER/SHANK INTERFERENCE

A Thesis by

CARL CLAYTON CORNELL

Submitted to the Graduate College of
Texas A&M University
in partial fulfillment of the requirements for the degree of

MASTER OF SCIENCE

May 1986

Major Subject: Aerospace Engineering

EXPERIMENTAL AND THEORETICAL STUDY OF PROPELLER
SPINNER/SHANK INTERFERENCE

A Thesis by

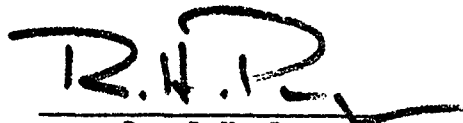
by

CARL CLAYTON CORNELL

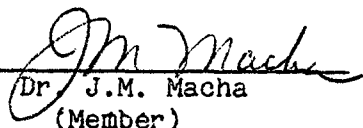
Approved as to style and content by:



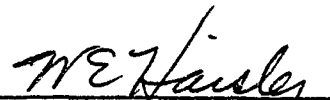
Dr. K.D. Korkan
(Chairman of Committee)



Dr. R.H. Page
(Member)



Dr. J.M. Macha
(Member)



Dr. W.E. Haisler
(Head of Dept.)

May 1986

ABSTRACT

Experimental and Theoretical Study of Propeller Spinner/Shank

Interference (May 1986)

Carl Clayton Cornell, B.S., Texas A&M University

Chairman of Advisory Committee: Dr. K.D. Korkan

A fundamental experimental and theoretical investigation into the aerodynamic interference associated with propeller spinner and shank regions has been conducted. The research program involved a theoretical assessment of solutions previously proposed, followed by a systematic experimental study to supplement the existing data base. As a result, a refined computational procedure has been established for prediction of interference effects in terms of interference drag and resolved into propeller thrust and torque components. These quantities have been examined with attention to engineering parameters such as two spinner finess ratios, three blade shank forms, and two/three/four/six/eight blades. Consideration of the physics of the phenomena aided in the logical deduction of two individual interference quantities, i.e., cascade effects and spinner/shank juncture interference. These interference effects have been semi-empirically modeled using existing theories and placed into a compatible form with an existing propeller performance scheme which provided the basis for examples of application.

ACKNOWLEDGEMENT

The author would like to thank Dr. J.M. Macha and Dr. R.H. Page for their consideration of serving as graduate committee members and the time which they will have devoted to this thesis. Thanks also to Dr. K.D. Korkan for his invaluable guidance and assistance throughout the course of my graduate career, not only on this endeavor but on numerous other projects of professional interest as well.

Special thanks also to my family for their support, my friends and working constituents who have assisted in this project, and especially to Carol for her enduring understanding and patience.

Finally, thanks to Dr. L. Bober, Mr. C. Hughes and NASA Lewis Research Center for their funding of and expressed interest in my research.

TABLE OF CONTENTS

	Page
ABSTRACT	iii
ACKNOWLEDGEMENT	iv
TABLE OF CONTENTS	v
LIST OF FIGURES	vii
LIST OF TABLES	x
NOMENCLATURE	xi
I. INTRODUCTION	1
II. SUMMARY OF PREVIOUS WORK	5
III. THEORY	18
A. Propeller Performance Computer Analysis	19
B. Sarsfeld Model	21
C. Borst/Reid Model	24
D. Present Model	29
IV. TEST ARRANGEMENT/PROCEDURE	36
A. Experimental Apparatus	36
B. Data Acquisition	41
C. Data Reduction	43
D. Tunnel Corrections	44
E. Test Procedure	47
V. RESULTS AND DISCUSSION	49
A. Interference Values	50
1. Cylindrical Shanks	51
2. Airfoils/Tapered Shanks	54
VI. SUMMARY/CONCLUSIONS	56

REFERENCES	59
APPENDIX I. FIGURES	62
APPENDIX II. DATA ACQUISITION/REDUCTION PROGRAM LISTING	111
VITA	129

LIST OF FIGURES

	PAGE
Figure 1. Comparison of theoretical prediction of thrust coefficient to experimental data (Clark Y-NACA 16 Propeller, Cruise condition).....	63
Figure 2. Comparison of theoretical prediction of power coefficient to experimental data (Clark Y-NACA16 Propeller, Cruise condition).....	64
Figure 3. Comparison of theoretical prediction of efficiency to experimental data (Clark Y-NACA16 Propeller, Cruise condition).....	65
Figure 4. Drag characteristics of two circular cylinders placed in tandem.....	66
Figure 5. Drag characteristics of a air of streamline struts in tandem.....	67
Figure 6. Drag characteristic of two circular cylinder placed side by side.....	68
Figure 7. Drag characteristic of a pair of streamline sections placed side by side.....	69
Figure 8. Interference drag originating at the junction of wings to a plane wall as a function of airfoil thickness ratio.....	70
Figure 9. Interference drag at wall junctions of wings as a function of lift coefficient.....	71
Figure 10. Interference drag loss effects on propeller performance at typical climb and cruise conditions.....	72
Figure 11. Thrust coefficient comparison between experimental data and theory, with Borst correction (Clark Y-NACA16 Propeller, Cruise condition)....	73
Figure 12. Power coefficient comparison between experimental data and theory, with Borst correction (Clark Y-NACA16 Propeller, Cruise condition)....	74
Figure 13. Efficiency comparison between experimental data and theory, with Borst correction (Clark Y-NACA16 Propeller, Cruise condition).....	75
Figure 14. Velocity diagram of a differential blade element.....	76

Figure 15.	Components of load distributions on propeller shank.....	77
Figure 16.	Three-dimensional sketch of cylindrical shank element showing radial variation of velocity and drag	78
Figure 17.	Photo of propeller test rig (PTR).....	79
Figure 18.	Components of PTR.....	80
Figure 19.	Contours of two spinners used in research program.....	81
Figure 20.	Baseline propeller blade and three representative shanks of present study (Reference 7).....	83
Figure 21.	Baseline blade planform with superimposed shank models.....	84
Figure 22.	Thickness distributions of baseline blade and shank models.....	85
Figure 23.	Twist distribution of baseline blade and shank models.....	86
Figure 24.	Clark Y airfoil section used on airfoil cuff and transition shank models.....	87
Figure 25.	Sectional view of modeled Clark Y airfoil shank illustrating foam core, composite layers, and retention shank spar.....	89
Figure 26.	PTR installation in TAMU 2ft. x 3 ft. low speed wind tunnel.....	90
Figure 27.	Schematic of instrumentation used in data acquisition.....	91
Figure 28.	Photo of wind tunnel and data acquisition installation.....	92
Figure 29.	Thrust load cell calibration.....	93
Figure 30.	Torque load cell calibration.....	94
Figure 31.	Pressure transducer calibration for tunnel velocity measurement.....	95
Figure 32.	Data acquisition/reduction program flowchart...	96
Figure 33.	Tunnel constraint corrections to tunnel datum velocity for propeller tests.....	97

Figure 34.	(a) Cylindrical shanks installed on PTR for Phase I.....	98
	(b) Transition shanks installed on PTR for Phase II.....	98
	(c) Airfoil cuff models installed on PTR for Phase III.....	98
Figure 35.	Spinners installed on PTR for: (a) $\lambda=1.0$, (b) $\lambda=1.6$	99
Figure 36.	Array of number of blades in installed configuration.....	100
Figure 37.	Representative raw thrust data ($B=6$).....	101
Figure 38.	Representative raw torque data ($B=6$).....	102
Figure 39.	Representative measured effects of number of blades (tapered shanks, $\beta=51^\circ$).....	103
Figure 40.	Cursory example of blade interference (tapered shanks, $\beta=51^\circ$).....	104
Figure 41.	Drag distributions of finite aspect ratio cylinder and two-dimensional equivalent.....	105
Figure 42.	Development of interference C_D with increasing number of cylindrical blade shanks.....	106
Figure 43.	Effect of rotation on interference C_D for cylindrical blade shanks.....	107
Figure 44.	Application of cylindrical shank interference drag values to Reid's baseline propeller efficiency.....	108
Figure 45.	Propeller performance prediction of shank contribution as compared to experimental measurements.....	109
Figure 46.	Application of cylindrical shank spinner/shank C_D 's and airfoil cuff C_D 's to efficiency curves of Reid's baseline blade.....	110

LIST OF TABLES

	Page
Table 1. Spinner coordinates	82
Table 2. Clark Y airfoil coordinates	88

NOMENCLATURE

a	speed of sound
b	geometric shank length
B	number of propeller blades
BHP	Brake Horepower
c	airfoil section chord
C	wind tunnel cross sectional area
C_d	section drag coefficient
C_D	drag coefficient based on frontal area, S
C_{Dc}	drag coefficient based on "chord area," c^2
C_{Dt}	drag coefficient based on "thickness area," t^2
C_l	section lift coefficient
C_p	propeller power coefficient, $\frac{P}{\rho n^3 d^5}$
C_Q	propeller torque coefficient, $\frac{Q}{\rho n^2 d^4}$
C_T	propeller thrust coefficient, $\frac{T}{\rho n^2 d^4}$
d	propeller diameter
D	drag force
ΔD	drag inerement due to interference
h	shank length
J	propeller advance ratio, V/nd
K	$\frac{900 a^2 b}{N^2 d^2}$
L	lift force
M	local Mach number

n	propeller revolutions per second
N	propeller revolutions per minute
P	power required
q, q_0	dynamic pressure, $1/2\rho V^2$
Q	torque required
S	shank frontal area
T	propeller thrust
V, V_0	freestream velocity
V'	corrected freestream velocity
V_G	geometric resultant velocity of freestream and rotational
V_r	rotational velocity, $2\pi rn$
V_{res}	resultant velocity
\bar{x}	dimensional propeller radial location
\bar{x}'	radial location in fraction by tip radius
\bar{x}_i	radial location of resolved interference load
Δx	dimensional radial length
$\Delta x'$	radial length normalized by tip radius
Δx_i	radial length of interference load
$\Delta x'_i$	radial length of interference load normalized by tip radius
α	angle of attack
β	propeller geometric pitch angle
δ	boundary layer height
η	propeller efficiency
$\Delta\eta_i$	change in efficiency due to interference
ρ	air density

σ_p	section solidity, $Bb/\pi d$
θ	induced angle
ϕ	resultant advance angle
ϕ_o	geometric advance angle
w	induced velocity

I. INTRODUCTION

Even though there are considerably more propeller-driven aircraft on the market today than any other type, the subtle aspects of propeller design and performance have not generally been appreciated until recently. The appearance of the turbofan/turbojet propulsion unit, and its exclusive use for large commercial aircraft, restricted technical interest in the propeller. In addition, use of the propeller as a propulsion device had been limited primarily to smaller aircraft and lower speeds. As of the early 1980's, most of these aircraft still used propeller designs based on technology that had not changed significantly since the 1940's and early 1950's. Because of the dramatic rise in fuel prices, however, a serious reappraisal of the propeller - being inherently more efficient than jet engines - has re-established this propulsion conversion device into a period of active technological development.

Several areas are currently under investigation to improve propeller performance and obtain higher cruise speeds, while still satisfying the more stringent noise regulations. These include concepts such as blade sweep, airfoils, proplets, increased number of blades, and counterrotation - accompanied by advanced materials and analytical capabilities. Another area which offers the potential of improved efficiency involves the in-board region of

the propeller blade and the junction with the hub/spinner. The influence of this segment of the propeller must be viewed in light of all the general engineering aspects, i.e., performance, structure, and noise as well as the additional phenomenon of interference drag.

At the interface where the blade enters the hub, the boundary layers of both the propeller shank and the hub combine resulting in additional pressure drag hence interference drag. Typically, the blade transitions from an airfoil profile to a cylindrical shank before entering the hub for structural and mechanical considerations. This exemplifies the detrimental problem in producing thrust losses and increased torque requirements. The actual magnitude of this drag contribution has been shown to be significant and warrants a fundamental experimental and concurrent theoretical study. Another type of interference drag arises when two bodies operate in close proximity of each other such as adjacent blade shanks and is referred to as cascade losses. This effect can be either positive or negative and may be significant, especially in the case of a propeller having many blades, in which case the magnitude of interference drag is increased and cascade losses are likely.

Physically, several approaches have been used to enhance the root section aerodynamic properties of propellers. The most dominating factor influencing this progress is that of structural integrity. When metal superseded the use of wood as a propeller blade material, the superior strength permitted the use of thinner airfoil sections not only at the propeller tip where the high speed

advantages of the NACA 16 airfoil section were utilized, but also at the blade root with a reduction in root losses. Direct benefits resulted in terms of propeller performance and pressure/velocity characteristics of turbine engine intakes. Planforms of the present metal propellers are still governed by the necessity of avoiding step-wise changes in cross-section and their associated stress concentrations in the heavily loaded shank segments of the blade. Current developments in composite blade technology are indicating similar potentials. Further refinements of the blade shank are being considered because airplane cruise speeds are rapidly approaching values wherein the drag of poorly faired shanks, when exposed to higher velocities, are assuming excessive proportions. Limited use of auxiliary "cuffs" and shanks of an airfoil profile has led to conflicting opinions on the practicality of such enhancements due to the lack of fundamental knowledge and experimental data. Other methods include improved spinner/shank integration and spinner/hub contouring.

Theoretically, most propeller performance analyses do not account for performance degradation from spinner/shank interference, and to the authors knowledge there has been little progress. Those existing methods that attempt to predict spinner/shank interference have not been sufficiently supported by experimental verification, and fail to include pertinent engineering parameters such as spinner geometry, number of propeller blades, advance ratio, and Reynold's number.

The primary objective of this study therefore is to quantify the influence of spinner/shank interference drag on propeller

thrust, torque, and efficiency through a systematic series of experiments whereby the existing semi-empirical theories can be scrutinized. Thus, the present study serves to improve the understanding of spinner/shank interference effects, verify and improve on analytical methods in terms of proper correlation with measured performance, and provide guidelines to the treatment of the spinner/shank region.

II. SUMMARY OF PREVIOUS WORK

The attempt of acquiring a smooth integration between propeller blades and the hub is not a new concept. Robert's patent boss, which in 1851 displayed a hub/shank integration with unexcelled streamlining while still allowing for pitch adjustment⁽¹⁾. Where the blades mounted, the hub was spherical and the blades had a matching semi-spherical contour maintaining fluency at all blade pitch angles. Eventually, a number of marine propellers manufactured in the 1945 to 1950 era exploited this design. Similar techniques, with blades mounted on "turn-table" type assemblies of cylindrical or otherwise axi-symmetric hubs, have been suggested but have yet to be implemented on full-scale propellers. Meanwhile, the benefits of these "ideal" junctures as opposed to conventional and proposed configurations are ascertained by experimental and theoretical research.

In 1938, Biermann and Hartman⁽²⁾ reported on wind tunnel tests of five 3-bladed propellers including typical round blade shanks, and those having airfoil cuffs extending into the hub operating in front of a radial and a liquid-cooled engine nacelle. Furthermore, two spinners were tested in conjunction with the liquid-cooled nacelle. The authors concluded that the propellers with airfoil shank cuffs outperformed those with round shanks, and the differentiation between measurements of the two spinners was only marginal. In similar tests, the same authors showed that propellers with planforms of maximum width occurring closer to the hub had higher peak efficiencies but lower take-off efficiencies⁽³⁾. These efficiencies translate directly into fuel economy, power available,

and cruise speed. Preliminary calculations by McCoy⁽⁴⁾ in 1939 showed that a propeller with proper spinner and blade shank fairings as compared to a conventional propeller should increase the propulsive power available by a conservative estimate of 10 to 15 percent.

Some of the most comprehensive experimental work has been conducted by Reid⁽⁵⁾. In a 1941, Reid accounts for the effects of hub drag, solidity, dual rotation and number of blades. Extensive conclusions were drawn from tests of two different spinners/hubs which covered different amounts of faired in-board blade segments. Slightly greater efficiencies were found with a spinner of 0.12D than 0.28D. This result appears to contradict the results of Hammack⁽⁶⁾, in which flight measurements of thrust losses due to shanks showed marked reductions of about 60 percent with a 19 percent larger diameter spinner. The trend is intuitive in that a larger diameter spinner would eliminate part of the in-board negative thrust and thereby improve performance. Reid was, however, quick to point out that his results were due to differences in root conditions between the two runs. This fact proved to be an important discovery in itself. That is, small irregularities of form at the junction of propeller blades and spinners, e.g., sealed junctions versus unsealed, may have a greater influence upon the efficiency of the propeller than does doubling the spinner diameter. It therefore follows that a fair appraisal of the relative merits of different spinners can be made only when comparable conditions exist at the blade roots. More over, since the detrimental effects of such irregularities increase with blade angle, this discovery has an

important bearing on the design of spinners and blade shanks/cuffs intended for high-speed aircraft. Reid also noted that as spinner diameter increases, the associated changes in disk loading and axial velocity tend to nullify the benefits of suppressing shank drag. Furthermore, Hammack's tests incorporated a propeller blade with rapid transition from the airfoil sections to round blade roots as opposed to faired blades or those with airfoil cuffs. The implication being that, on the general question of optimum spinner sizing, spinner diameter is not as critical with propellers of faired shanks as those containing transition shanks. The trade-off appears to be whether to cover unacceptable shank regions with an appropriate spinner or to improve the shank regions in the design phase. For present and future propellers, the latter seems more reasonable. Hammack determined shank losses based on integration of the negative thrust areas on the order of 9 percent loss in efficiency, most of which was speculated to be recoverable by proper spinner/shank integration thus bringing overall efficiencies upwards of 90 percent.

The basis for much of the work of this study was a 1945 study by Reid⁽⁷⁾. A wind tunnel program was carried out at Stanford University to investigate the influences of blade root form by testing model propellers with conventional round shanks, similar models equipped with replicas of streamlined cuffs of Clark Y profile adequate for the enclosure of such shanks, and still other models incorporating relatively thin airfoil profiles for the shank. It was found that the faired blade shanks offered substantial improvements in efficiency which increased with advance ratio. The

effect was to augment both the thrust and power coefficients corresponding to given pitch settings. The improvement in efficiency which consisted of approximately 4 percent at peak and as much as 10 percent off-design is the result of the greater proportional increase of thrust than power. Reid addresses the effects of augmenting propeller solidity by increasing the number of blades through tests of models which had both three and four blades of the same form. It was observed that experimentally determined efficiencies closely approached ideal values, η_i , throughout a wide range of advance ratios for small C_p 's, but fell at large values of the power coefficient. Furthermore, the adverse effects of increasing C_p were much greater with three blades than with four blades. Since momentum theory predicts no change of efficiency as long as C_p and J remain fixed,

$$(V/nd)C_p^{-1/3} = \eta(2/\pi(1-\eta))^{1/3} \quad (\text{II-1})$$

the advantages of the four-blade model could result only from reduction of the forces on individual blades. Reid supplements this hypothesis by showing that both propellers of three and four blades attained practically identical fractions of the corresponding ideal efficiencies (η/η_i) when the loading of the individual blades (C_p/B) at equal values of J are the same. This fact led to the conclusion that there was an absence of any measurable consequential effect of the actual number of blades, and emphasized the use of blade loading rather than disc loading in data evaluation and design analysis.

This result is of interest to the present study as secondary effects are indeed apparent and measurable with a larger array in number of blades (2,3,4,6 and 8), especially when focusing attention to the shank region. Barlow⁽⁸⁾, during a series of flight tests conducted in 1946, determined the high speed drag of models simulating propeller shanks in the form of a circular cylinder and three airfoils; the NACA 16-025, NACA 16-040, and NACA 16-040 with the rear 25 percent chord eliminated. The models were cantilevered to the lower surface of an XP-15 airplane. Profile drag at Mach numbers from 0.3 to 0.8 and over a small range of angle-of-attacks were determined using a wake-survey rake and, in the case of the circular cylinder, surface pressure distribution and force measurements. Pressure gradients due to a propeller spinner were simulated to some degree by judicious chordwise positioning of the models. Likewise, the finite aspect ratio of the models was said to approximate the radial relieving conditions normally experienced by propeller shanks due to rapid spanwise decreases in blade thickness. It was shown that this did not, however, reproduce the radial variation of an actual propeller shank of equivalent length because of the lack of the rotational velocity component. On the basis of the drag calculations, Barlow estimated that a "present-day" fighter airplane could achieve an increase in speed of about 4 to 6 miles per hour by fairing the exposed round shanks of a four-blade propeller.

Although Barlow's tests provided a preliminary data base for propeller strip analysis techniques, they were skeptically fundamental in approach but supplemented by propeller tests along

the same theme - attention to blade shank form for high-speed applications. Tests of model propellers made in the NACA 8 foot high-speed tunnel⁽⁹⁾ have shown that the highest efficiencies can be realized if the shanks are very broad and thin. Model tests by Delano⁽¹⁰⁾ and full-scale tests by Maynard⁽¹¹⁾ were then mutually conducted to exploit the effect of shank design and to determine the effects of scaling on measured efficiencies. As a baseline, two 10-foot diameter two-blade propellers differing only in shank design were tested in the Langley 16-foot high-speed tunnel. The maximum envelope efficiency of the propeller with airfoil shank sections was measured at about 0.95 and approximately 5 percent less for the round shanks. At constant power and rotational speed, the efficiency of the airfoil shank propeller was from 2.8 to 12 percent higher than that of the round shank propeller over a range of air speeds from 225 to 450 miles per hour. Comparisons to Delano's model tests of a 4-foot diameter propeller indicated that the efficiency envelope of the full-scale propeller was higher than that of the model case by 1.5 to 0.5 percent. The difference in the two sets of data was noted to be within the limits of experimental accuracy. However, it was suggested that Reynolds number or the difference in spinner scaling, e.g. $0.217D$ in the full-scale tests and $0.333D$ in the model tests, may have also been a source of error.

Another area in which shank geometry and spinner/shank integration is important concerns cowling intakes. The power and economy of gas-turbine engines are markedly dependent on the efficiency of the air-induction system. In the case of turbo-propellers equipped with conventional annular cowling/spinner

combinations, the problem of obtaining low intake losses is complicated by the presence of an initial boundary layer on the spinner ahead of the inlet and by interference effects introduced by the propeller root. Determining cowl, spinner, and blade root forms for this case requires knowledge of the effects of propeller operation on the spinner boundary layer and on the flow in the vicinity of the cowl. To this end, Prince⁽¹²⁾ and Keith, Bingham, and Rubin⁽¹³⁾ have contributed. Unfortunately, the author of this thesis was not able to obtain a copy of Reference 12 but the study by Keith, et.al, was sufficiently rigorous. Keith, et.al., conducted tests of several propeller planforms to investigate the effects of variations in shank geometry and spinner-juncture on the aerodynamic characteristics of a NACA 1-series cowl/spinner combination equipped with an eight-blade dual-rotation propeller. This configuration is of great interest to the industry at the present time for subsonic/transonic turbo-propeller powered aircraft. A particularly difficult design problem is presented from the viewpoint of obtaining low intake losses because of the large spinner, number of blades, blade-root disturbances, and the counterrotation of the propeller elements. It is of interest in the present study because of the meaningful qualitative and quantitative insight into the physics of the problem.

The propellers tested consisted of three airfoil-type shank blades with root thicknesses of 12, 24, and 40 percent, and two round shank blades which had root diameters equal to the maximum thickness of the 24 and 40 percent thick airfoil shank propellers. Because of power and tunnel size limitations, the outer 36 percent

of the blades were removed. All propellers tested were identical in geometry and section lift coefficient with the exception of the thickness distribution in-board of the 55 percent radial station. Each propeller was tested with an aerodynamically "ideal" spinner/shank juncture, i.e., the shank was extended to the spinner surface and sealed. One of the propellers was then tested with four "practical" juncture configurations that permitted blade rotation. The first of these junctures involved removing a section of the blade root to allow the necessary blade angle change. The second consisted of a low airfoil-type riser mounted on the spinner which was positioned to coincide with the blade at cruise. The third juncture was a larger riser which extended above the spinner boundary layer. The fourth juncture was a broad, hemi-spherical riser which spanned the gap between the blade and spinner over a 20 degree blade angle sweep from the assumed climb and high speed cruise blade angles. Total and static pressure surveys were recorded and data reduced in the form of total pressure coefficient distributions across the annulus of the cowling inlet.

It was found that at the simulated design cruise condition, the propeller with the 12 percent thick shanks and "ideal" spinner/shank juncture produced the most favorable average total pressure coefficients at the cowling inlet which was nearly equal to those obtained with the propeller removed. Increases in shank thickness caused significant reduction in average total pressure coefficients, with round-shank blades causing much greater losses of as much as 26 percent more than the airfoil shank of the same thickness. Propeller/spinner juncture arrangements that permitted

blade rotation also reduced the total pressure coefficients when the juncture was located inside the spinner boundary layer. Whereas the high airfoil - land - type with land-shank gap located well above the spinner surface gave total pressure coefficients approximately equal to those of the "ideal" juncture on-design, and was superior off-design in climb. This enhanced off-design performance was explained to be due to the riser acting as a vortex generator, energizing the spinner boundary layer and thereby delaying separation at lower inlet-velocity ratios.

It is apparent that much effort has been expended experimentally on the broad concern of propeller root losses and the work has continued to date by the propeller industry. As recent as May of 1985, in a series of unpublished wind tunnel tests by Dowty Rotol, Ltd. on a commuter aircraft 4-bladed composite propeller⁽¹⁴⁾, gains of around 2 1/2 percent in peak efficiencies for full-scale tests and 10 percent in model tests resulted from fairing the blades into the spinner. Employing these efficiency gains could provide a 2.6 mph increase in cruise speed for the particular aircraft with a further 2 mph increase estimated due to improved flow into the engine intake.

Unfortunately, the numerous accounts of experimental programs dealing with performance benefits due to propeller root enhancements have failed to extrapolate the results to the fundamental mechanism of efficiency gain and in a compatible form to allow implementation into a theoretical methodology. Since the tests were oriented toward specific commercial products, the results were not widely distributed. It was also assumed that the performance

characteristics of various propeller root configurations were solely a result of the two-dimensional properties of the in-board blade sections and therefore could readily be accounted for in the present day strip analysis numerical routines. In a review of propeller performance methodologies by Korkan, et.al.⁽¹⁵⁾, the short comings of such a philosophy were revealed. Theoretical predictions of C_T , C_p and η versus J were shown to overpredict experimental data (Figures 1, 2 and 3), dictating the need to account for secondary sources of performance losses. One such source is the interference drag which is inherent at the junction of the propeller blade and spinner and between blades. Isolating this component is often difficult, but Hoerner⁽¹⁶⁾ provides a valuable compilation of data for several cases. For example, when two bodies operate in tandem in a flow field, drag can be significantly different than when isolated in free flow. Further, the effect is not the same for bluff bodies as for streamlined shapes as shown in Figures 4 and 5. This is a phenomena which Hoerner terms the "shielding effect" and is employed to advantage in motorcar and bicycle racing under the terminology of "drafting". Another example of cases in which mutual interaction exists between bodies operating in close proximity is shown in Figures 6 and 7. Here, Hoerner shows the effects on drag of cylinders and airfoils placed side by side. In all instances shown in Figures 4 through 7, interference effects are evident up to dimensionless gap distances of four. This distance is within the range in which propeller blade roots are accommodated, especially with a large number of blades. However because of the resultant velocity of rotational and free-stream velocity components of a

propeller system, the blade-to-blade interference effects will not be a single case of operating either in tandem nor side by side, but a combination of the two and furthermore, changing as a function of advance ratio.

Interference drag also originates at the junction of bodies where two boundary layers coalesce. Hoerner considered the case of an airfoil at zero angle-of-attack meeting a flat plate as shown in Figure 8, and provided an expression for the resulting interference C_{D_i} in the form of:

$$C_{D_c} = \Delta D / q c^2 = 0.8(t/c)^3 - 0.0003 \quad (\text{II-2})$$

or

$$C_{D_t} = \Delta D / q t^2 = 0.75(t/c) - 0.0003(t/c)^2 \quad (\text{II-3})$$

Note that the expressions are based on the "chord area", c^2 , or the "thickness area", t^2 . This is suitable since this type of interference drag was found to be independent of the span of the respective wing or strut. Caution must be exercised in interpreting these results since C_D was also found to increase appreciably with lift coefficient as given in Figure 9.

The analogy of this interference drag to the case of a propeller blade joining a hub is obvious, and several investigators have recognized the idea in contributing to the scheme of theoretical calculations. Sarsfeld⁽¹⁷⁾ used the interference C_{D_i} expression of Equation (II-2) in postulating the change in propeller efficiency. In a more direct check of blade/spinner interference

drag loss, Reid⁽¹⁸⁾ measured the drag of a spinner with four round stub blade shanks attached. The shank length was established to duplicate that of a typical unfaired blade shank. From Reid's data Borst^(19,20) deduced a drag interference loss of $C_D = 0.517$ which is approximately equal to the primary drag coefficient of cylinders at the tested Reynolds number. The drag due to the spinner/shank interference was expressed in terms of a drag area, $SC_D = \text{Drag}/q$. Borst then expressed the change in thrust and power coefficients due to the drag area change between the spinner with and without stub shanks, which resulted in a semi-empirical model that could be incorporated into analytical propeller performance codes. Borst's work, as shown in Figure 10 indicates that the reduction in efficiency due to interference losses can range from one to five percent depending on the flight condition. The mathematical models of Borst and Sarsfeld are discussed in more detail in Chapter III.

Korkan, et.al,⁽¹⁵⁾ took a similar approach in applying Borst's correction to the predicted values of propeller performance methodologies, but elaborated by directly comparing the theoretical predictions to experimental data. It was shown that although the inclusion of interference drag improved the correlation between the theoretical predictions and experiment, yielding acceptable results in some cases, complete agreement was still not achieved. These results are shown in Figures 11 through 13.

In summary, the paucity of experimental data specific to the effects of interference, and the deficiencies/limitations of the existing analytical models of Borst and Sarsfeld clearly indicate a need for improvement. Clarifying the interference C_D value and

identification and examination of the variables that affect its magnitude and functional form is required. For instance, previous studies have failed to account for such associated engineering parameters as spinner geometry, shank form, number of blades, and advance ratio in any compatible, systematic form. Each of these variables have been shown to influence propeller performance as a whole, but prior investigations often neglect to identify the physics of the more pertinent issue of interference drag. Furthermore, the problem is complicated by the various types of interference phenomena, i.e., shank/shank or spinner/shank. Fortunately, the task of isolating these various mechanisms is eliminated by the empirical nature of the solution, which takes into account both types of interferences under a common heading of a single overall interference effect -- provided experimental data is available from a complete, systematic program.

III. THEORY

At the present time, there is no complete theoretical method to account for interference drag. Such models would be difficult to formulate since the primary physics of the phenomena is not well understood, therefore empirical, or semi-empirical models which can be incorporated into existing propeller performance prediction routines have been utilized. The acquisition and continued development of such aerodynamic tools allows the design and analysis of current and future propellers to be more rigorously treated. The approach during the present research effort has been to mathematically develop applicable corrections from first principles of blade element theory and supplement unknown quantities using experimentally gathered data with attention to the important physical parameters. This approach reduces the empirical qualifications to basic lift and drag loads, while maintaining the practicality of the contribution in terms of compatibility and adaptability to propeller performance techniques.

As an example of analysis methodologies and as a theoretical foundation, a propeller performance computer code has been adopted which uses strip-analysis. The method has been used extensively for many years with a history of progressive improvements, and is still widely used today. In this Chapter the propeller performance code used in this study is briefly discussed, followed by a detailed summary of the interference models of Borst and Sarsfeld .

A. Propeller Performance Computer Analysis⁽²¹⁾

The propeller performance computer code chosen to supplement the current study utilizes conventional strip analysis techniques as carried out in the 1920's by Lock and Goldstein. The particular program described herein was developed by Cooper⁽²¹⁾ and involves the calculation of aerodynamic forces at selected spanwise blade locations for given operating conditions and propeller geometry (Figure 14). From these differential forces, the differential thrust and torque coefficients can be expressed as:

$$\frac{dC_T}{dx} = k(c/d)Mx^2(C_\ell \cos \phi - C_d \sin \phi) \quad (\text{III-1})$$

$$\frac{dC_Q}{dx} = \frac{x}{2} \frac{dC_T}{dx} \frac{C_d \cos \phi + C_\ell \sin \phi}{C_\ell \cos \phi - C_d \sin \phi} \quad (\text{III-2})$$

Thrust and torque coefficients may be obtained by integrating over the radius of the blade. Alternatively, thrust and torque contributions due to limited portions of the propeller, such as the inboard blade regions, can be ascertained by integrating over a discrete radius fraction. Propeller efficiency and power absorbed may then be calculated by:

$$\eta = J \frac{C_T}{C_P} = (V/nd) \frac{C_T}{2\pi C_Q} \quad (\text{III-3})$$

$$\text{BHP} = \frac{C_P \rho n^3 d^5}{550} \quad (\text{III-4})$$

Cooper's propeller performance analysis approximates a linear induced inflow distribution on the propeller blade. Typically, an iterative process is required to resolve the induced angle of attack and lift coefficient at a specific radial location because of the interrelationship. However Goldstein⁽²²⁾ has solved the radial distribution of circulation for a lightly loaded propeller having a finite number of blades, and has established the relationship between $\sigma_p C_l$ and α_i . Cooper approximated the $\sigma_p C_l - \alpha_i$ curves by straight lines and plotted the slopes versus advance ratio for spanwise locations and number of blades. From these plots, and using available aerodynamic data, induced angles of attack can be determined.

In addition to induced velocities, the propeller performance code also requires an inflow velocity distribution. This inflow velocity profile accounts for nacelle effects and, while many prediction schemes assume a uniform inflow, is actually input into the current computer analysis. A potential flow solution has been utilized to estimate the inflow velocities applicable to the experimental configurations used in the present study.

Cooper's analysis also employs a tip correction factor to account for the three-dimensional propeller tip effect. Here, the two-dimensional lift curve slope is reduced according to correlations with pressure distribution measurements made on a NACA operating propeller.

In summary, Cooper's procedure for calculating propeller performance is useful as a fast and simple numerical computation. Further, the method appears to be the most versatile approach since

treatment of such physical conditions as nacelle effects and tip relief can be easily included. However, it cannot be regarded as rigorous because of difficulties in obtaining reliable aerodynamic data and lack of consideration to such engineering particulars as aeroelastic twist, spanwise flow and blade-to-blade/spinner-shank interference. It is the aim of the current study to diagnose the latter phenomenon with a review of Borst's and Sarsfeld's previous attempts, leading to further development and suggestive improvements.

B. Sarsfeld Model (17)

In a limited study, Sarsfeld conducted an analysis of propeller spinner/shank interference drag to determine its magnitude for the current round-shanked propeller blades and define its effect on efficiency. Sarsfeld used a basic approach which relied on the interference drag coefficients compiled by Hoerner (16) for an airfoil meeting a flat plate (Figure 8). Being independent of the span of the respective wing or strut, the interference drag coefficients are based on sectional dimensionalizations i.e., chord area, c^2 , or thickness area, t^2 and interpolated in the form of:

$$C_{D_c} = \frac{\Delta D}{qc^2} = 0.8(t/c) - 0.0003 \quad (\text{III-5})$$

$$C_{D_t} = \frac{\Delta D}{qt^2} = 0.75(t/c) - 0.0003(t/c)^2 \quad (\text{III-6})$$

Sarsfeld postulated that the change in efficiency can be represented by a ratio of interference drag to thrust produced by the propeller, starting with the expression:

$$\Delta\eta_i = \frac{\Delta D}{T_{\text{net}}} \quad (\text{III-7})$$

Using the data provided by Hoerner, and extrapolating the points to the case of a cylinder joining a plane wall corresponding to a $t/c = 1$, Sarsfeld determined that a 3.4% increase in efficiency could be realized for a typical three-bladed model propeller if the spinner/shank interference drag could be eliminated. Estimates were also made of the increase in efficiency available from fairing the hub region blade sections with airfoil shapes instead of cylindrical, based on pressure drag correlations provided by Hoerner for faired bluff sections.

It may be noted that a general efficiency expression⁽¹⁵⁾ can be written by combining equations (III-5) and (III-7) such that:

$$\Delta\eta_i = \frac{(0.8(t/c)^3 - 0.0003) c^2 q_{\text{loc}}}{T_{\text{net}}} \quad (\text{III-8})$$

where q_{loc} is the local dynamic pressure. Using potential flow analysis:

$$q_{loc} = q_o (V_{loc}/V_o)^2 \quad (III-9)$$

and therefore:

$$\Delta\eta_i = \frac{(0.8(t/c)^3 - 0.0003) c^2 q_o (V_{loc}/V_o)^2}{T_{net}} \quad (III-10)$$

where q_o and V_o are the free stream dynamic pressure and velocity, respectively and V_{loc} is the local velocity at the shank location. Utilizing the thrust coefficient (C_T) and advance ratio (J) where :

$$T = \frac{2 C_T d^2 q_o}{J^2} \quad (III-11)$$

(III-10) becomes:

$$\Delta\eta_i = \frac{(0.4(t/c)^3 - 0.00015) (V_{loc}/V_o)^2 J^2}{C_T (d/c)^2} \quad (III-12)$$

For a given propeller/test condition:

$$\Delta\eta_i = \frac{k_1 J^2}{C_T (d/c)^2} \quad (\text{III-13})$$

where k_1 is a constant. As pointed out by Korkan, et.al⁽¹⁵⁾, the expression indicates that $\Delta\eta_i$, the decrease in efficiency due to spinner/shank interference, increases as advance ratio increases, C_T decreases, or D/C decreases - none of which is intuitive nor borne out by experimental evidence. The efficiency expression also contains no implications of the effect of interference drag upon propeller torque as related to the radial location of the interference. Furthermore, extrapolation of interference C_D values for thickness ratios approaching unity is questionable since it is expected that the wake pressure drag effects will become important. This concern is compounded since no accurate experimental interference drag data has been collected for cylinders in conjunction with plane walls.

C. Borst/Reid Model^(18,20)

The nearest evidence of drag measurements for cylindrical proturbences is due to Reid⁽¹⁸⁾, who measured the drag of a spinner with four round stub blade shanks. The objective was to account for the effect of a 1/4 inch long circular shank of one inch diameter, which seperated the propeller blades from the spinner surface. Reid made experimental measruements of the drag of a plain spinner, and with cylindrical stubs of 0.45 inches in length in place of the

blades. The additional length is intended to compensate for the finite aspect ratio of the stub shanks using C_D data of Hoerner⁽¹⁶⁾ and Goldstein⁽²³⁾ for cylinders with exposed ends. The stub shanks produce the same drag, or SC_D , as the end-plated blade shanks. The difference between the measured SC_D with stubs and without stubs, neither of which involved spinner rotation, gave the increment in drag due to the stubs. These quantities were reported as:

$$SC_D = 2.1 \text{ for } Re/ft < 6 \times 10^6$$

$$SC_D = 1.5 \text{ for } Re/ft > 6 \times 10^6$$

with a potential error band due to recorded limits of balance repeatability of $\pm 10\%$.

Borst then elaborated upon Reid's results by subtracting the equivalent drag coefficient of the stubs, with recognition to aspect ratio effects, to arrive at the spinner/shank interference contribution. For example at a Reynold's number of 500,000, Reid's total drag coefficient is found to be 1.167 per blade. The corresponding drag coefficient of a cylinder with a diameter-to-span ratio of $h/b = 1/(2 \times 0.45)$ including imaging is approximately 0.65 (Ref 16, Figure 3-28). Hence the interference drag coefficient is 0.517.

Using a propeller blade element approach for a section, Δx , operating at zero lift, Borst then resolved the interference drag contributions into components of thrust and torque, such that:

$$\Delta C_T = \frac{\Delta T}{\rho n^2 d^4} = \frac{\Delta D \sin \phi}{\rho n^2 d^4} \quad (\text{III-14})$$

$$\Delta C_P = \frac{2\pi n Q}{\rho n^3 d^5} = \frac{2\pi (\Delta D \cos \phi) \bar{x}}{\rho n^3 d^5} \quad (\text{III-15})$$

per blade. In these equations, ϕ is the angle between the resultant and rotational velocities which are known based on the freestream velocity and revolution speed, n . Therefore, Equations (III-14) and (III-15) can be derived into convenient forms of:

$$\Delta C_T = \frac{Bc \Delta C_D J}{2d^2} (J^2 + 4(\pi \bar{x})^2/d^2)^{1/2} \Delta x \quad (\text{III-16})$$

$$\Delta C_P = \frac{2Bc (\pi \bar{x})^2 \Delta C_D}{d^4} (J^2 + 4(\pi \bar{x})^2/d^2)^{1/2} \Delta x \quad (\text{III-17})$$

Borst showed that these corrections to propeller thrust and power coefficients take on more simplistic forms if dimensionless values of Δx and x are used based on propeller radius, such that:

$$\Delta C_T = \frac{Bc \Delta C_D J}{4D} (J^2 + (\pi \bar{x}')^2)^{1/2} \Delta x' \quad (\text{III-18})$$

$$\Delta C_P = \frac{Bc (\pi \bar{x}')^2 \Delta C_D}{4D} (J^2 + (\pi \bar{x}')^2)^{1/2} \Delta x' \quad (\text{III-19})$$

Although these expressions are mathematically precise with no simplifying assumptions, complications in applying them were revealed due to the subtleties of expressing the interference drag coefficient, ΔC_D , in terms of frontal area, or per radial length. This subtlety incurs implicit restrictions upon the choice of Δx , which is arbitrary, and requires knowledge of the length over which the interference drag acts. In other words, similar testing of

cylinders of different length would result in different magnitudes of the interference ΔC_D , where:

$$\Delta C_D = \frac{\Delta D}{qc \Delta x} \quad (\text{III-20})$$

since ΔD is changing disproportionately to Δx . In fact, ΔD has been shown to be independent of Δx providing Δx is much larger than the boundary layer height. If this form of the drag coefficient is to be assumed, Δx should be the distance over which the interference acts e.g.,; Δx_i . Hence, an appropriate value and functional form of the interference drag coefficient can be determined by:

$$\Delta C_{D_i} = \frac{\Delta D}{qc \Delta x_i} = (C_{D_{\text{meas}}} - C_{D_{\text{shank}}}) \frac{\Delta x}{\Delta x_i} \quad (\text{III-21})$$

The obvious short-coming of expressing interference drag coefficients based on frontal areas is now explicit.

If Reid's and Borst's drag coefficients are recast into forms based on sectional dimensions as Sarsfeld's and Hoerner's, the interference value becomes:

$$\Delta C_{D_t} = C_D (\Delta x/c) = 0.517 (0.45/1) = 0.233 \quad (\text{III-22})$$

Note that this can now be directly compared to Sarsfeld's extrapolated value of 0.75 and has been plotted on Figure 8 for comparative purposes, illustrating that the discrepancy of

almost 70%. The same 70% discrepancy exists between Borst's and Sarsfeld's interference thrust and torque corrections in application to propeller sections operating at zero lift since for a given condition, ΔC_T and ΔC_p depend solely on ΔC_D as does efficiency for $\Delta \eta = \Delta D/T_{net}$.

Two hypotheses can be suggested to explain the disagreement, disregarding the errors in Reid's experiment or Hoerner's drag compilations. Since there is no experimental data beyond t/c of 0.6 for the tests of airfoils joining a plane wall, Sarsfeld's extrapolation to the case of a cylinder ($t/c = 1$) may be inaccurate. Secondly, the height of Reid's cylinder stub may be of comparable proportion to the spinner boundary layer such that the condition $h \gg \delta$ is violated. Attention to this detail using drag forces under such conditions⁽²⁴⁾ increases Borst's value in the direction of Sarsfeld's. Still, the interference phenomena may yet to be fully developed in Reid's case.

The previous studies by Sarsfeld and Borst warrant further examination to clarify the discrepancy in the interference C_D value for cylindrical shanks. To supplement the understanding and applicability of interference thrust and torque corrections, interference drag coefficients need to be determined with attention to parameters such as advance ratio, number of blades, spinner effects, and airfoil shank sections. The latter requires that Equations (III-18) and (III-19) be re-derived for the general case to include lift. A suggestive method of extracting interference drag coefficients from the thrust and torque data of the concurrent

experimental program (Chapter IV) is also beneficial and thus developed herein.

D. Present Model

The interference models of Borst and Sarsfeld were independently determined as a first approximation to a problem in which very little experimental confirmation was available. Closer inspection of the two methods, aside from the comparisons of Korkan, et.al.⁽¹⁵⁾ with experiment, has indicated discrepancies and areas of potential improvement. In view of the previously discussed deficiencies in Borst's and Sarsfeld's methods, a more thorough examination of interference drag and its associated effects on propeller performance can be attempted, beginning with a procedural development of the generalized performance parameter equations for a differential blade element.

Referring again to the velocity diagram of Figure 14, the differential thrust and power coefficients can be resolved in terms of their respective lift and drag components as :

$$\frac{dC_T}{dx} = \frac{L \cos\phi - D \sin\phi}{\rho n^2 d^4} \quad (\text{III-23})$$

$$\frac{dC_P}{dx} = \frac{2\pi(L \sin\phi - D \cos\phi) \bar{x}}{\rho n^2 d^5} \quad (\text{III-24})$$

where x is the radial distance of the blade section from the center of rotation. Expressing the angle ϕ in terms of the known geometric angle, ϕ_0 , and induced angle, θ , where $\phi = \phi_0 + \theta$, Equation III-21 and III-22 become:

$$\frac{dC_T}{dx} = \frac{L \cos(\phi_0 + \theta) - D \sin(\phi_0 + \theta)}{\rho n^2 d^4} \quad (\text{III-25})$$

$$\frac{dC_P}{dx} = \frac{2\pi(L \sin(\phi_0 + \theta) + D \cos(\phi_0 + \theta)) \bar{x}}{\rho n^2 d^5} \quad (\text{III-26})$$

Using trigonometric relations:

$$\frac{dC_T}{dx} = \frac{L}{\rho n^2 d^4} (\cos\phi_0 \sin\theta - \sin\phi_0 \cos\theta) - \frac{D}{\rho n^2 d^4} (\sin\phi_0 \cos\theta - \cos\phi_0 \sin\theta) \quad (\text{III-27})$$

$$\frac{dC_P}{dx} = \frac{2\pi\bar{x}}{\rho n^2 d^5} (L(\sin\phi_0 \cos\theta - \cos\phi_0 \sin\theta) + D(\cos\phi_0 \cos\theta - \sin\phi_0 \sin\theta)) \quad (\text{III-28})$$

Equations III-26, 27 are general but not in a functional form useful to strip analysis. Assuming that dx is a small radial width of blade section, Δx , and small enough to where there are no severe load variations across Δx such that x , now the radial distance to the load centroidal location, can be approximately resolved. Equations III-26, 27 can therefore be rewritten in terms of rotational and freestream velocities as

$$dC_T = \frac{1}{\rho n^2 d^4} \left(L \left(\frac{V_r}{V_G} \cos \theta - \frac{V_\infty}{V_G} \sin \theta \right) - D \left(\frac{V_\infty}{V_G} \cos \theta - \frac{V_r}{V_G} \sin \theta \right) \right) \Delta x \quad (\text{III-29})$$

$$dC_P = \frac{2\pi \bar{x}}{\rho n^2 d^5} \left(L \left(\frac{V_\infty}{V_G} \cos \theta - \frac{V_r}{V_G} \sin \theta \right) + D \left(\frac{V_r}{V_G} \cos \theta - \frac{V_\infty}{V_G} \sin \theta \right) \right) \Delta x \quad (\text{III-30})$$

where

$$V_r = 2\pi x n$$

$$V_G = (V_\infty^2 + V_r^2)^{1/2} = (J^2 + 4(\pi \bar{x})^2/d^2)^{1/2} (nd)^2$$

$$V_{res} = (V_G^2 - w^2)^{1/2} = (J^2 + 4(\pi \bar{x})^2/d^2 - w^2/(nd)^2)^{1/2} (nd)^2$$

The fully expanded form of the above equations can be manipulated to involve lift and drag coefficients with the use of $1/2 c \Delta x V_{res}^2$.

Therefore:

$$dC_T = \frac{c \Delta x V_{res}^2}{2n^2 d^4 V_G} (C_L V_r \cos \theta - C_L V_\infty \sin \theta - C_D V_\infty \cos \theta + C_D V_r \sin \theta) \quad (\text{III-31})$$

$$dC_P = \frac{\pi \bar{x} c \Delta x V_{res}^2}{n^2 d^5 V_G} (C_L V_\infty \cos \theta - C_L V_r \sin \theta + C_D V_r \cos \theta - C_D V_\infty \sin \theta) \quad (\text{III-32})$$

where dC_T and dC_P is taken as per blade. Note that for the cylindrical shank or zero lift regions where w and θ approach zero, Equations III-31 and III-32 reduce to those used by Borst.

Therefore if the interference drag coefficient is known and substituted in Equations III-31 and 32 for C_D , the change in thrust and power coefficients can be calculated. The interference C_D values can be determined from experimentally measured thrust and power coefficients by:

$$C_{T_{meas}} = C_{T_{shank}} + C_{T_i} \quad (\text{III-33})$$

$$C_{P_{meas}} = C_{P_{shank}} + C_{P_i} \quad (\text{III-34})$$

However, Equations III-33 and 34 yield two equations and three unknowns, i.e., C_{Di} , Δx_i and \bar{x}_i . Ratioing Equation III-33 to Equation III-34 yields:

$$\bar{x}_i = \left(\frac{C_{P_{meas}} - K(\pi\bar{x})^2 C_{D_{shank}}}{C_{T_{meas}} - K J C_{D_{shank}}} \right)^{1/2} J / \pi \quad (\text{III-35})$$

It is evident that knowledge of the distribution of C_{Di} over Δx_i must be known to proceed further. A better understanding of the concepts used in this development can be gained from Figure 15 which illustrates the primary and interference drag components. The problem arises because of the form in which C_D is expressed ($C_D = D/qs$), and can be eliminated by re-deriving Equations (III-16) and (III-17) for $C_{Dt} = D/qt^2$ where:

$$dC_T = \frac{B c^2 J}{2 D^2} C_{Dt} (J^2 + 4(\pi\bar{x})^2/d^2)^{1/2} \quad (\text{III-36})$$

$$dC_P = \frac{2B c^2 (\pi\bar{x})^2}{D^4} C_{Dt} (J^2 + 4(\pi\bar{x})^2/d^2)^{1/2} \quad (\text{III-37})$$

For dimensionless \bar{x} :

$$dC_T = \frac{B c^2 J}{2 D^2} C_{Dt} (J^2 + (\pi\bar{x})^2)^{1/2} \quad (\text{III-38})$$

$$dC_P = \frac{B c^2 (\pi\bar{x})^2}{2 D^2} C_{Dt} (J^2 + (\pi\bar{x})^2)^{1/2} \quad (\text{III-39})$$

Note that Δx_i is no longer a factor, leaving a properly posed problem in two equations and two unknowns such that with \bar{x}_i

determined from Equation (III-35), C_{Dti} can be obtained from either of the following two expressions:

$$C_{T_{meas}} = KJC_{D_{shank}} + \frac{Bc^2 J}{2D^2} C_{D_{ti}} (J^2 + (\pi \bar{x}'_i)^2)^{1/2} \quad (III-40)$$

or

$$C_{P_{meas}} = K(\pi \bar{x})^2 C_{D_{shank}} + \frac{Bc^2 (\pi \bar{x}'_i)^2}{2D^2} C_{D_{ti}} (J^2 + (\pi \bar{x}'_i)^2)^{1/2} \quad (III-41)$$

Because of the mathematical form of Equation III-35, numerical quantities of \bar{x}_i are very sensitive to the components $C_{p_{meas}}$, $C_{T_{meas}}$, $C_{D_{shank}}$, and \bar{x} of the fraction. Small differences in any of these values produce large errors in extracted interference C_{Di} 's. Therefore, an alternative approach of determining interference C_{Di} 's from experimental measurements is suggested.

The drag coefficient of a propeller section operating at zero lift can be expressed directly in terms of thrust and torque loads as:

$$C_D = \frac{(T^2 + (Q/\bar{x})^2)^{1/2}}{0.5\rho V_{loc}^2 S} = \frac{T/\sin\phi}{qS} = \frac{Q/\bar{x}\cos\phi}{qS} \quad (III-42)$$

or

$$C_{D_t} = \frac{(T^2 + (Q/\bar{x})^2)^{1/2}}{0.5\rho V_{loc}^2 t^2} = \frac{T/\sin\phi}{qt^2} = \frac{Q/\bar{x}\cos\phi}{qt^2} \quad (III-43)$$

Henceforth, coefficients based on qt^2 will be used for interference drag computations in light of the problems associated with basing C_{Di} 's on qS .

From experimental tests similar to Ried's for spinners with cylindrical stubs attached with velocity and load distributions as shown in Figure 16, the interference drag, $C_{D_{ti}}$ can be directly determined from thrust measurements by:

$$C_{D_i} = \frac{T/\sin\phi}{qt^2} - C_{D_{shank}} (\Delta x/c) \quad (III-44)$$

The respective resolved load location, \bar{x}_i , is determined from torque measurements. Referring to Figure 15, \bar{x}_i can be written from centroidal moment considerations in terms of measured and equivalent 2-D loads as:

$$\bar{x}_{meas} = \frac{C_{D_{shank}} \bar{x} - C_{D_i} \bar{x}_i}{C_{D_{shank}} + C_{D_i}} = \frac{C_{D_{shank}} \bar{x} - C_{D_i} \bar{x}_i}{C_{D_{meas}}} \quad (III-45)$$

From Equation III-43

$$(C_{D_i} \bar{x})_{meas} = Q/Bqt^2 \cos\phi \quad (III-46)$$

and therefore:

$$\bar{x}_i = (Q/Bqt^2 \cos\phi - C_{D_{shank}} (\Delta x/c))/C_{D_{ti}} \quad (III-47)$$

Knowledge of C_{D_i} and \bar{x}_i allows the effect of interference drag on the propeller thrust and torque coefficients, hence efficiency, to be determined from Equations III-36 and III-77. Note that an interference efficiency correction cannot be written solely based

on interference C_T and C_p as $\eta_i = \frac{C_{Ti}}{C_{pi}}$ J, but

expressed as:

$$\eta_{\text{corrected}} = \frac{C_{T_{\text{theory}}} - C_{T_i}}{C_{P_{\text{theory}}} - C_{P_i}} J \quad (\text{III-48})$$

Using this approach, it is anticipated that although interference drag may have small effects on overall propeller thrust and torque coefficients, significant decrements in efficiency may result as previously shown by Korkan, et.al., (Figures 11-13). In order to determine these effects quantitatively, and account for rotation, blade-to-blade interference, spinner/shank interference and number of blades, an experiment was developed and conducted in the present study. The theoretical development can then be used to reduce thrust and torque measurements into a resolved drag, form which the interference contribution can be determined. Finally, the reverse process of incorporating these interference C_D values into existing propeller performance codes, using the above theory, can be achieved as an application to the general case.

IV. TEST ARRANGEMENT/PROCEDURE

The experimental segment of this study to examine the program to study the effects of interference drag on propeller performance has been conducted in the Texas A&M University 2 ft x 3 ft subsonic wind tunnel using a propeller test rig (PTR) specifically designed and constructed for this purpose at Texas A&M University. The wind tunnel is a closed circuit, single return-type with test section dimensions of two feet high by three feet wide. Maximum attainable airspeed as supplied by a 30-horsepower DC motor with fixed pitch, four-blade fan, is approximately 90 ft/sec and can be adjusted by varying the motor RPM.

A. Experimental Apparatus

The PTR, shown in Figures 17 and 18, incorporates a 1.5 horsepower AC motor which is rated at 12,000 RPM. The design utilizes two bulkheads with linear bearings to support the motor, yet permits free rotational and translational movement. This movement is restrained only by properly oriented load cells, which in turn provide measurements of thrust and torque (Figure 19). The thrust cell is actuated directly along the axis of the PTR and is oriented to provide non-interference with the rotational movement of the PTR. The torque unit is oriented off-axis with a moment arm of 1.3 inches to provide pure torque measurements. The actuating arm also incorporates a miniature linear bearing to uncouple the torque reaction from the thrust direction.

The load cells are small modular force-sensing units relying on a full-bridge arrangement of strain gages placed on flexures, and are commercially available in capacities of 5, 10, 25 and 50 pounds. For the present tests, it was found that a 10 pound capacity load cell provided adequate sensitivity on both the thrust and torque axes without risk of permanent deformation of the flexure or strain gage. Factory specifications in terms of non-linearity and hysteresis were provided as less than 0.03 percent of the rated output. However, calibration in their present application was necessary and is detailed in later sections of this thesis.

An extension of the motor shaft through the front bulkhead drives the propeller assembly, which consists of a primary hub with attached spinner and stub blade shanks. Two hubs were fabricated to facilitate the testing of 2, 4, or 8 blades, and 3 or 6 blades, respectively. Various propeller model configurations can then be assembled with one of two spinners, and one of three types of blade shanks.

The spinners are scaled versions of an existing Hartzell Propeller, Inc.⁽²⁵⁾ spinner and differ only in finess ratio, i.e., length to diameter ratio (l/D). Initially, three spinner finess ratios of 1.0, 1.3, and 1.6 were proposed, but preliminary checks on the two extreme cases (1.0, 1.6) indicated only small differences in thrust and torque measurements. Coordinates of the spinners tested are provided in graphical form in Figure 19 and tabulated in Table 1. As noted in Table 1, the fineness ratio is altered by scaling the x-axis.

The propeller shank models tested were chosen to simulate the shank region of a typical propeller and sized in accordance to the model tests of Reid⁽⁷⁾. The prototype blade model of Reid⁽⁷⁾ was adopted as a "base configuration" to define the dimensional form of the three models of the current tests, and as a representation of the outboard propeller blade segment. This approach was required since the full propeller blade was not included in these experimental tests, but was utilized in the theoretical analysis. Figure 20 shows the representative prototype, and the three shank types modeled for this study. The principal design characteristics of the various blade forms are presented in Figures 21 through 23, i.e., the radial distribution of twist ($\beta/\beta_{0.75}$), non-dimensional thickness (t/c), and non-dimensional planform (h/D) of the shank stubs superimposed upon the referenced prototype propeller. As noted earlier, the selected models are intended to provide a fundamental foundation for the development of a spinner/shank interference data base, and therefore do not exactly duplicate the prototype propeller.

The models tested include a baseline circular cylinder, a transition shank from a round root to an airfoil, and a constant chord airfoil shank representing a cuff fitted to the stub section of the cylindrical shank region of the prototype propeller. All shanks have the same maximum thickness and length -- representing the inboard 35% of the referenced propeller radius as scaled based on the spinner diameter. Assuming the same type of spinner/propeller diameter scaling of Reid's study, i.e., spinners of 15 percent propeller diameter, the full propeller diameter, D ,

for the present series of tests is given. The airfoil profile section of the transition and cuff shanks are matched at the tip ($r/R=0.35$) for both shank blade-types by a 43 percent thick double-cambered Clark Y airfoil⁽²⁶⁾ shown in Figure 24 (Table 2). These shank forms are a compromise between conventional blade shanks, with radially varying geometry, and an absolute two-dimensional representation. The intent is to maintain the fundamental nature of the study without the complication of radially varying twist and thickness, while accurately representing root dimensions dictated by structural considerations. This work is an extension of Hoerner and Reid's work, and supplements the gap between previous work and those which utilized full propeller blades. It is also assumed that minor discrepancies in radial modeling would not significantly influence absolute interference values since this effect is primarily confined to the root where the blade and hub adjoin. However, blade-to-blade consistency was presumed to be important for purposes of aerodynamic balance and dimensional accuracy. A molding construction technique similar to that of industrial composite blade manufacturers was adopted.

The construction process of molding the transition and airfoil cuff propeller shanks was initiated with the fabrication of an aluminum master. Templates for the Clark-Y airfoil section master were determined from dimensionless coordinates, plotted on a 500% enlarged scale, and photographically reduced to actual size. Polyester casting resin was then used to create molds from the master from which eight identical cuff and transition shanks were cast. The process also involved molding an undersized foam core of

1.5 lbs / ft³ urethane foam onto an aluminum fir-tree shank for centrifugal retention. A preform is then obtained by wrapping the core with a dry lay-up consisting of three layers of uni-directional graphite cloth, one layer of woven graphite cloth oriented $\pm 45^\circ$ to the blade axis, and an outer layer of fiberglass cloth (Figure 25). This preform is then placed into the mold for resin injection. After curing for a prescribed period, the blade is removed and deflashed. The final product exhibits a smooth surface finish with minimal dimension and weight variation between blades.

Other features of the PTR include an electro-magnetic sensor triggered from the back of the hub to register RPM on a Spectral Dynamics SD 340 Spectrum Analyzer, an air cooling system, and a thermocouple to monitor internal nacelle temperatures. The cooling arrangement passes low pressure air over the electric motor and exhausts through small ports at the rear of the nacelle, thus maintaining an acceptable temperature environment for the motor. Indications from the thermocouple were also well within the load cell tolerances as specified by the compensated range of 0°F to 150°F with associated zero shift of $\pm 0.08\%$ rated output per 100°F. Speed control is afforded by a Variac power supply. The rig is compactly contained within a minimum-body, fiberglass fairing and supported along the centerline of the wind tunnel test section by a truss arrangement of streamline stringers as shown in Figure 26. This configuration results in minimal aerodynamic disturbances in the propeller disc plane.

B. Data Acquisition

Data acquisition was primarily devoted to recording thrust and torque measurements at pre-set tunnel velocities and PTR RPM's. This was required for the array of propeller configurations entailing variations in number of blades, spinner fineness ratio, shank type, and airfoil blade pitch angles $\beta_{0.35}$, of 46, 51, and 56 degrees. The necessary instrumentation was arranged according to Figures 27 and 28.

Voltage signals from the Ametek thrust load cell and the Interface MB-10 torque load cell were passed through individual amplifiers and into an 8-bit analog-to-digital (A/D) conversion board interfaced with the Apple II+ computer. The principle features of the load cell amplifier/conditioner system included variable and regulated excitation from 1 to 12 Vdc which were set to the factory recommended excitation of 10 Vdc, independently variable gain, and LED null indicators for balance. A third channel of the A/D board was dedicated to tunnel velocity by means of a pressure transducer input, which was supplied from a pitot-static probe located ten inches ahead of the propeller disk plane and halfway between the blade tips and tunnel wall. An Apple II+ computer with appropriate software is then used to read, sample, and average three channels of data independently, which is automatically displayed prior to storage or printing.

With this arrangement, the necessary calibrations of thrust, torque, and tunnel velocity were accomplished. Thrust and torque voltage readings were calibrated by applying static thrust and

torque loads in the form of weights to the propeller hub while recording the respective signals at the computer terminal. This process also provided a measurement of the mechanical and/or electrical interaction between the two load cells, which was observed to be negligible. Amplifier gains were adjusted to exploit the full voltage range of the A/D board ($\pm 5V$) for sensitivity, with allowances to prevent signal "chopping" and was verified using a dual-trace oscilloscope. Calibrations resulted linear functions of weight versus volts in with less than $\pm 0.5\%$ deviation as shown in Figures 29, 30. These calibrations were accomplished with the model installed in the wind tunnel and repeated at several intervals during the experiment, showing repeatability to within ± 1 percent. Tunnel velocity was calibrated against an ammeter-type micromanometer in terms of voltage output versus displacement of water hence velocity (Figure 31). The calibration routines were included into the Apple II+ software for data acquisition and reduction, thus providing a direct measure of the desired data. A flowchart of the data acquisition/reduction program is given in Figure 32, with a listing and sample input/output contained in Appendix II.

In the data collection phase of the tests, capacitors were used to filter noise content of the thrust and torque channels by shunting high frequency information, thereby bringing the magnitude of the voltage signal to within tolerances of the A-D system. Electronic interference was also suppressed by determining proper excitation voltages, amplifier gain settings, and using the

necessary electronic grounding to minimize electromagnetic interference.

The Apple II+ was used interactively during test run sequences for "real-time" acquisition and reduction of the data. Atmospheric and operating conditions of a given case, e.g. run number, number of blades, blade type, spinner type, temperature, barometric pressure, and propeller RPM were input by the operator, who also set the sampling value. A minimum of 500 samples of signal information per channel were averaged for the data contained in this experimental program and a maximum of 1000 depending on the operating condition and data point repeatability. Sampling rate and software/hardware efficiency resulted in "on-station" times for data feedback of approximately fifteen seconds per data point.

C. Data Reduction

The experimental thrust, torque, velocity and RPM data have been reduced at the time of data acquisition, and placed into coefficient forms:

$$C_T = \frac{T}{\rho n^2 d^4} \quad (IV-1)$$

$$C_P = \frac{P}{\rho n^3 d^5} = \frac{2\pi Q}{\rho n^2 d^5} \quad (IV-2)$$

$$\eta = \frac{C_T}{C_P} J \quad (IV-3)$$

Note that the coefficients are based on the full propeller diameter of 2.528 feet, and not on the diameter of the stub shanks. This

form maintains compatibility with conventional propeller coefficients resulting in Δ 's related to spinner/shank interference.

Caution must be exercised in interpreting the results and determining how well these values represent a free-air propeller. Through various phases of the planning and testing, there was considerable discussion about the corrections which may be appropriate. Conventional practice has been to subtract spinner drag as a tare from thrust readings. Corrections to account for tunnel interferences are also commonly required in wind tunnel tests of propellers. In order to assess the accuracy of the experimental data, a review of three corrections based on previous theoretical and experimental work was conducted.

D. Tunnel Corrections

The accepted authoritative work on spinner drag corrections is a series of propeller tests conducted by Reid⁽²⁷⁾. Reid applies this correction to thrust readings and shows that these values can be divided into two parts, referred to as ΔT_1 and ΔT_2 . ΔT_1 is the force on the rear face of the spinner and ΔT_2 has been taken as the spinner forebody drag. ΔT_1 is used to correct the measured thrust to values which would have prevailed had the pressure on the back of the spinner been equal to the static pressure of the air stream, and calculated using the pressure differential at the rear face and the spinner area. In the report used as a basis for the present tests, Reid showed that the ΔT_1 correction was inconsequential with spinners of the diameter tested

Measurement of ΔT_2 is typically accomplished by either pressure plotting across the spinner or measuring thrust with the blades removed such that ΔT_2 is equal to the balance thrust minus ΔT_1 . This method assumes that the spinner drag remains unchanged when the blades are installed. This component was unmeasurable indicating an order of magnitude less than the desired quantities.

Two other corrections due to tunnel wall constraints must be resolved to fully simulate free air conditions. These are typically termed tunnel-blockage and wake-blockage effects. Owing to the wall constraints upon the contraction of a propeller slipstream, the effective advance ratio is less than that corresponding to the measured tunnel datum velocity. It is therefore necessary to determine an equivalent free airspeed, V' , corresponding to the tunnel velocity, V , at which the propeller would produce the same thrust and torque. A theoretical solution attributed to Glauert, has been developed from extending simple actuator-disk and momentum theory ⁽²⁸⁾. This correction applies to the advance ratio and hence efficiency, but does not affect thrust and torque coefficients. The equivalent airspeed is obtained from curves of V/V' against observed $T/\rho AV^2$ for a range of model sizes given by A/C , where A is the propeller disk area and C the tunnel cross sectional area (Figure 33). From these curves, which can be approximated by:

$$\frac{V' - V}{V} = \frac{D^2}{2C} T_c / (1 + 8T_c/\pi)^{1/2} \quad (\text{IV-4})$$

where

$$T_c = \frac{T}{\rho V^2 d^2} \quad (\text{IV-5})$$

this correction is justifiably neglected in the present tests based on A/C of 0.09, and measured thrust values of less than one pound corresponding to a T_pAV^2 value of 0.16. The maximum correction to airspeed is accordingly less than one percent. Physically, the explanation of such a negligible wake interference effect is that very little stream tube contraction is produced from the current propeller arrangement.

The final correction due to tunnel blockage is detailed by Rae and Pope⁽²⁹⁾ based on continuity and blockage area ratios. The form for solid blockage for a three-dimensional body is given by:

$$\frac{\Delta V}{V} = \frac{(\text{model volume})}{C^{3/2}} \quad (\text{IV-6})$$

This expression is more appropriate for propeller applications than direct area ratioing using the propeller disk area, since the individual blades can be handled by approximating their volume. The permeability or effective volume of the rotating blades is in question since the swept disk does not constitute a solid blockage to the airstream, but does present some degree of restriction. In either case, the magnitude of the correction is conservatively estimated from Rae and Pope as approximately 1 percent.

The treatment of the various tunnel interference effects infers that individually, the corrections are not appreciable. A

point of general concern in model wind tunnel tests of propellers is how the effects manifest themselves in conjunction with one another, and how valid the assumptions are in their derivation. It is certain, however, that the use of the propeller shanks as opposed to full blades was beneficial in minimizing the effects.

E. Test Procedure

The experiment was conducted to collect performance data over a range of advance ratios, J . The established practice of varying advance ratio was to set the wind tunnel velocity and vary the propeller rotational velocity. Wind tunnel velocity was nominally set at 65 ft/sec and RPM ranged from 200 to 2000, which resulted in advance ratios of 7.7 to 0.77, and covered the range of peak propeller efficiency of the prototype propeller blade as measured by Reid.

In order to investigate the effect of the parameters of interest and propeller configurations under study, the experimental tests were organized into three Phases according to shank type.

Phase I (Cylindrical Shanks): The initial segment consisted of measuring thrust, torque, propeller speed, and tunnel airspeed for the cylindrical shanks (Figure 34a). Shank configurations of 2, 3, 4, 6, and 8 shanks were tested with each spinner of fineness ratio equal to 1.6 and 1.0. The propeller RPM sweep consisted of 200 to 2000 RPM in nominal increments of 120 RPM. This series of tests served as a baseline for means of comparison to Reid's experiments, as well as the transition and airfoil shanks.

Phase II (Transition Shanks): The matrix of Phase I was repeated with the airfoil transition shanks (Figure 34b) installed at blade angles of 46° , 51° , and 56° . These angles are defined between the disk plane of rotation and the airfoil longest chordline at the tip of the stub shanks ($r/R=0.35$). The angle of 51° was chosen to correspond to the design propeller blade angle at the 75% radial location of 35° of the referenced prototype propeller model. Propeller pitch changes of $\pm 5^\circ$ were then effected from this datum point.

Phase III (Airfoil Shanks): The matrix of testing the propeller shanks representing airfoil cuff blades was identical to that of the transition airfoil shanks and cylindrical shanks (Phases I, II). The only difference was the added necessity of filling the void between the base of the propeller blade shank and the hub with modeling clay. This task was required at each propeller blade angle to eliminate the added parameter of gap size/geometry, and served to provide the "ideal" faired juncture. Figure 34c shows a photo of the Phase III configuration. configurations for the matrix of two spinner and 2,3,4,6 and 8 blades are shown in Figures 35 and 36, respectively.

V. RESULTS AND DISCUSSION

Prior to resolving quantitative interference values from the experimental observations, the collected data was plotted in terms of thrust and torque coefficients versus propeller advance ratio for the entire test matrix in order to review the preliminary performance aspects of each model configuration. Representative plots for Phases I, II and III of the tests are given in Figures 37 through 39 .

It was immediately apparent that no consistent trends due to the two spinner finess ratios could be established, and is therefore eliminated as a factor from future discussion. That is the spinner effects were not measureable in these model tests, however it is not known how the spinner results would scale to full-scale spinners and propellers. For instance, based on the resultant velocity at the hub and running length of the spinner, Reynold's numbers are on the order of 300,000. Coupled with the favorable pressure gradient, the Reynold's number indicates that a laminar boundary layer would exist at the spinner/shank juncture which would not be the case for a full-scale propeller. This factor is important with regards to spinner/shank interference drag and therefore warrants further study.

It should also be noted that the magnitude of the thrust and torque coefficients are indicative of the force measuring capability of the PTR in that the scales correspond to a maximum thrust measurement of 1.2 lbs and 0.2 ft-lbs of torque. Figures 37 through 39 do reveal the relative differences in the performance

characteristics of the three shank forms. Small distinctions are indicated in the negative thrust magnitudes of the various shanks. Because of the negatively stalled operating condition of the untwisted propeller cuff and transition models, forward thrust is not produced over these regions until RPM's above 2500, or low J's. Therefore these plots are not illustrative of the relative merits of the various shank forms which is not within the scope of the current study. The reader is referred to Reid's⁽⁷⁾ paper for detailed overall performance aspects of model propellers with similar shank geometry.

A cursory example of the cascade losses, or blade-to-blade interference effects, can be ascertained by plotting the coefficients for the array of 2,3,4,6 and 8 blades with respect to the individual contribution of each blade, such as C_T/B as shown in Figure 40. Secondary effects are revealed since the thrust per blade increases with the number of blades. The spinner/shank interference effect cannot, however, be discerned in this manner since an account of the primary shank contribution is still required.

A. Interference Values

The experimental data for Phase I was reduced to interference values using the method of the present study as discussed in Chapter III. Subtraction of the drag of the cylinders from those indirectly measured in the sense that the thrust and torque components of drag were actually measured, but can be resolved in terms of drag. Segments of Chapter III are repeated here for convenience.

1. Cylindrical Shanks

Initially, the equivalent drag of the cylinder was estimated using the C_D values of Hoerner for cylinders of finite aspect ratio as did Reid and Borst. The drag coefficient based on frontal area for a cylinder with a length of three inches and diameter of 0.819 inches was found to be 0.840. For torque considerations, an estimate of the radial load distribution is required to accurately model the point of application radially, or moment arm, \bar{x} , of the C_D . An elliptical distribution shown in Figure 41 was thus chosen, which provides the same integrated C_D as an equivalent two-dimensional length of cylinder. This equivalent two-dimensional length was calculated by equating the SC_D of the tested shanks to the SC_D of a two-dimensional cylinder where $C_D = 1.17$ and S is taken as diameter times length. Assuming the same diameters, the two-dimensional length is given by:

$$b_{2D} = \frac{(0.84) (3) (0.819)}{(1.17) (0.819)} = 2.154 \text{ inches} \quad (V-1)$$

The major axis of the desired ellipse is known and the minor axis, which corresponds to the sectional (C_D) at the base, is found from:

$$\text{Area} = SC_D = \frac{\pi (\text{length})}{4} C_{d_{\text{base}}} \quad (V-2)$$

Therefore, $C_{D_{\text{base}}}$ is given as 1.069 as compared to a two-dimensional C_D of 1.17 which reflects the extent of the tip effects being about 90 percent of the two-dimensional drag coefficient. The final form

of the ellipse is thus defined. The radial centroid can be calculated by:

$$\bar{x} = \frac{4 \text{ (length)}}{3\pi} = 0.424 \quad (\text{V-3})$$

resulting in a resolved moment arm, \bar{x} , of 3.548 inches. The drag and moment arm can now be subtracted from the measured quantities as determined by Equation III-41 and recalculated based on thickness area, t^2 , to provide interference values.

At zero RPM, this method of reduction can be directly compared with Sarsfeld's and Borst's results which is given in Figure 42. If it is assumed that no blade-to-blade interferences exist for the non-rotating, two and three blade runs resulting in purely spinner/shank interference, it can be concluded that the interference agrees well with the extrapolation of Sarsfeld (Figure 42). It would be interesting to more accurately resolve the effects upon the wake pressure drag for high thickness ratio struts in conjunction with a wall to span the gap of Hoerner's data between thicknesses of 0.5 and 1.0. It is difficult to ascertain whether the wall presence can further impair the shed wake, thereby increasing C_{Di} , or improve the wake and reduce C_{Di} . The three blade run indicates the former, whereas the two blade run suggest the latter. In either case, Sarsfeld's interference C_D is acceptably verified. Interference data above this value for higher number of blades can be attributed to blade-to-blade effects and follow the results of Hoerner as provided in Figure 6. The magnitude of these

interference C_D 's can be compared to the shank C_D of 0.840, or C_{Dt} of 3.077.

Interference CD 's for the case of spinner rotation consistently exceeded the spinner/shank only interference over the range of RPM's examined (Figure 43). This result indicates that the interference drag at the spinner drag interface is increasing with local velocity, or additional blade-to-blade interferences are increasing, or both. Closer inspection of Figure 43 discloses that the occurrence is developing at nominally the same rate, irrespective of the number of blades. This behavior is particularly difficult to relate to the interference phenomena based on the reasoning that: (1) blade-to-blade interference should develop slower, or at higher RPM, for lesser number of blades, and (2) spinner/shank interference should not exhibit the "hump" pattern unless Reynold's number effects are playing an important role. Without supportive Reynold's data, it is suggested that the mathematical form of the data reduction (Equations III-16,17) is predominating in this form of presentation and will be clarified in thrust and power expressions. It is noted that, the CD peak is found in the vicinity of maximum efficiency of Reid's baseline propeller.

Applying the interference drag values to PROPPERF predictions of Reid's four blade configuration for the currently tested conditions yields the corrected efficiency curves as shown in Figure 44. The benefits of suppressing interference drag is thus apparent. The difference in efficiencies are pessimistic at this stage since the 35% inboard section of a propeller blade does not constitute a

circular cylinder. An appraisal of transitioning shanks and airfoil cuffs must therefore be made.

2. Airfoils/Tapered Shanks

The absolute interference values for the shanks tested in Phase II and III could not be accurately deduced without an adequate tip correction. The raw data is compared to integrated shank contributions predicted by PROPPERF without end effects in Figure 45. At the low values of advance ratio, where the shank is operating at a lower angle of attack, the difference in the measured and predicted values may be indicative of interferences. At higher advance ratios, the blade sections are operating at increasingly negative lift coefficients through stall and thus increasing the extent of tip losses. An account of the tip relief as a function of J must be applied in order to reduce the predicted values to satisfactory norms. The experimental results of Phases II and III are therefore inconclusive with respect to interferences at this stage.

The effects of spinner/shank interference drag on Reid's model propeller efficiency can however be evaluated as an application of the experimental data and theoretical method. Assuming that the propeller blade which transitions into a round shank possesses the same spinner/shank interference as determined in Phase I, the C_D defined by Figure 42 can be applied to PROPPERF runs of the modeled propeller. The corrected efficiency is shown in comparison to that with interference neglected in Figure 46. Similarly, a conservative estimate of the spinner/shank interference C_D can be assumed for the

airfoil shank for Hoerner's data and applied to PROPPERF predictions for the modeled propeller with shank cuffs. This was done for the three blade pitch angles tested and shown in Figure 47. A comparison of Figure 46 and 47 reveals the benefits of the faired shanks over round shanks in higher efficiencies and smaller interference corrections.

VI. SUMMARY/CONCLUSIONS

In the review of previous work it was found that although much commercial attention has been given to applied research of propeller spinner/shank junctions in the attempt of enhancing overall performance, there has been a lack of fundamental understanding into the problem. In this sense, the current research program has proved successful in several ways.

A theoretical treatment has been outlined primarily as an extension of Borst's approach with refinement to the otherwise arbitrary Δx variable in the pertinent expressions based on Hoerner's dimensionalizations. Borst's thrust and torque corrections due to the interference drag of cylindrical shanks has also been re-derived for the general case of a streamline, lift-producing shank. Because of the semi-empirical form of the solution along with discrepancies disclosed between Borst's and Sarsfeld's interference CD values, a supportive experimental program was conducted.

The baseline segment of the experiment using cylindrical shanks similar to Reid verified Sarsfeld's extrapolated interference drag value. The major reason for the discrepancy in Borst's value being too low was given as failure to meet the $h \gg \delta$ condition. Thus the interference effect was not fully developed and the primary contribution of the shank stub not accurately resolved. This result was circumvented in the present study by use of longer shanks. The significance of Borst's work should not be understated since this constitutes the first and most direct solution and provided the groundwork for the present study.

From this point, the concurrent experimental matrix was expanded to include two mutual interferences, i.e., spinner/shank and cascade effects as functions of the associated engineering parameters including spinner length, number of blades, blade planform, and advance ratio. It was revealed that spinners of the two finess ratios tested caused unmeasureable effects on the resulting data. However, a 35% increase in interference CD occurred in going from two cylindrical shanks to eight and further increased with advance ratio to as much as 46% of the shank contribution due to surmounting blade-to-blade interferences. Experiments of cylinders meeting flat plates has been suggested to further validate these findings.

Unfortunately, the blade-to-blade interfaces of the tapered and airfoil shank phases of the experiment could not be discerned because of difficulties in defining the primary shank contribution with end effects. However, argument is made for the validity of the spinner/shank interference values which are subtracted from the predicted efficiency envelope of the baseline blade as a final application of the methodology. It is thereby revealed that although the interference drag coefficients are small segments of the overall blade lift and drag components, significant reductions of 3% percent in propeller efficiency can result. These values can be reduced to 1.5% percent conservatively by properly fairing bluff shanks. Although these benefits can be directly measured experimentally, emphasis is placed upon the inclusion of the interference corrections into prediction schemes for purposes of rigorous analytical methodologies. While it is not proposed that

ultimate agreement between experiment and theory will be completely achieved since other sources of error such as radial flow are inherent, spinner/shank interference effects can be accounted for in an accurate manner using the results of the present study.

REFERENCES

1. Bass, R.M., "An Historical Review of Propeller Developments," The Aeronautical Journal of the Royal Aeronautical Society, Paper No.1089, August 1983.
2. Biermann, D. and Hartman, E., "Tests of Five Full-Scaled Propellers in the Presence of a Radial and Liquid-Cooled Engine Nacelle, Including Tests of Two Spinners," NACA Rept. No. 642, 1938.
3. Hartman, E.P., and Biermann, D., "The Aerodynamic Characteristics of Four Full-Scale Propellers Having Different Planforms," NACA Rept. No. 643, 1938.
4. McCoy, H.M., "A Discussion of Propeller Efficiency," J. Aero. Sci., Vol. 6, No. 6, April 1939, pp. 227-234.
5. Reid, E.G., "The Effects of Hub Drag, Solidity, Dual Rotation, and Number of Blades Upon the Efficiency of High-Pitch Propellers," NACA Wartime Rept., W-84, ACR, October 1941.
6. Hammack, J.B., "Investigation of Thrust Losses Due to Shanks of a Flared Two-Bladed Propeller on a Slender-Nose Airplane," NACA TN 1414, August 1947.
7. Reid, E.G., "Studies of Blade Shank Form and Pitch Distribution for Constant-Speed Propellers," NACA TN 947, 1945.
8. Barlow, W.H., "Flight Investigation at High Speeds of the Drag of Three Airfoils and Circular Cylinder Representing Full-Scale Propeller Shanks," NACA Rept. No. 852, June 1946.
9. Delano, J.B., and Carmel, M.H., "Effect of Shank Design on Propeller Performance at High Speeds," NACA ARR L6D23, June 1946.
10. Delano, J.B., "Investigation of Two-Blade Propellers at High Forward Speeds in the NACA 8-Foot High-Speed Tunnel," NACA ACR No. L5F15, 1945.
11. Maynard, J.D., "Aerodynamic Characteristics at High Speeds of Full Scale Propellers Having Different Shank Designs," NACA RM No.L6L27a, February 1947.

12. Prince, C.H., "The Effects of Three Types of Propeller Shanks on Pressure Recovery of a Conical-Spinner-Turbine Intake at Mach Numbers of 0.4 and 0.7," U.A.C. Rept. R-14018-2, United Aircraft Corp. Res. Dept., June 1948.
13. Keith, A.L., Bingham, G.J., and Rubin, A.J., "Effects of Propeller Shank Geometry and Propeller-Spinner-Juncture Configuration on Characteristics of an NACA 1-Series Cowling-Spinner Combination with an Eight-Blade Dual-Rotation Propeller," NACA RM L51F26, September 1951.
14. Bass, R.M., "Private Communication," 1985.
15. Korkan, K.D., Gregorek, G.M., and Mikkelsen, D.C., "A Theoretical and Experimental Investigation of Propeller Performance Methodologies," AIAA Paper No. 80-1240, June 1980.
16. Hoerner, S.F., Fluid Dynamic Drag, published by the Author, New Jersey, 1965, pp. 8-10.
17. Sarsfeld, L.P., "Private Communication," 1979.
18. Reid, J.V., "Advanced V/STOL Propeller Technology Cruise Performance Tests," Technical Report AFFDL -TR-71-88, Vol. III, September 1971.
19. Borst, H.V., "General Aviation Propeller Wind Tunnel Test Results," Report No. 3-5-80, H.V. Borst and Associates, Wayne, Pa., March 1980.
20. Borst, H.V., "Propeller Performance and Design as Influenced by Installation," SAE Tech. Paper Series No. 810602, April 1981.
21. Cooper, J.P., "The 'Linearized Inflow' Propeller Strip Analysis," WADC TR 56-615, March 1957.
22. Goldstein, S., "On the Vortex Theory of Screw Propellers," Proceeding of the Royal Aeronautical Society (London), Ser. A, Vol. 123, No. 792, April 6, 1929.
23. Goldstein, S., Modern Developments in Fluid Dynamics, Dover Publications, Inc., New York, 1966, p. 439.
24. Blevins, Robert D., Applied Fluid Dynamics Handbook, Van Nostrand Reinhold Co., New York, 1984, p. 308-312.

25. Edinger, R. Private Communication, Hartzell Propeller, Inc., Piqua, Ohio, 1984
26. Borst, H.V., Private Communication, Henry V. Borst and Associates, Wayne, Pennsylvania, 1985
27. Reid, J.V. "Advance V/STOL Propeller Technology -Cruise Performance Tests," Technical Report AFFDL -TR-71-88, Vol. I, II, and III.
28. Glauert, H., The Elements of Aerofoil and Airscrew Theory, The MacMillan Co., New York, 1943, pp. 222-226.
29. Rae Jr., W.H., and Pope, A., Low-Speed Wind Tunnel Testing, John Wiley and Sons, New York, 1984.

APPENDIX I

FIGURES

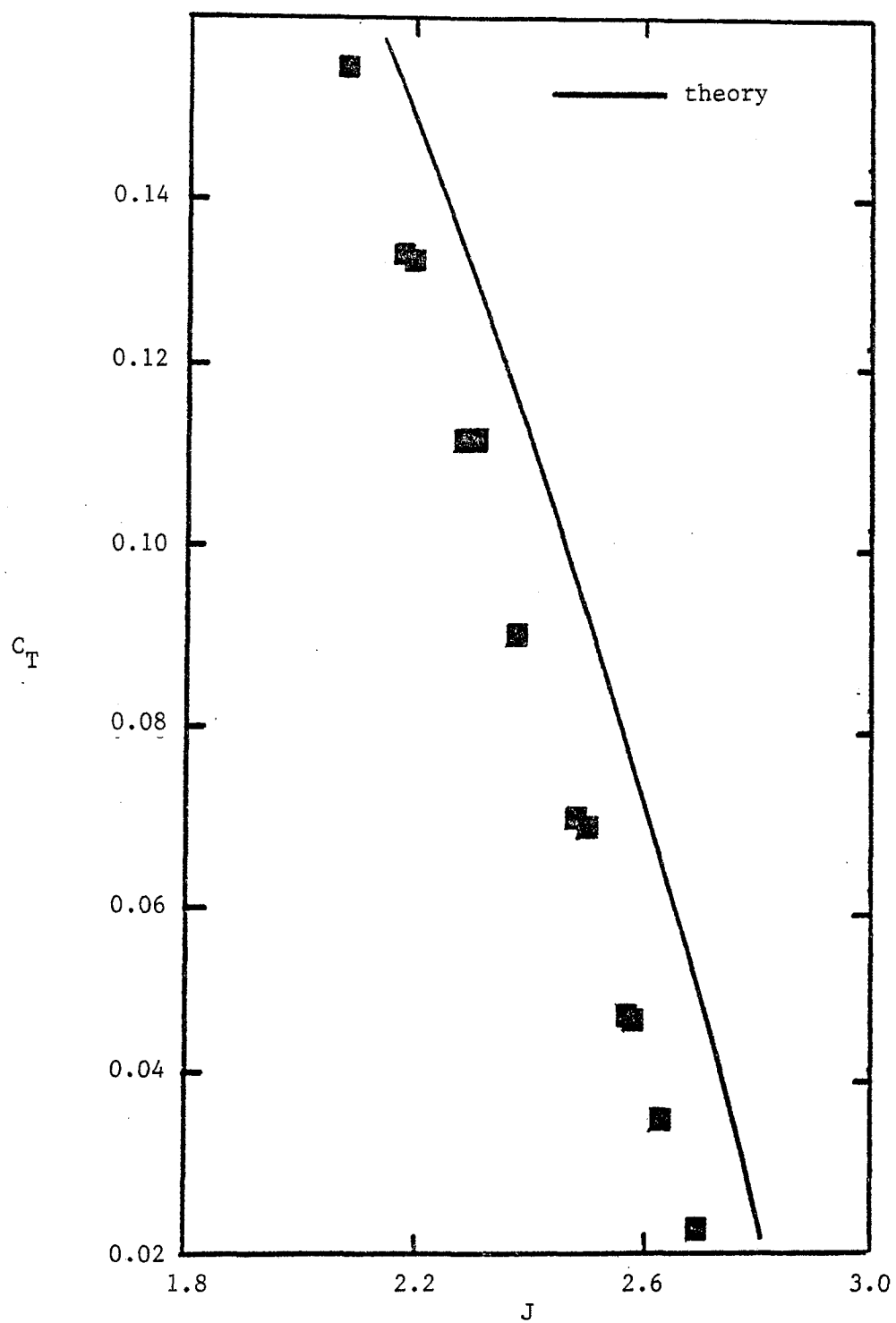


Figure 1. Comparison of theoretical prediction of thrust coefficient to experimental data (Clark Y-NACA16 Propeller, Cruise condition).

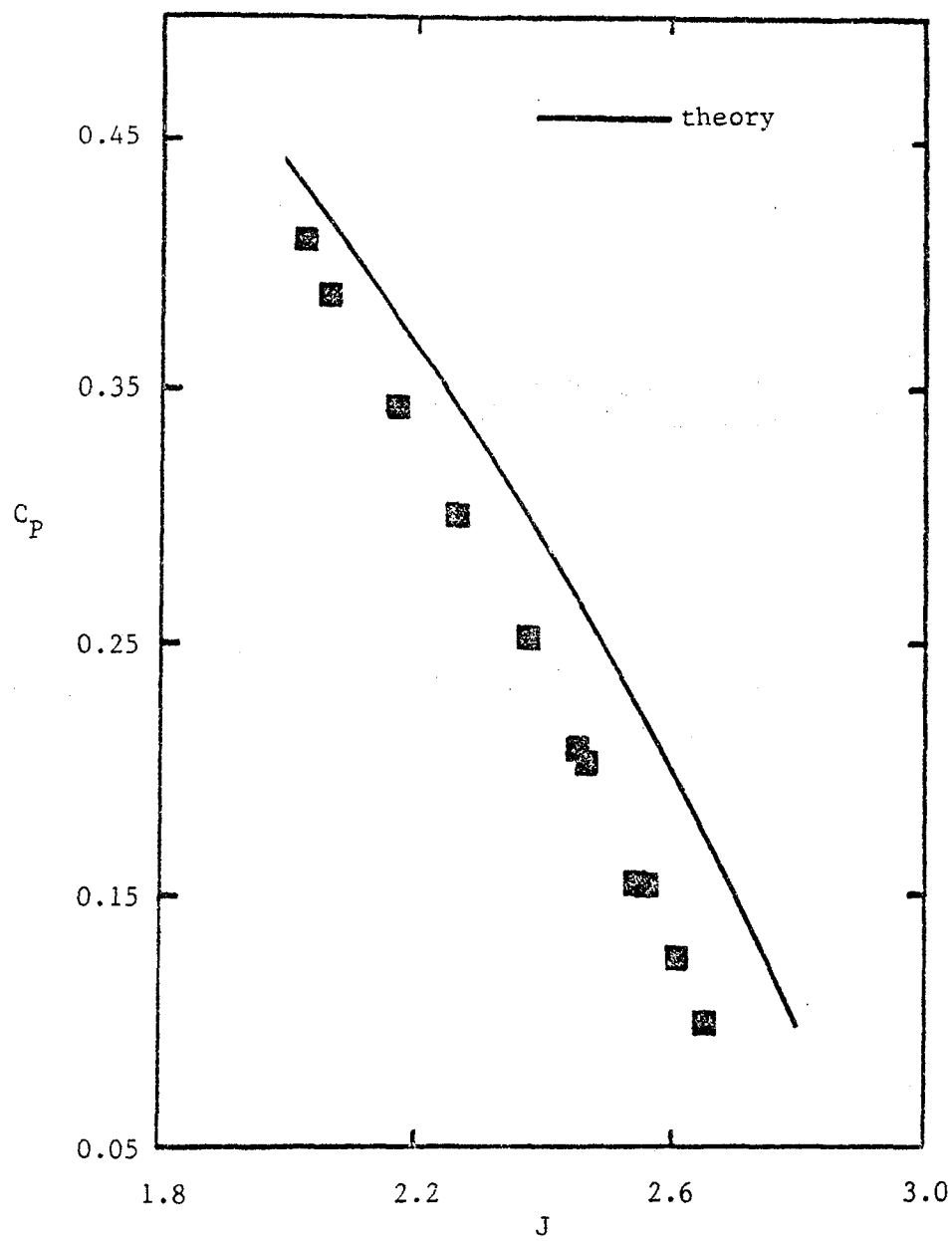


Figure 2. Comparison of theoretical prediction of power coefficient to experimental data (Clark Y-NACA16 Propeller, Cruise condition).

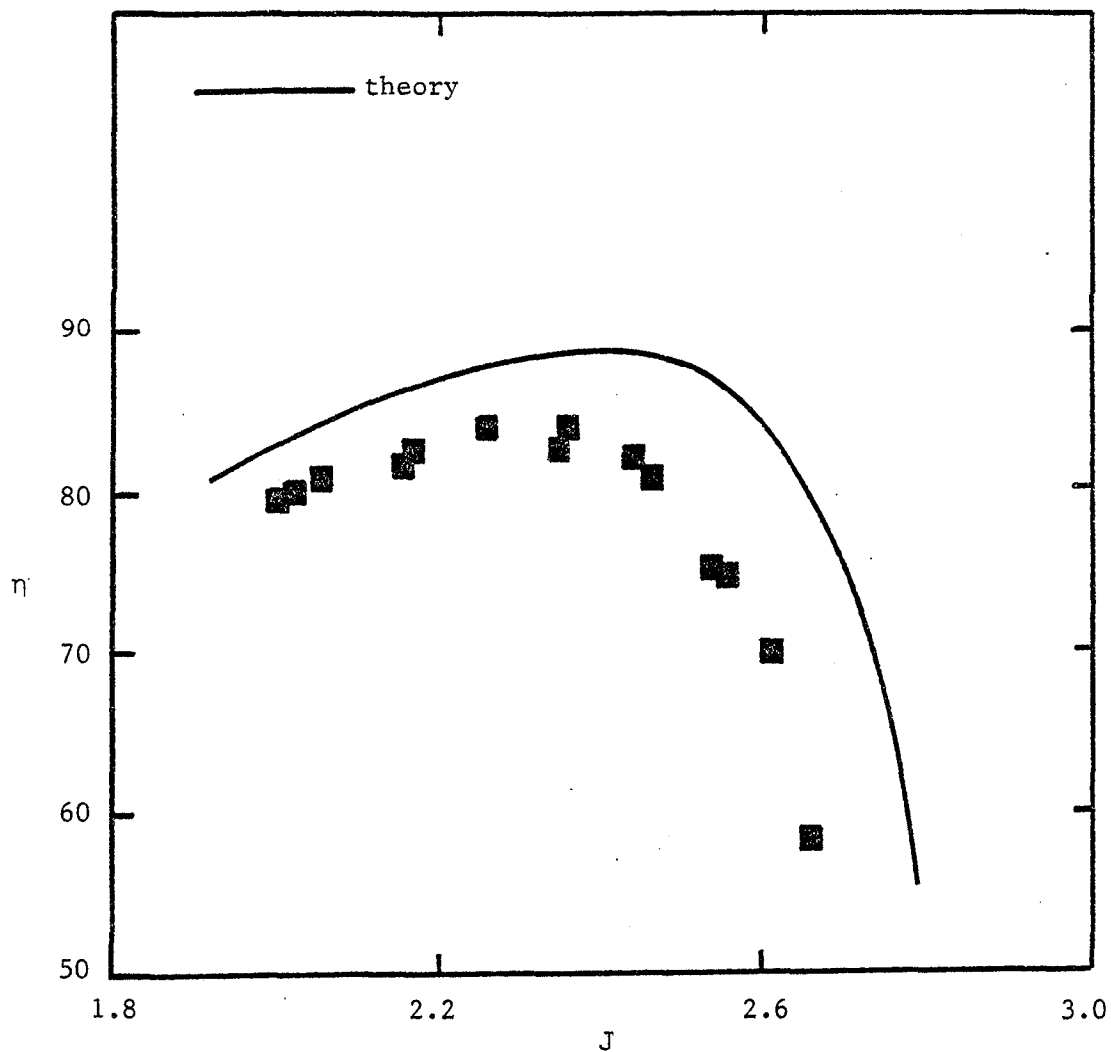


Figure 3. Comparison of theoretical prediction of efficiency to experimental data (Clark Y-NACA16 Propeller, Cruise condition).

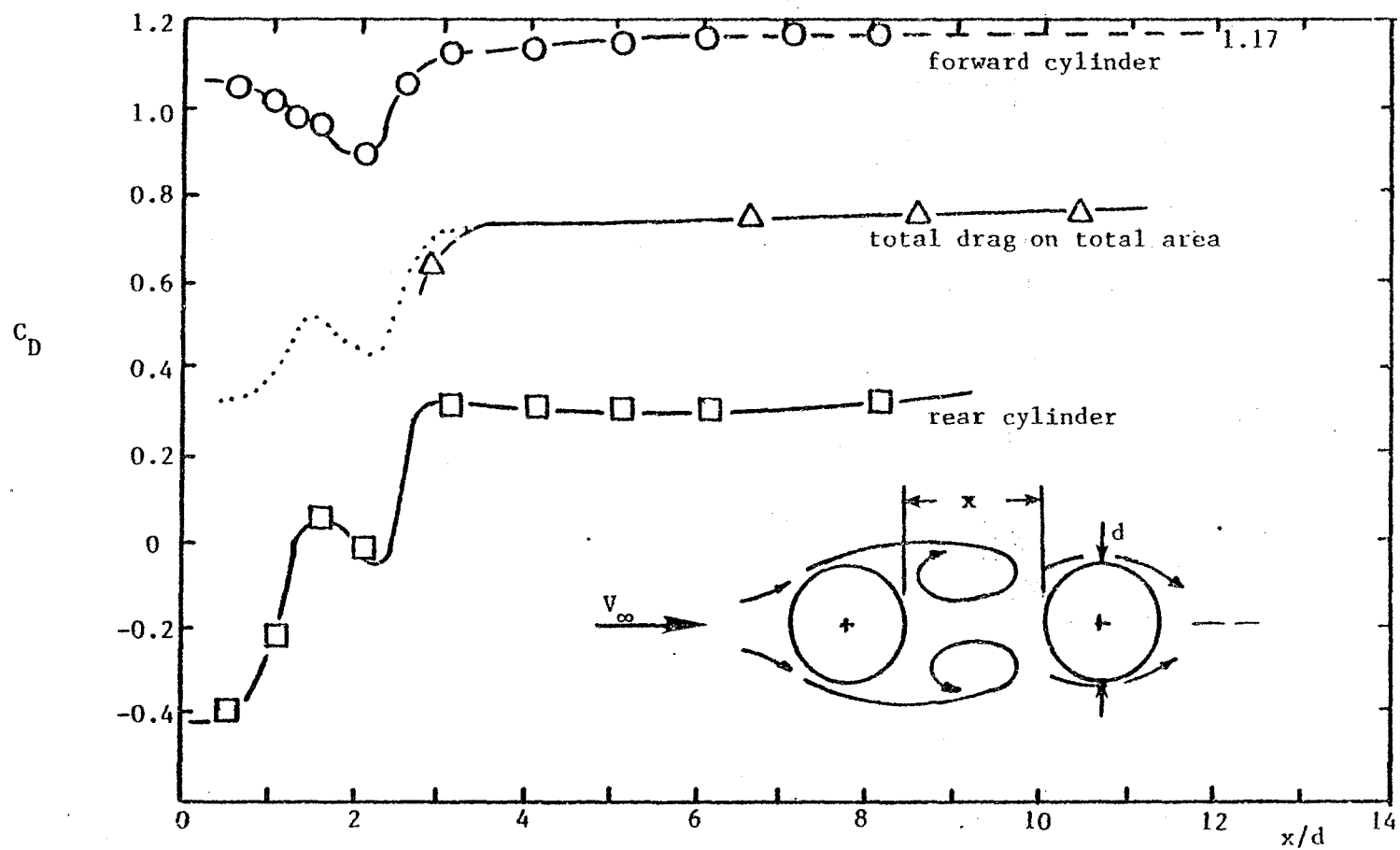


Figure 4. Drag characteristics of two circular cylinders placed in tandem.

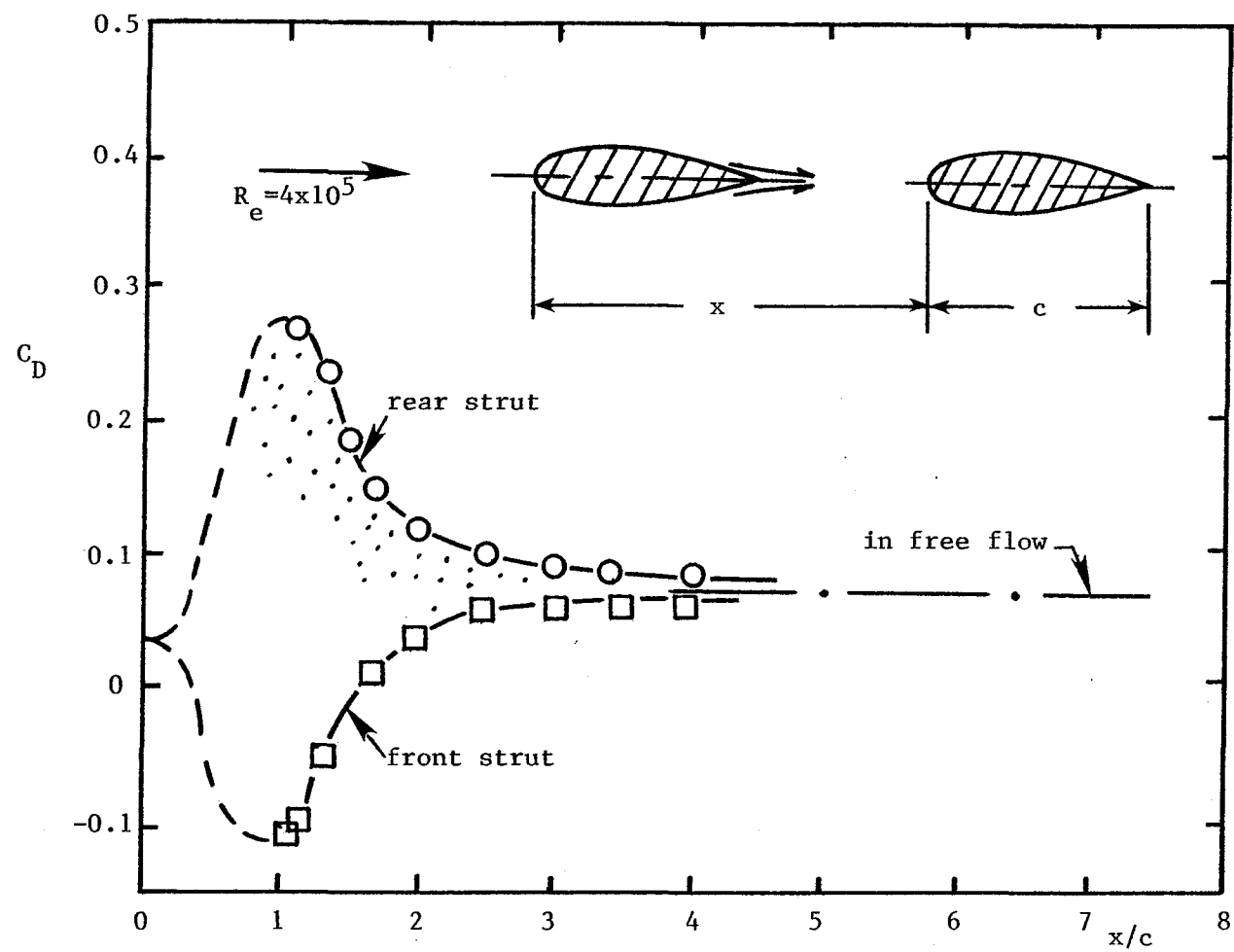


Figure 5. Drag characteristics of a pair of streamline struts in tandem.

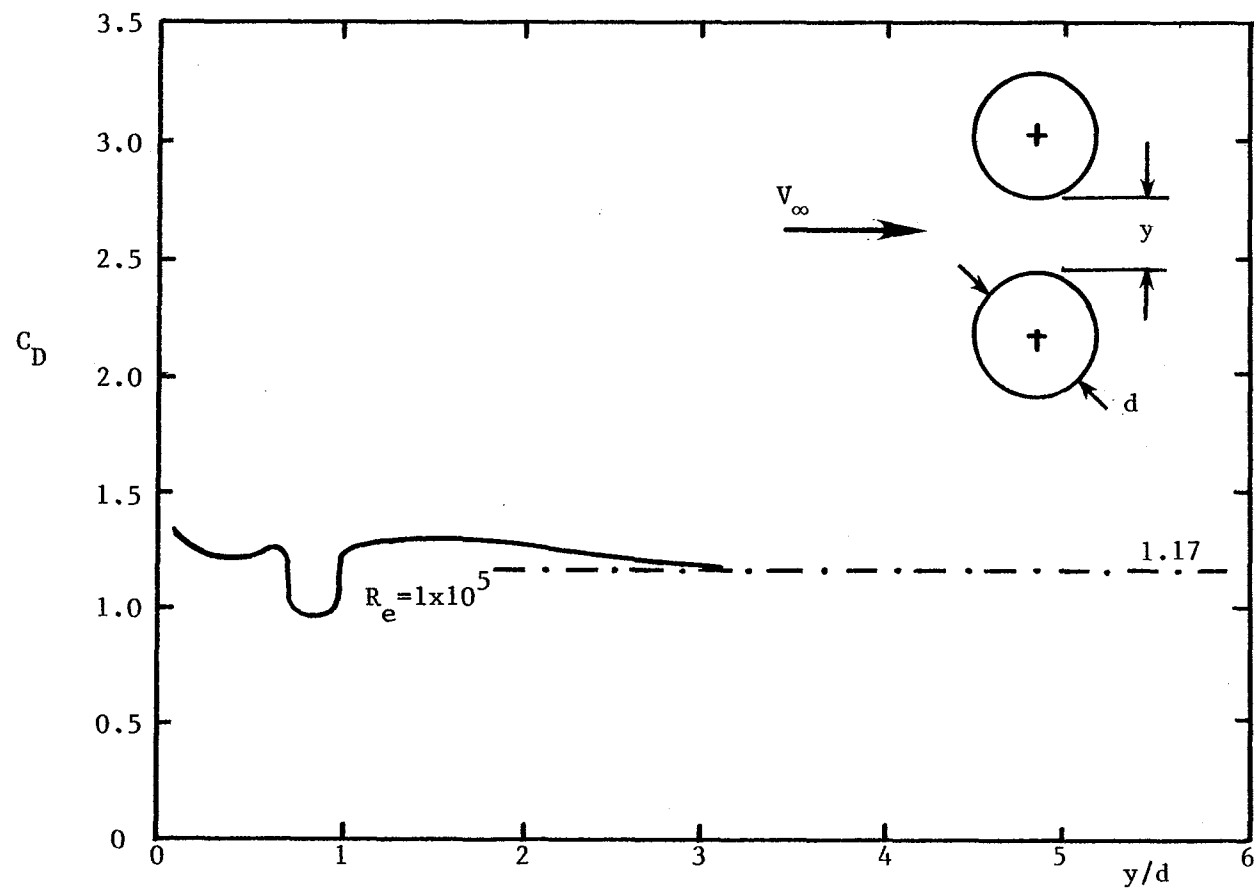


Figure 6. Drag characteristic of two circular cylinders placed side by side.

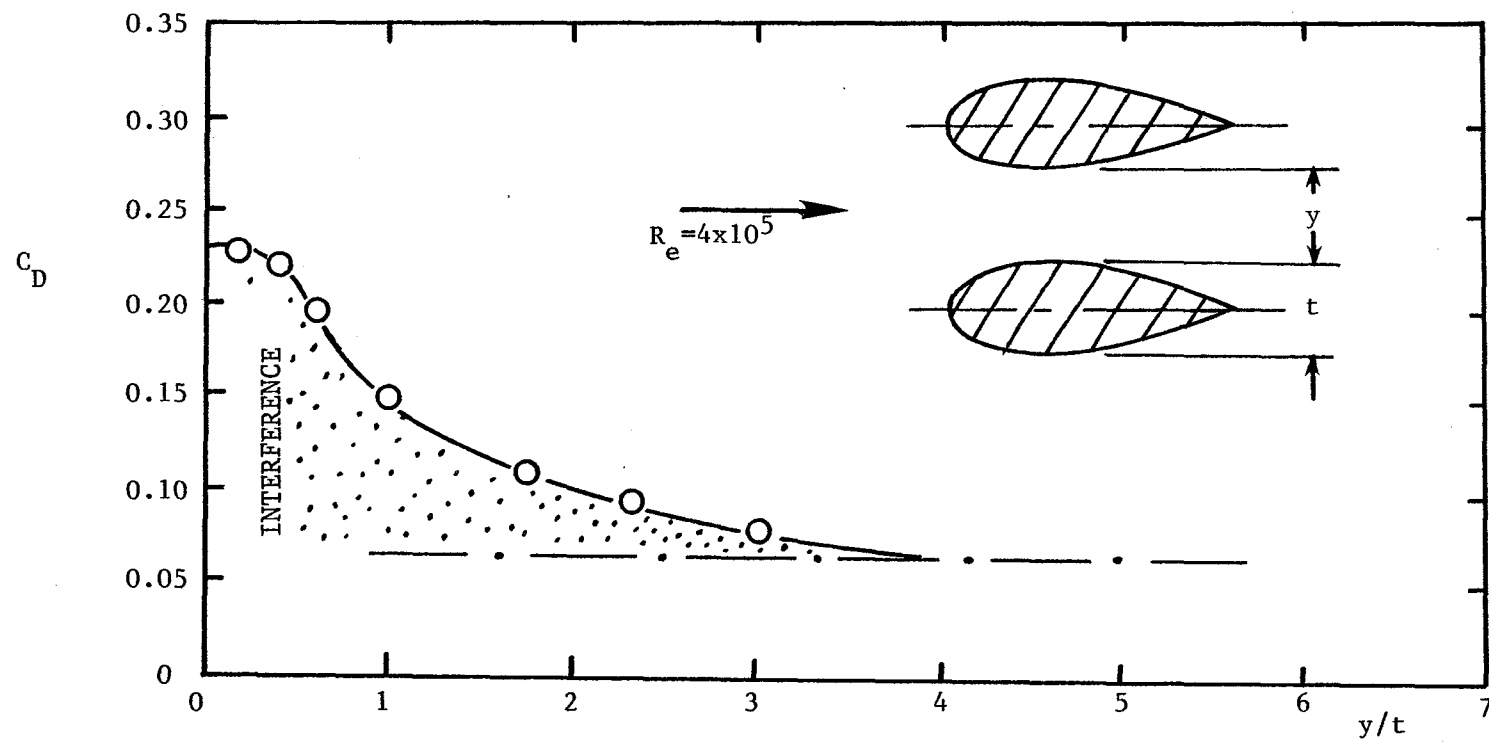


Figure 7. Drag characteristic of a pair of streamline sections placed side by side.

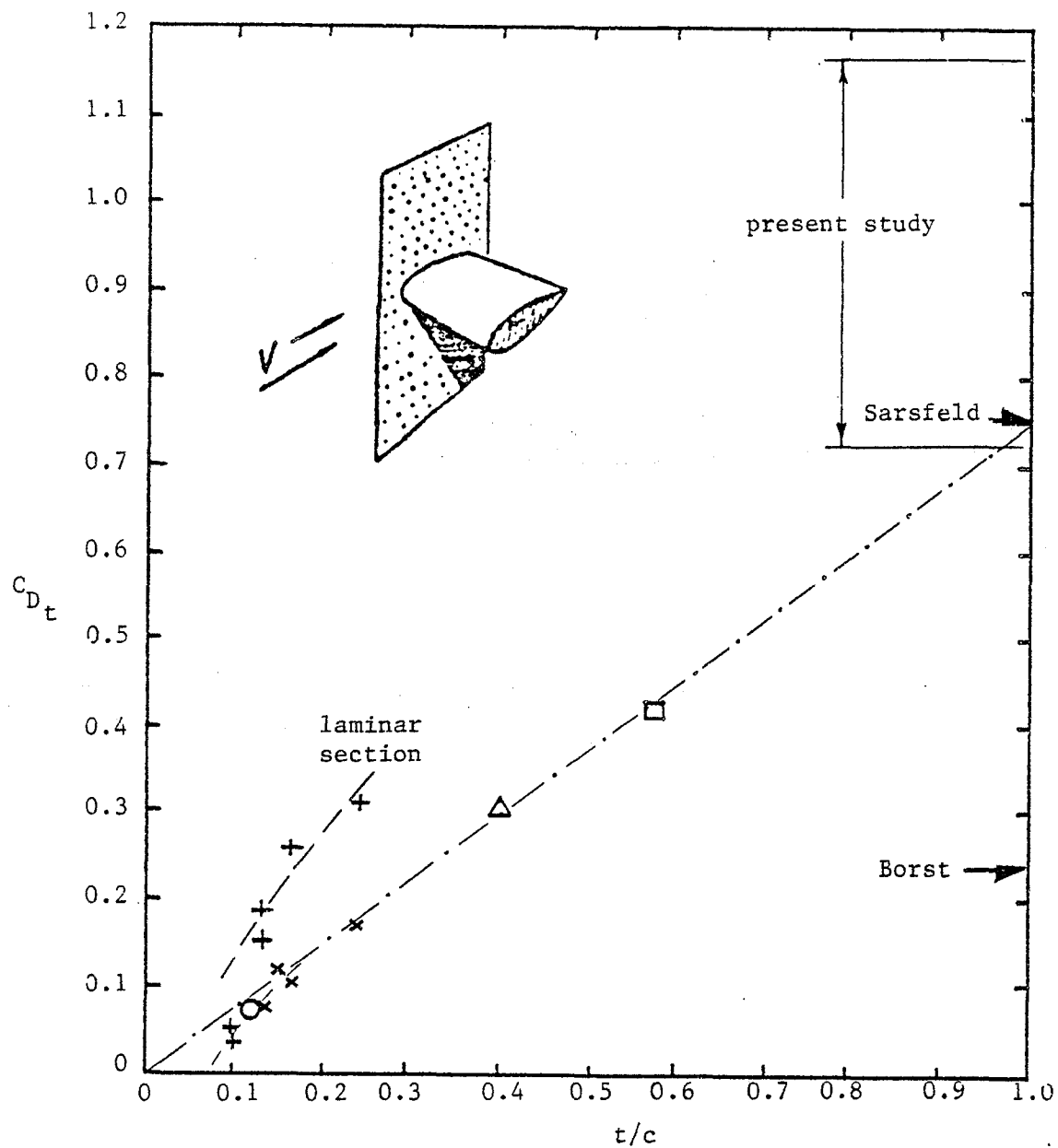


Figure 8. Interference drag originating at the junction of wings to a plane wall as a function of airfoil thickness ratio.

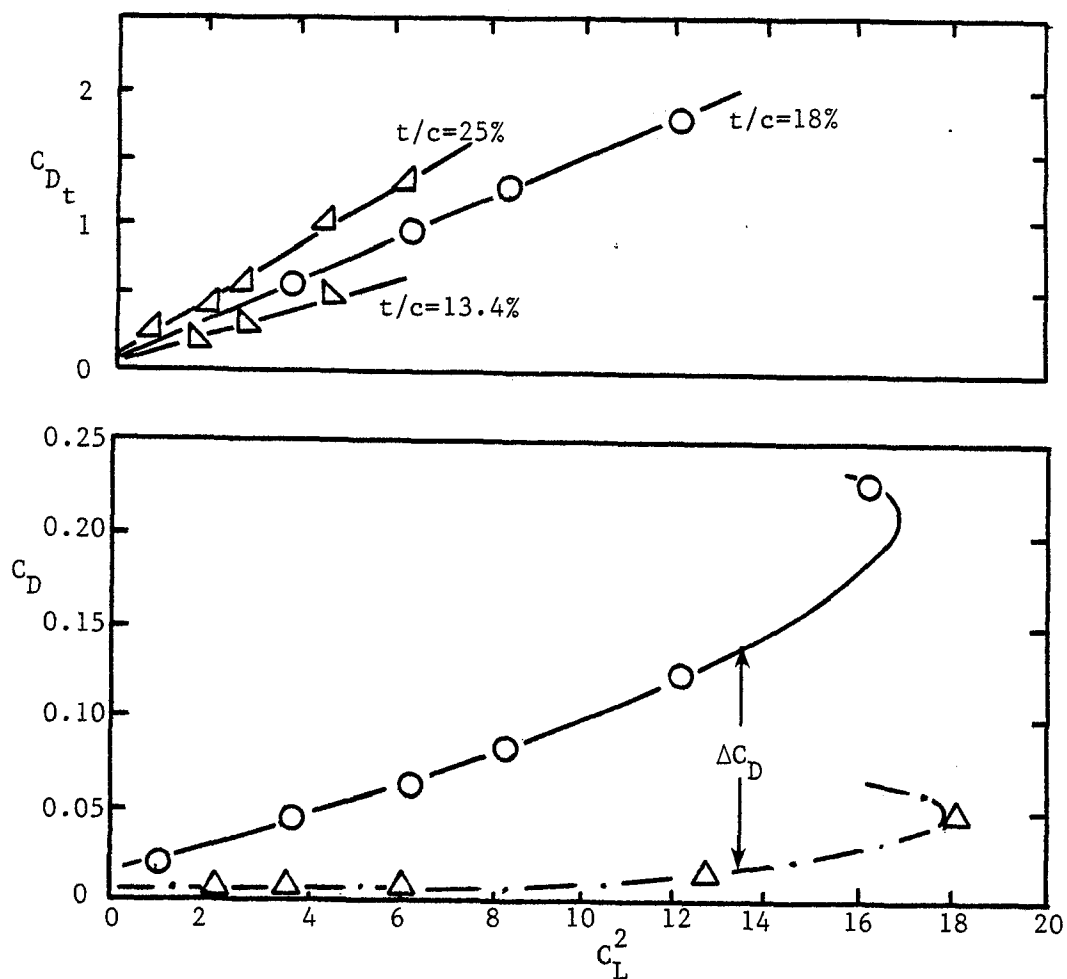


Figure 9. Interference drag at wall junctions of wings as a function of lift coefficient.

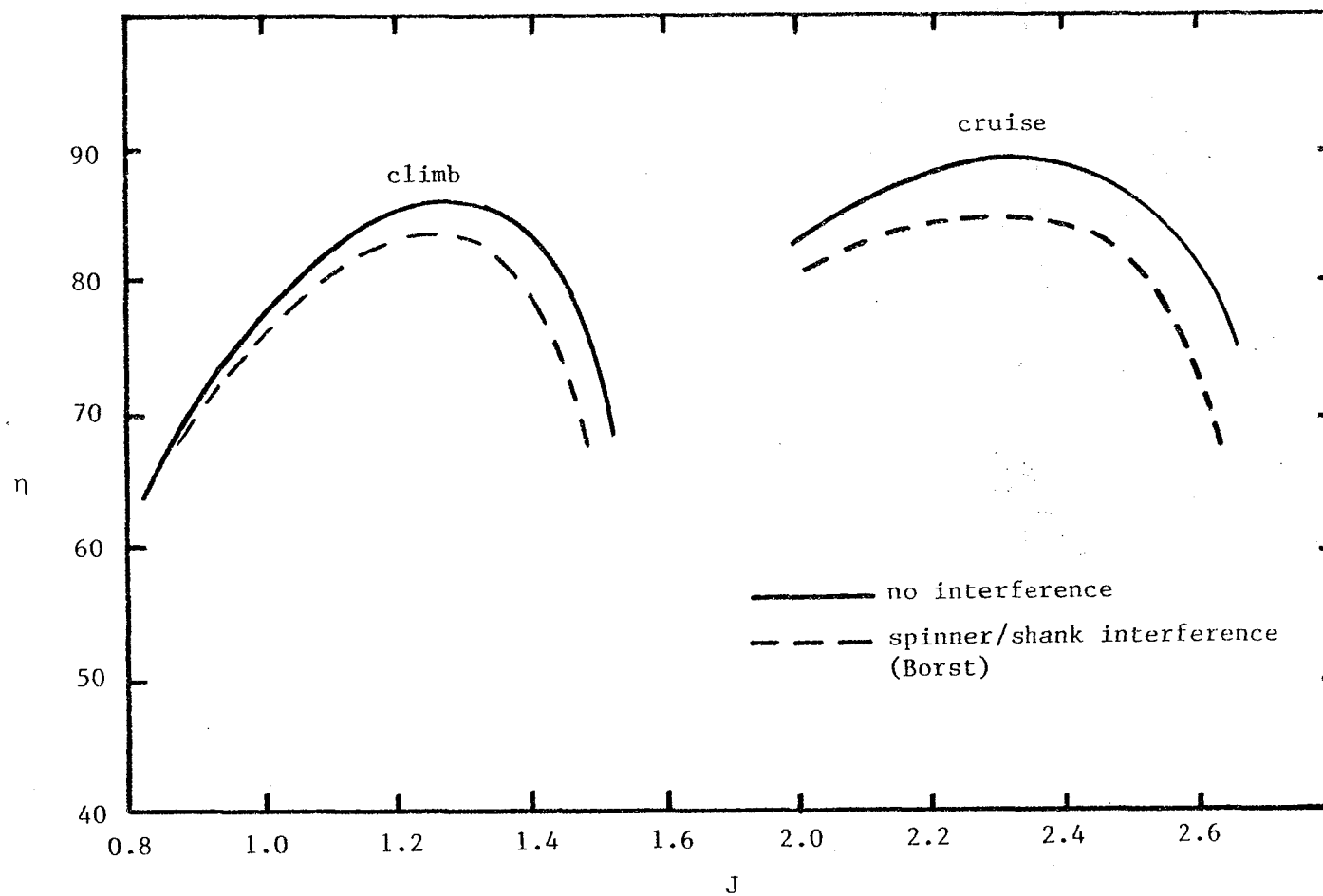


Figure 10. Interference drag loss effects on propeller performance at typical climb and cruise conditions.

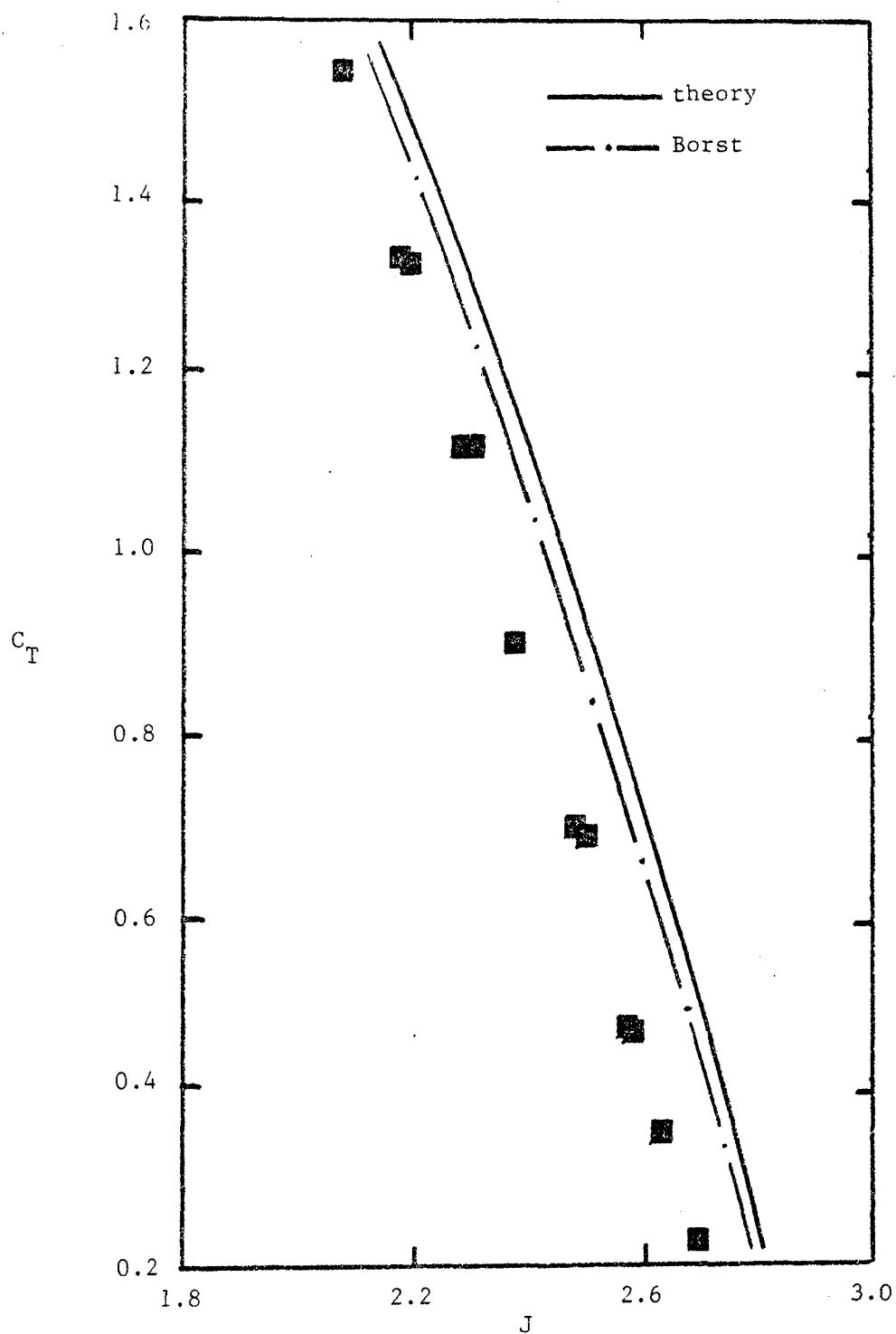


Figure 11. Thrust coefficient comparison between experimental data and theory, with Borst correction (Clark Y-NACA16 Propeller, Cruise condition).

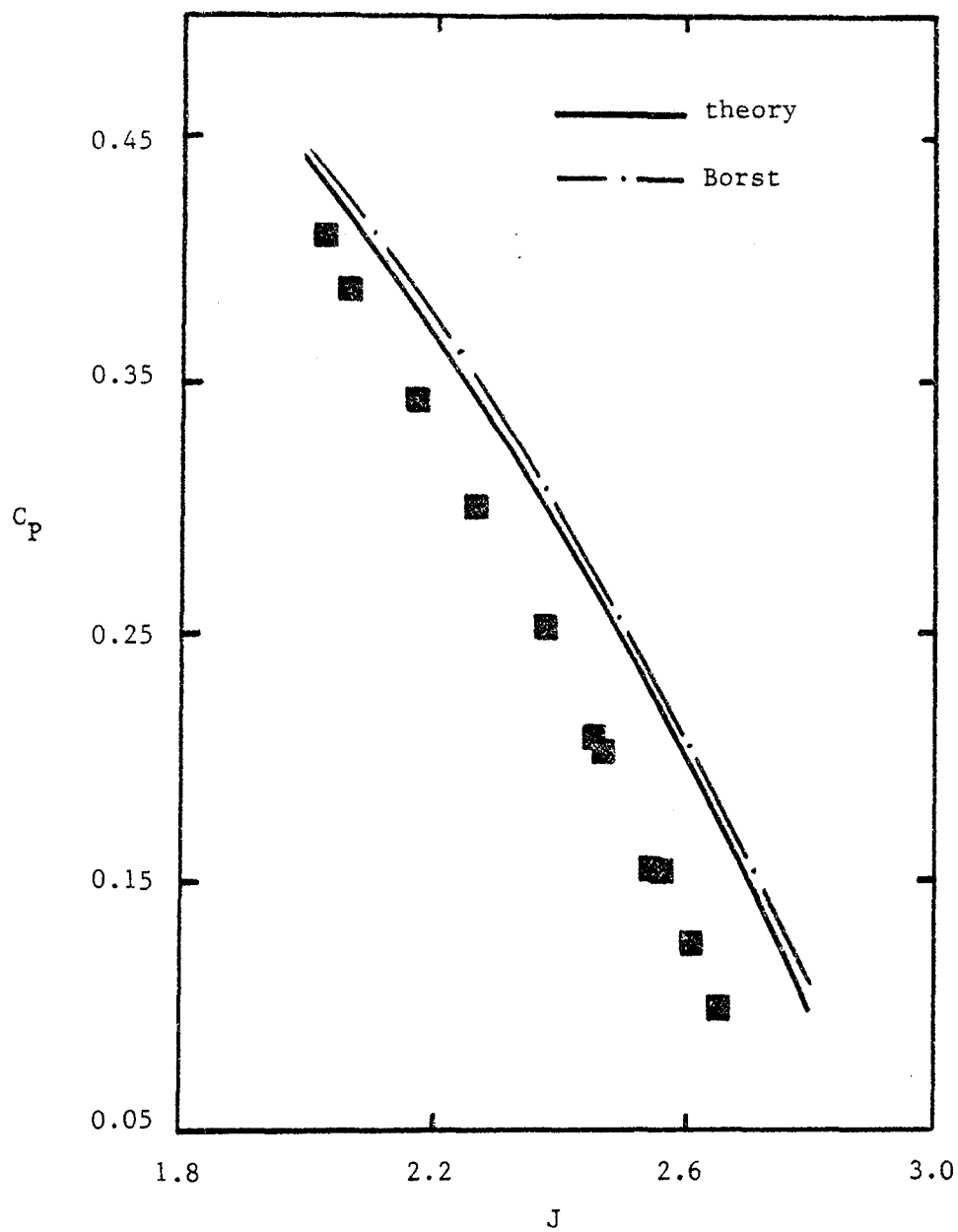


Figure 12. Power coefficient comparison between experimental data and theory, with Borst correction (Clark Y-NACA16 Propeller, Cruise condition).

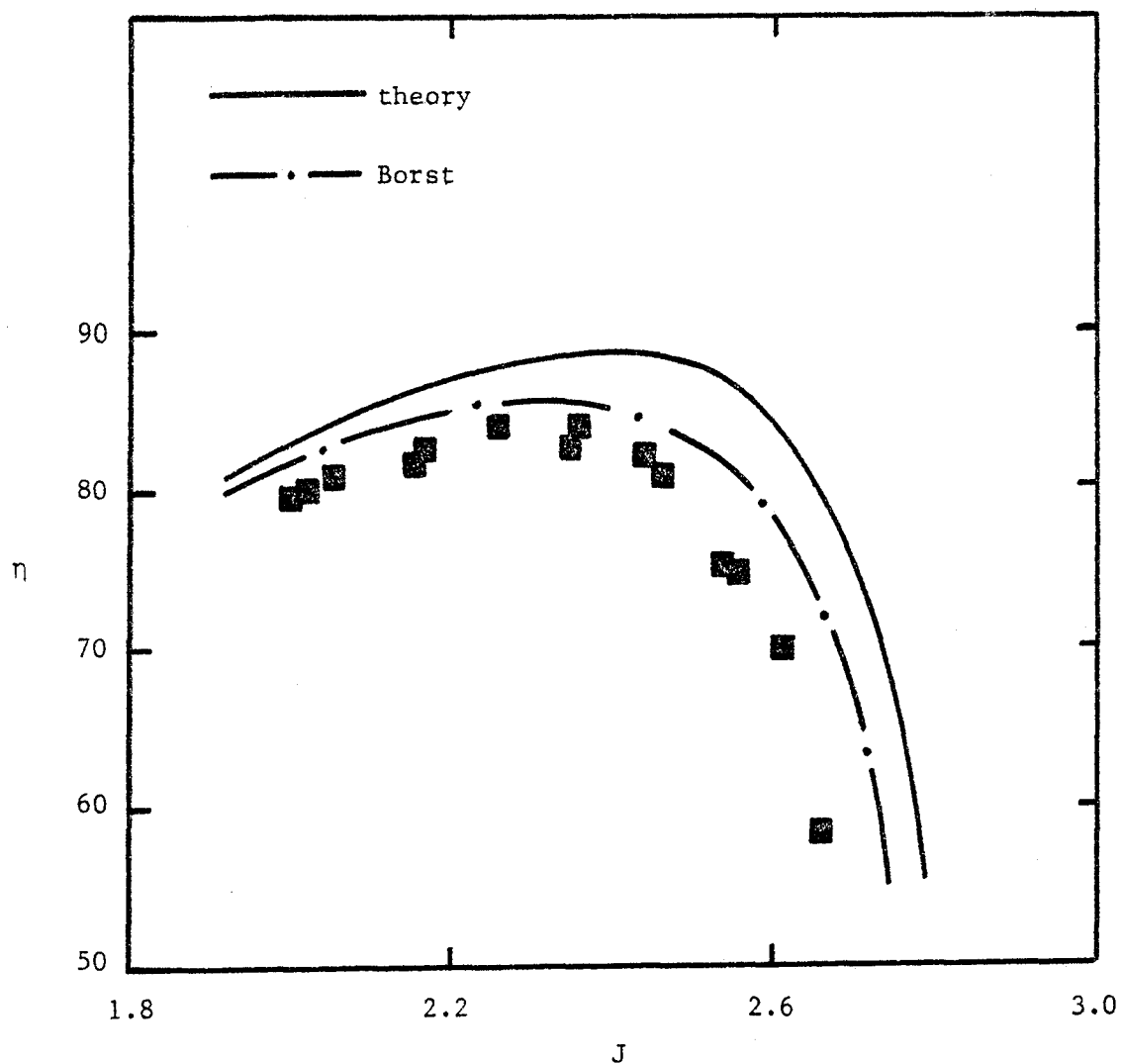


Figure 13. Efficiency comparison between experimental data and theory, with Borst correction (Clark Y-NACA16 Propeller, Cruise condition).

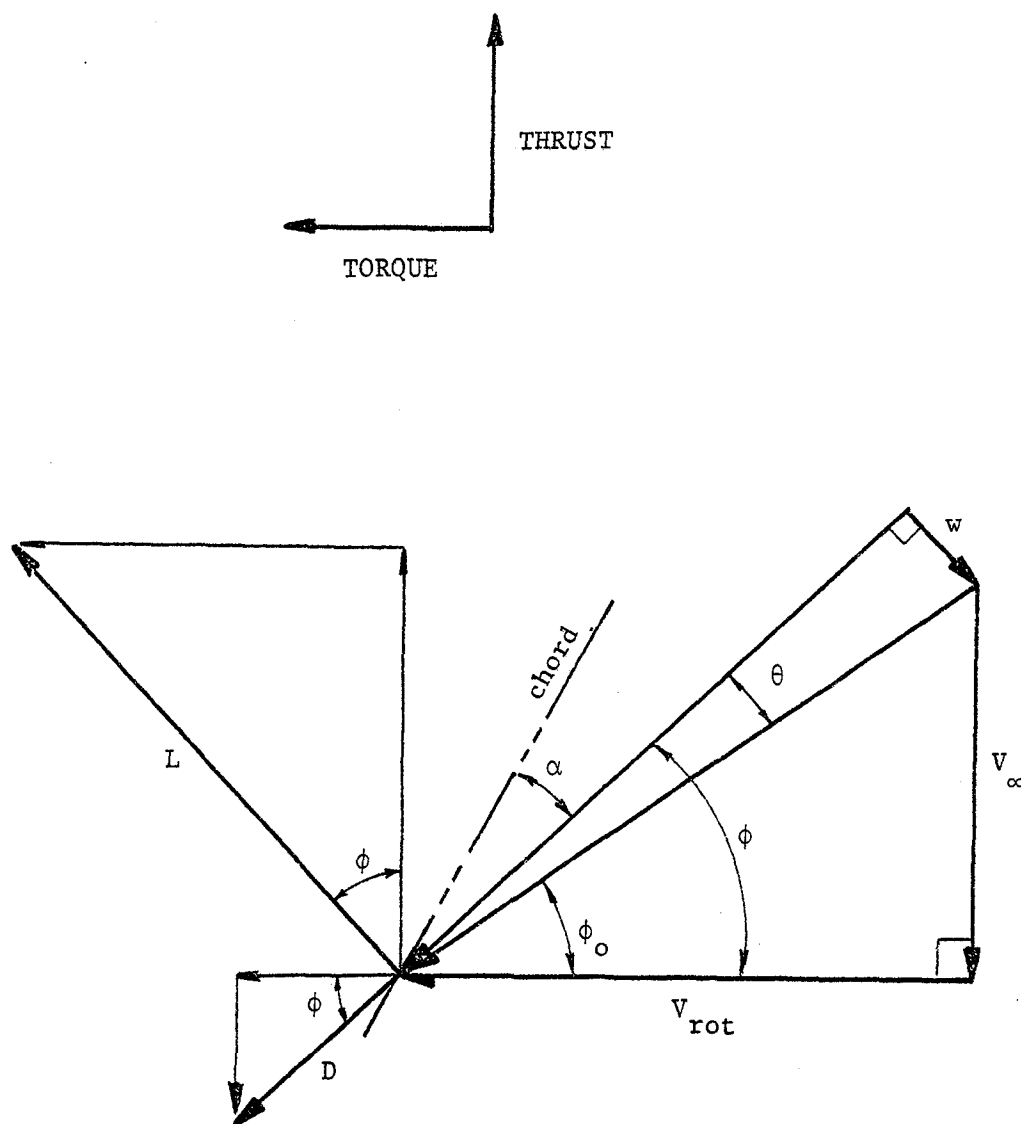


Figure 14. Velocity diagram of a differential blade element.

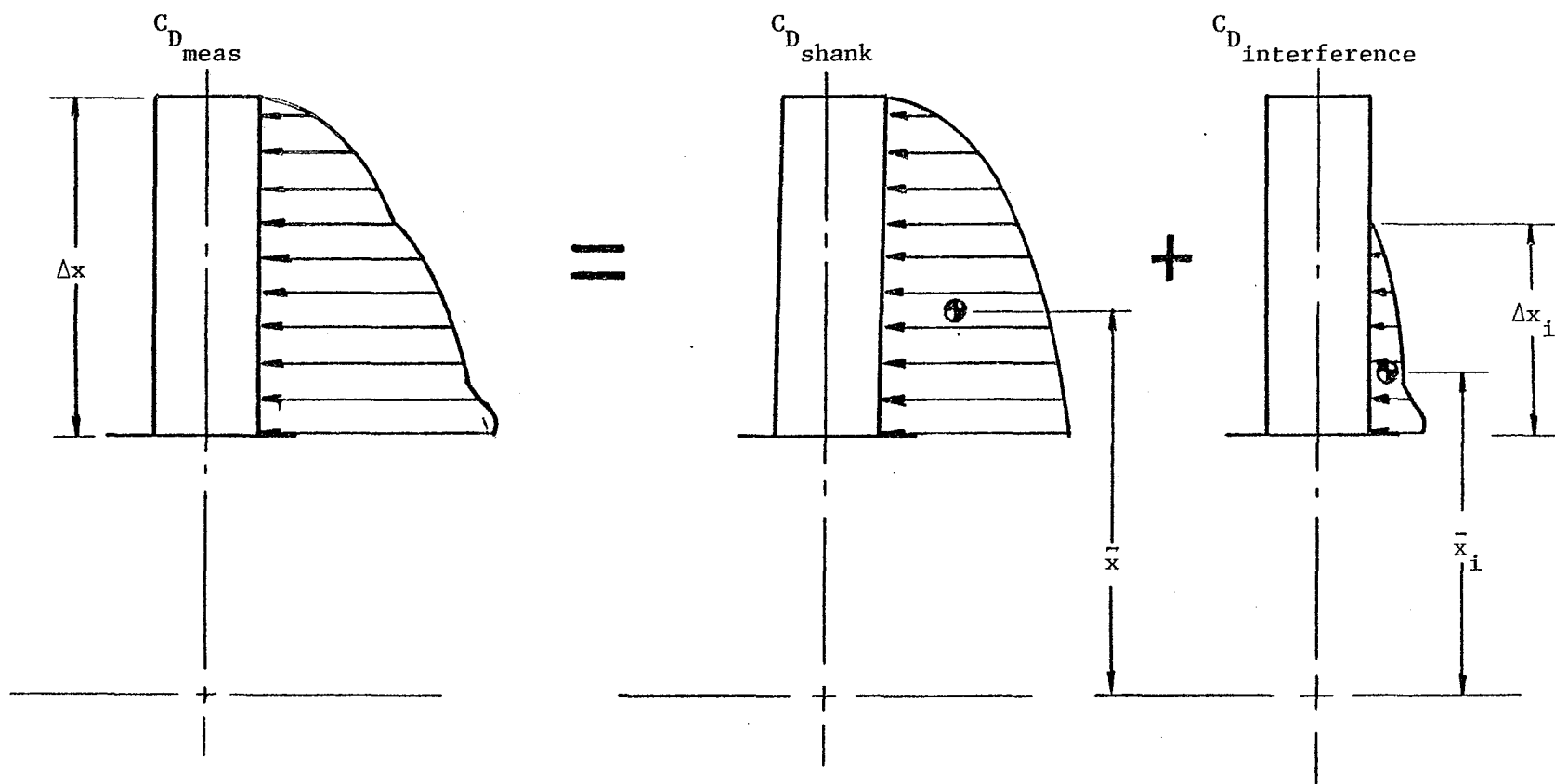


Figure 15. Components of load distributions on propeller.

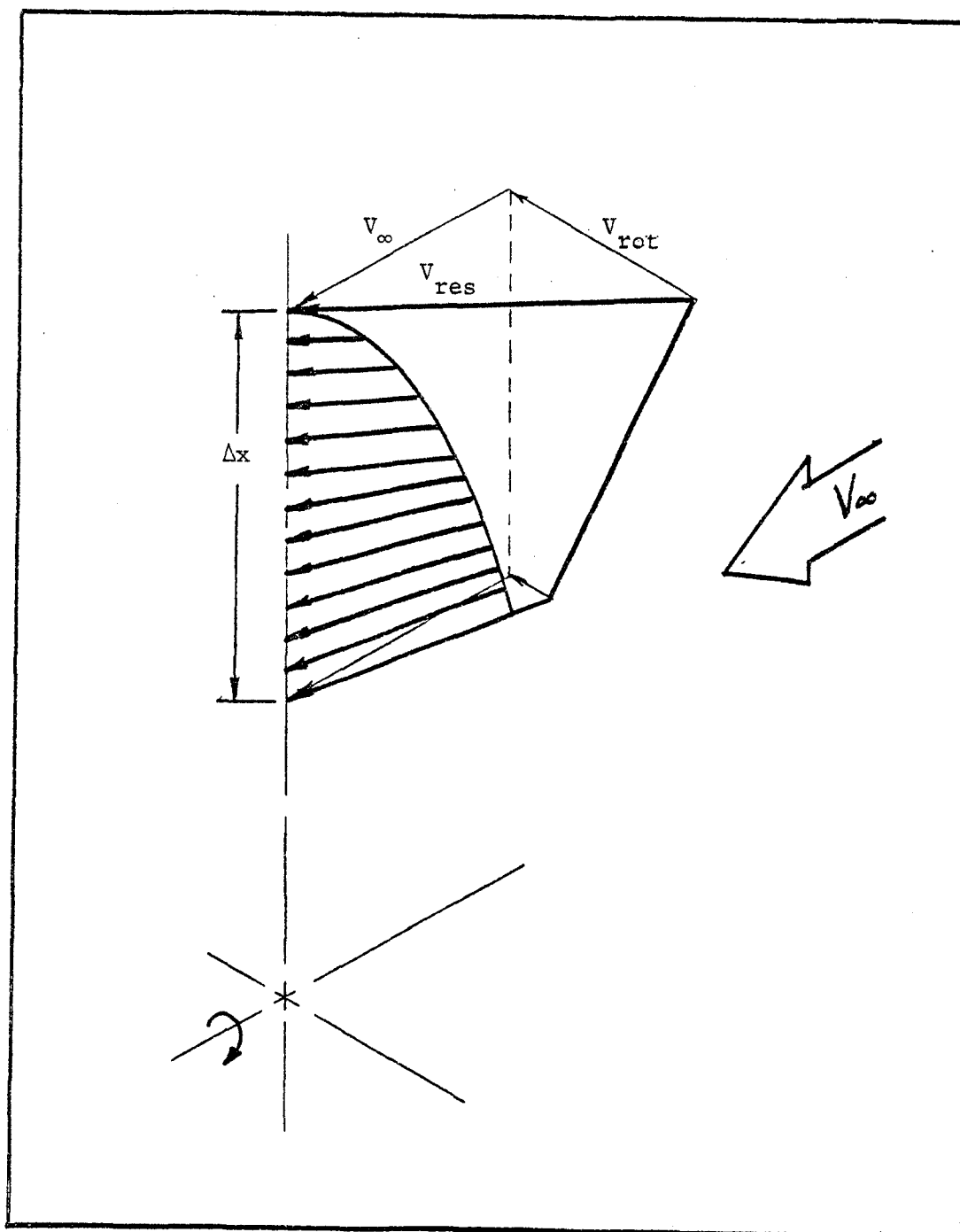


Figure 16. Three-dimensional sketch of cylindrical shank element showing radial variation of velocity and drag.

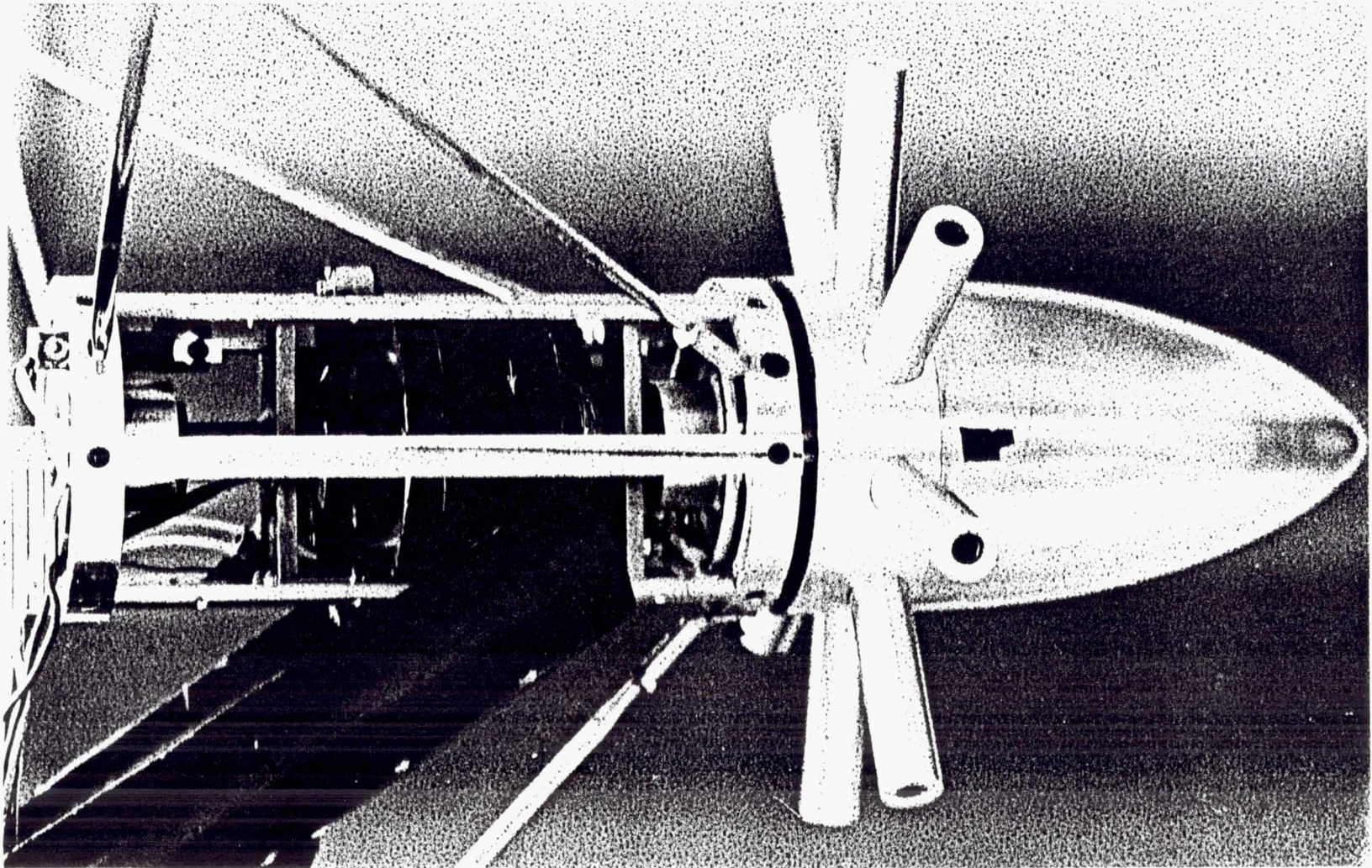


Figure 17. Photo of propeller test rig (PTR).

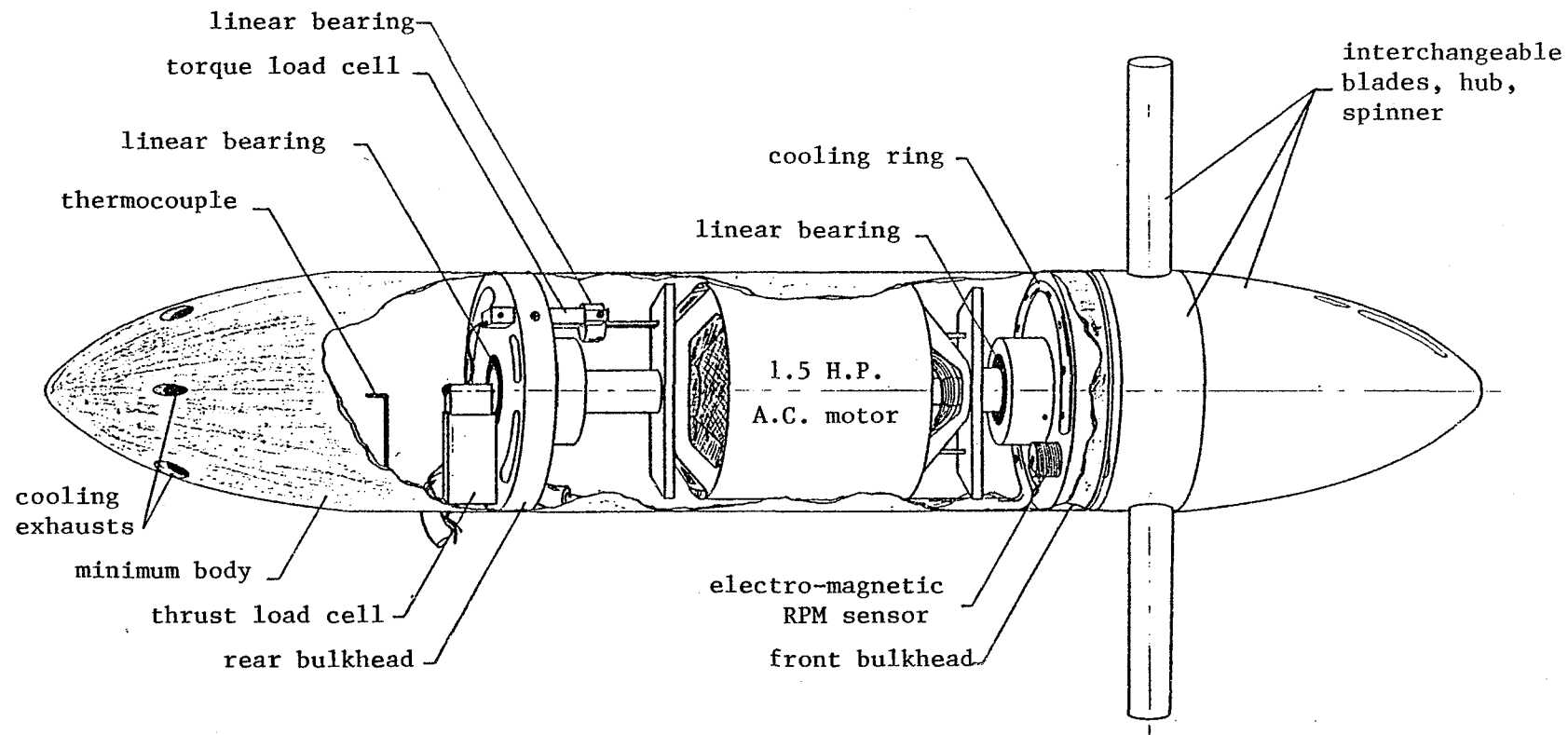


Figure 18. Components of PTR.

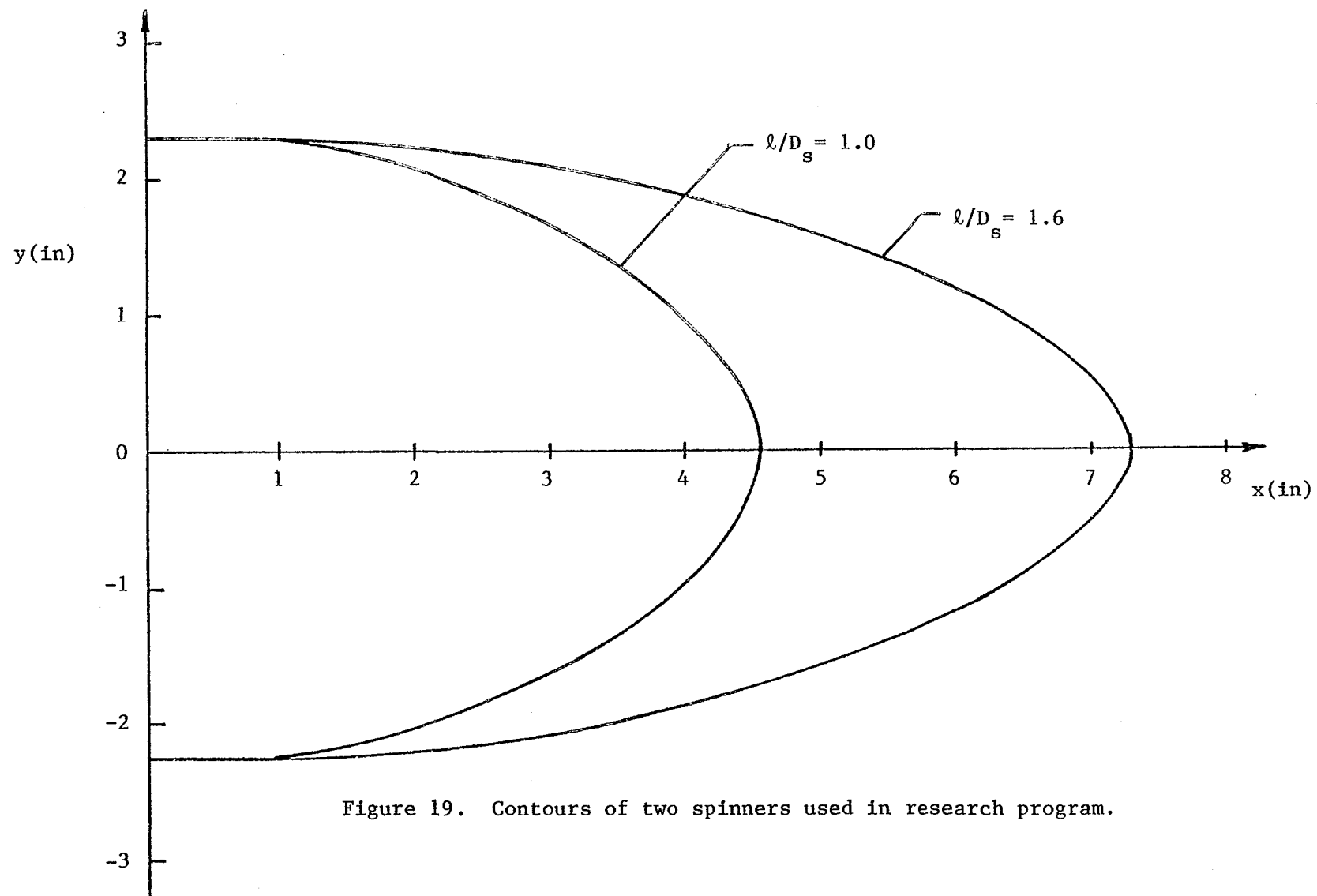


Figure 19. Contours of two spinners used in research program.

TABLE 1. SPINNER COORDINATES *

y	$x(l/D_s = 1.0)$	$x(l/D_s = 1.6)$
2.275	0	0
2.201	1.365	2.184
2.102	1.820	2.912
1.966	2.275	3.641
1.778	2.730	4.368
1.552	3.185	5.096
1.413	3.413	5.460
1.254	3.640	5.825
1.084	3.867	6.188
0.871	4.095	6.552
0.590	4.323	6.917
0.410	4.433	7.093
0.134	4.541	7.265
0	4.550	7.280

* All values are in inches.

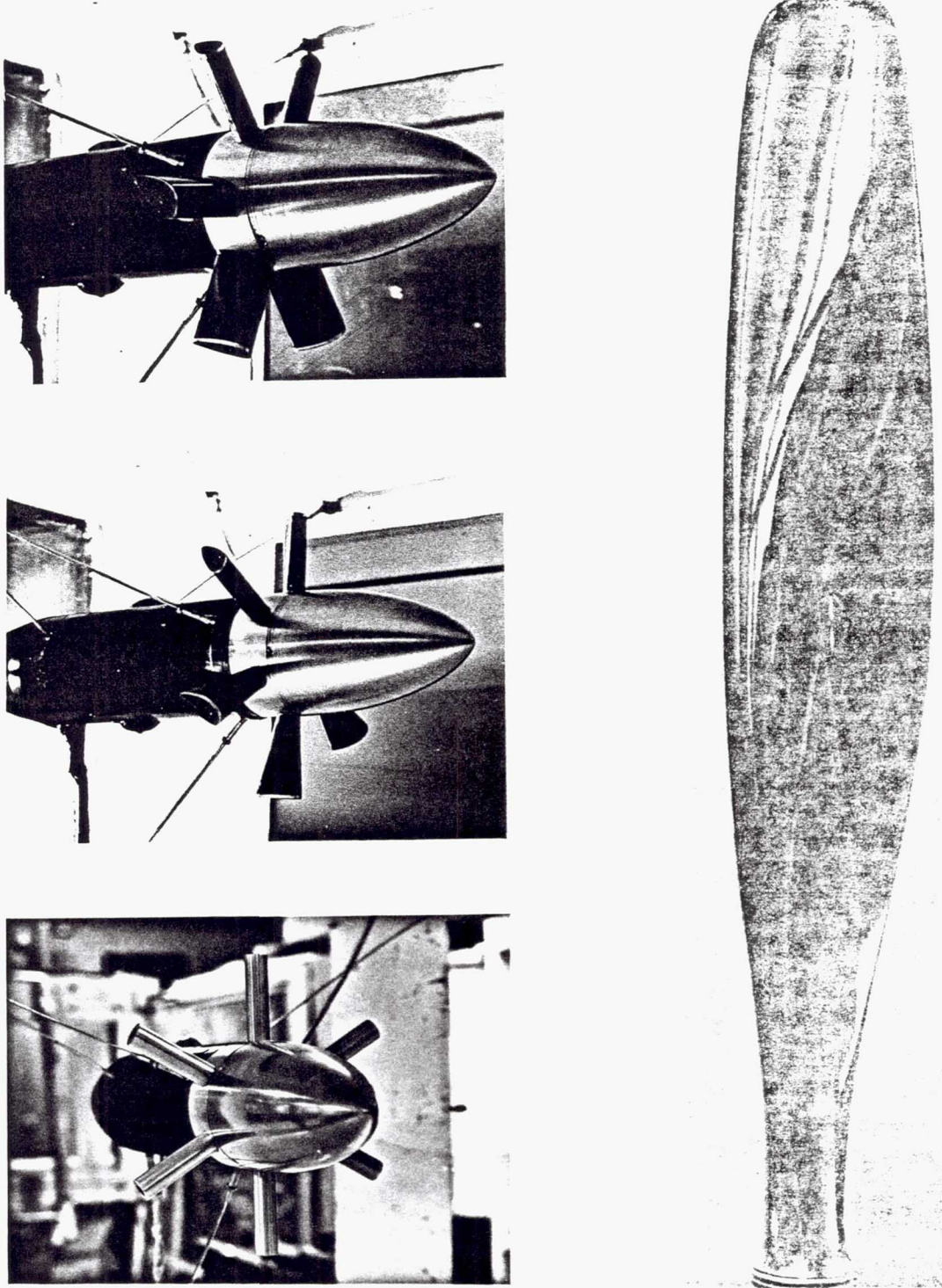


Figure 20. Baseline propeller blade and three representative shanks of present study (Reference 7).

c-2

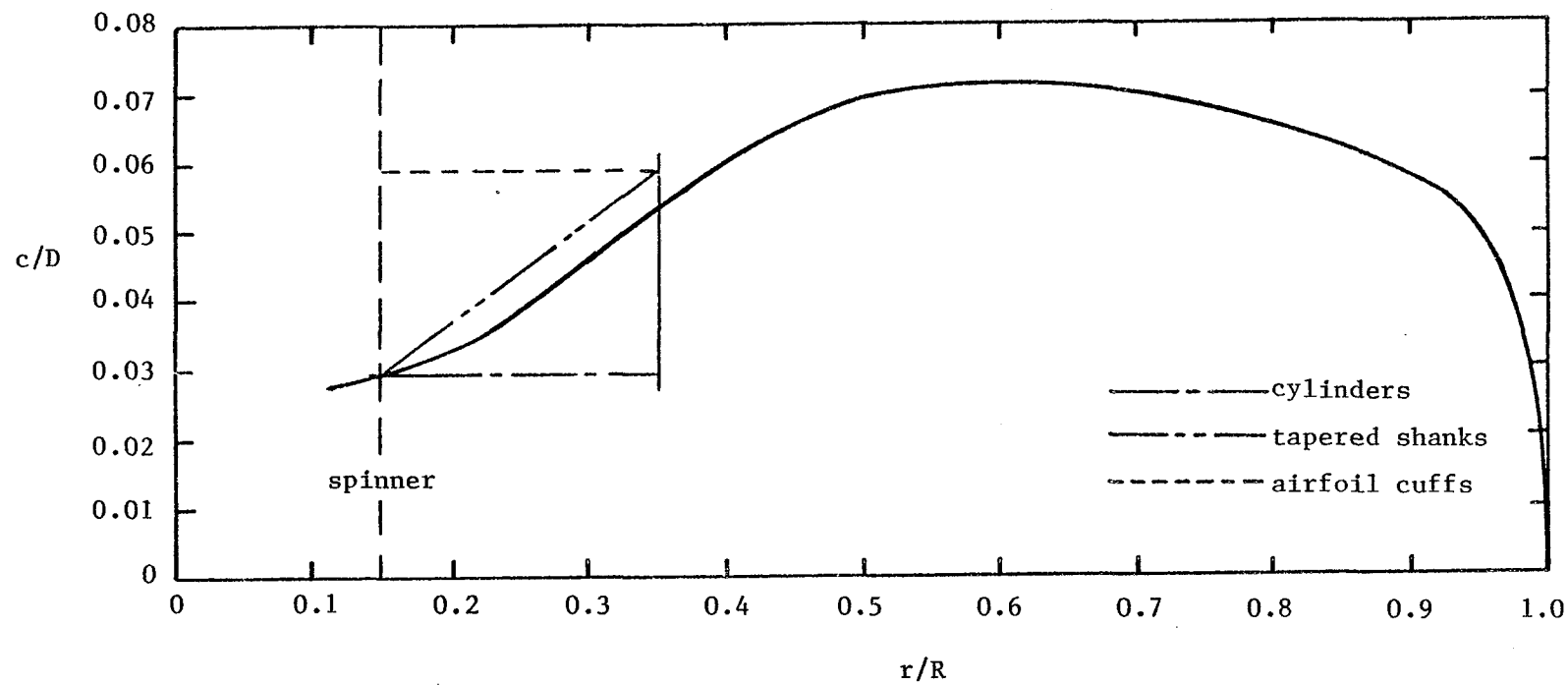


Figure 21. Baseline blade planform with superimposed shank models.

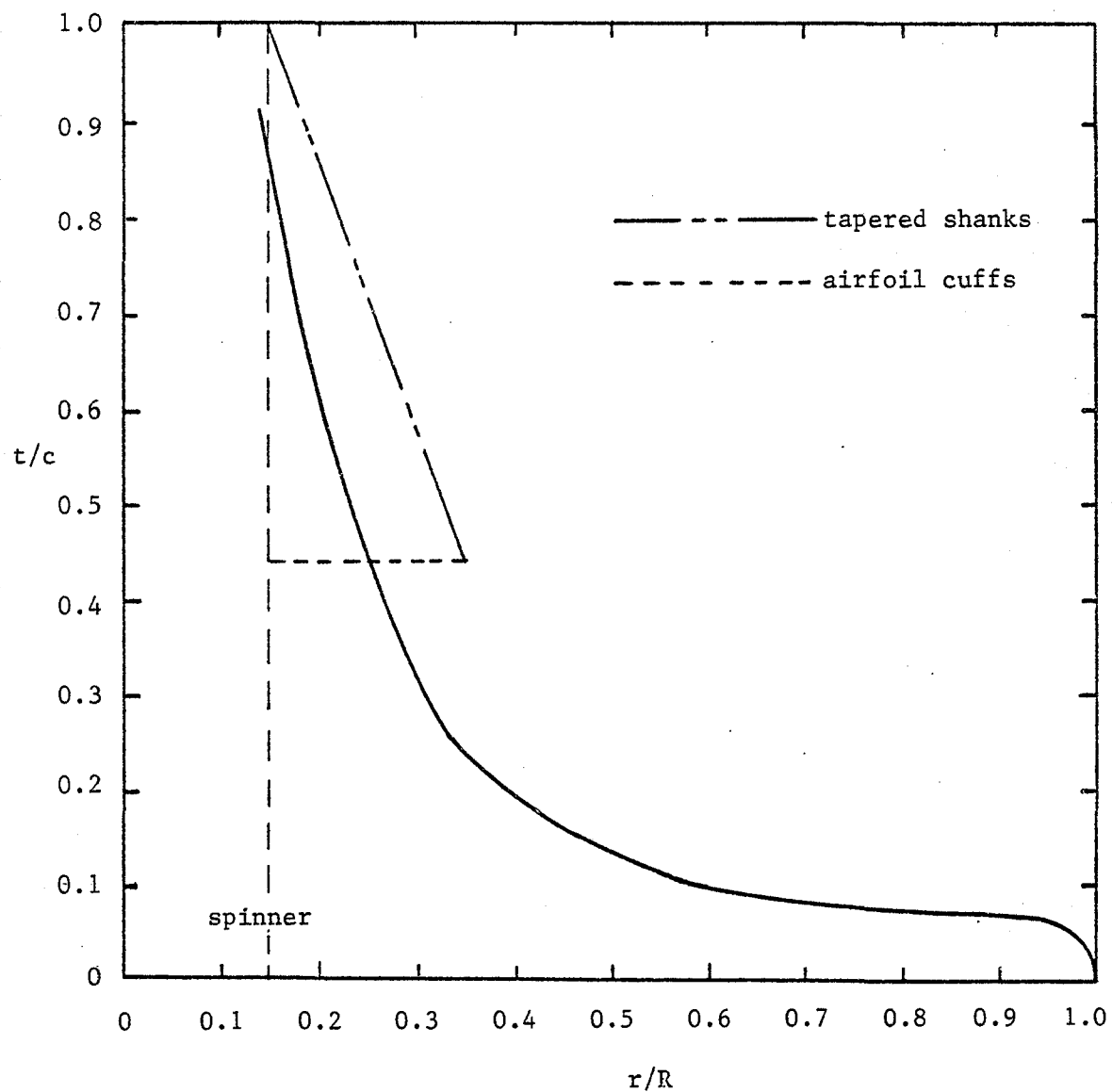


Figure 22. Thickness distributions of baseline blade and shank models.

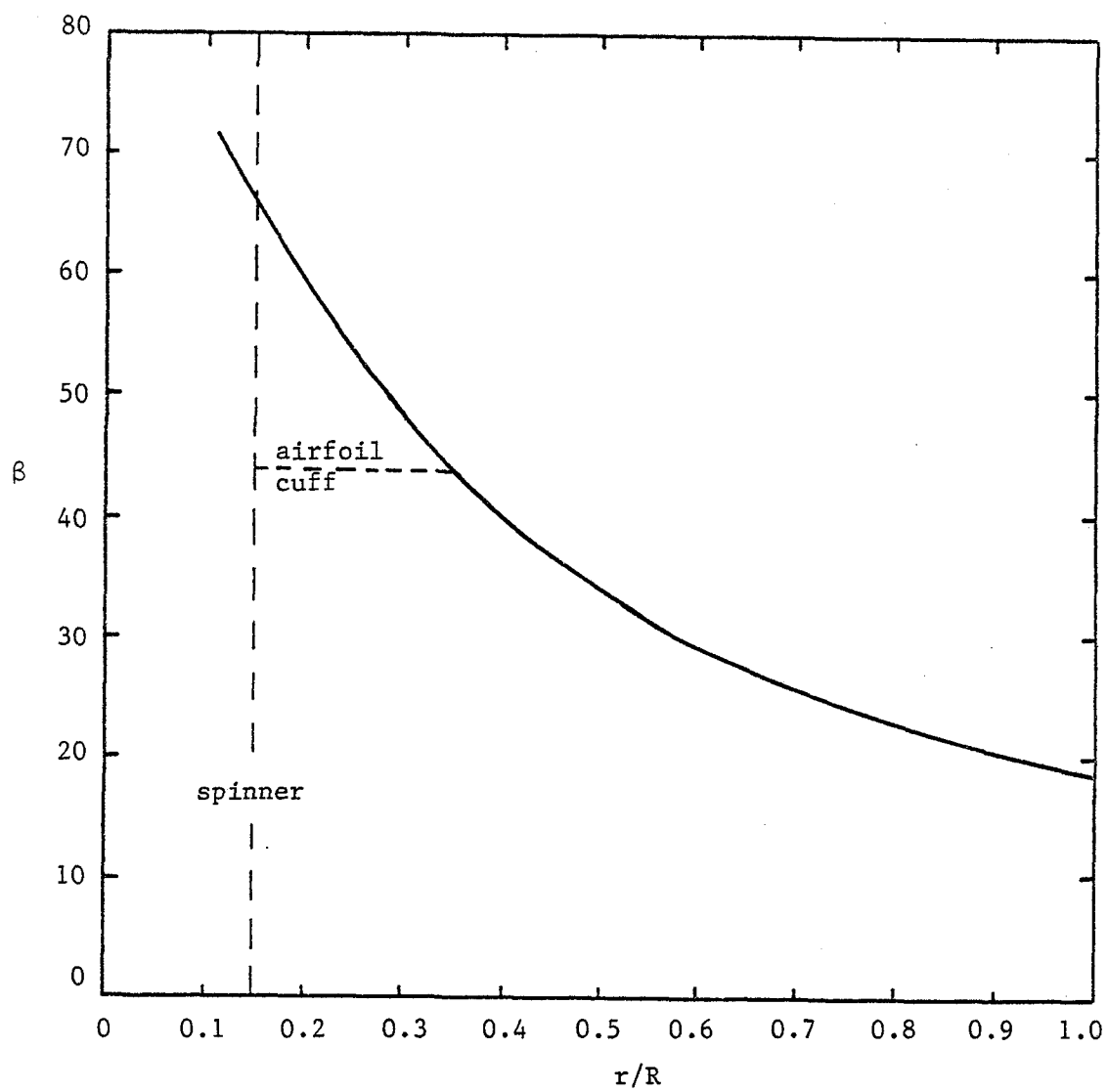


Figure 23. Twist distribution of baseline blade and shank models.

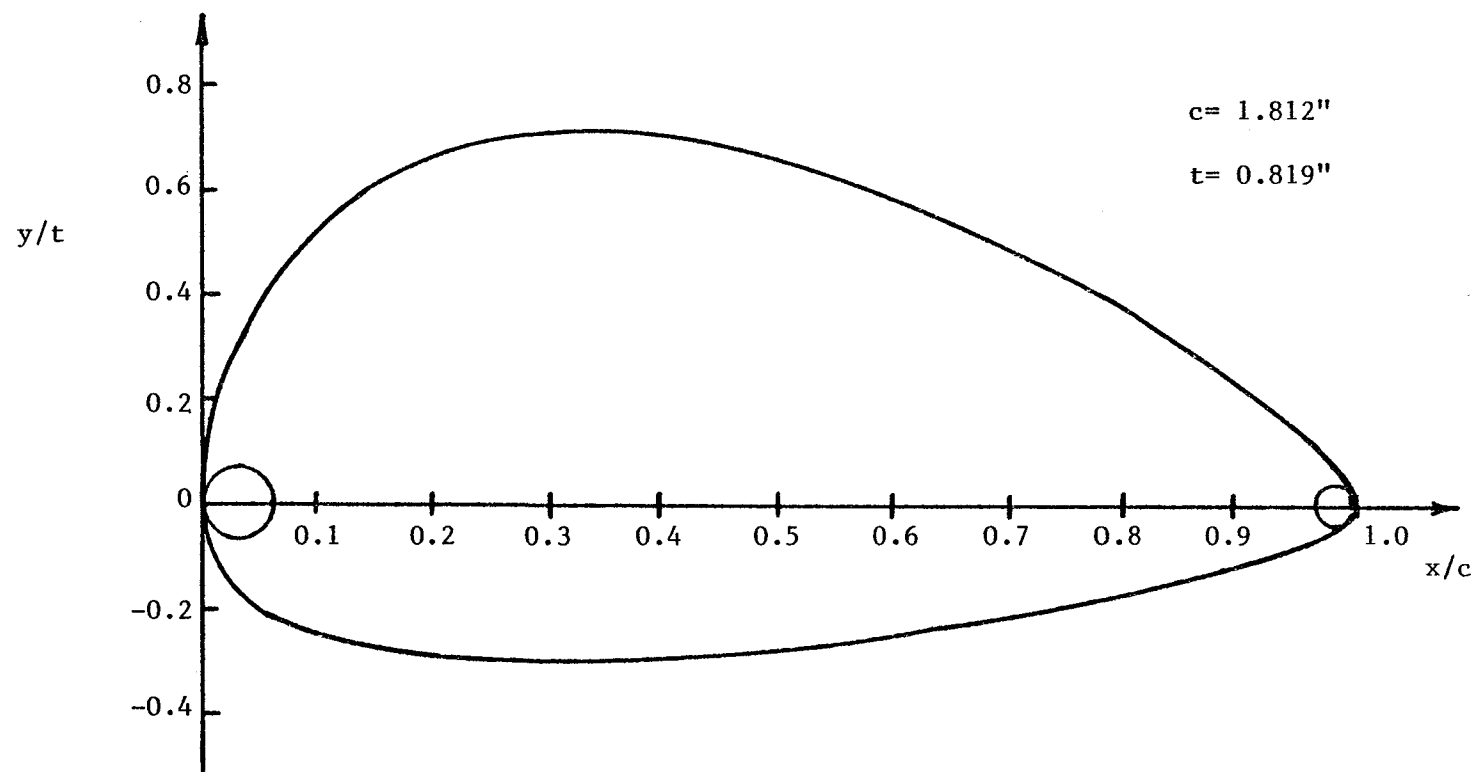
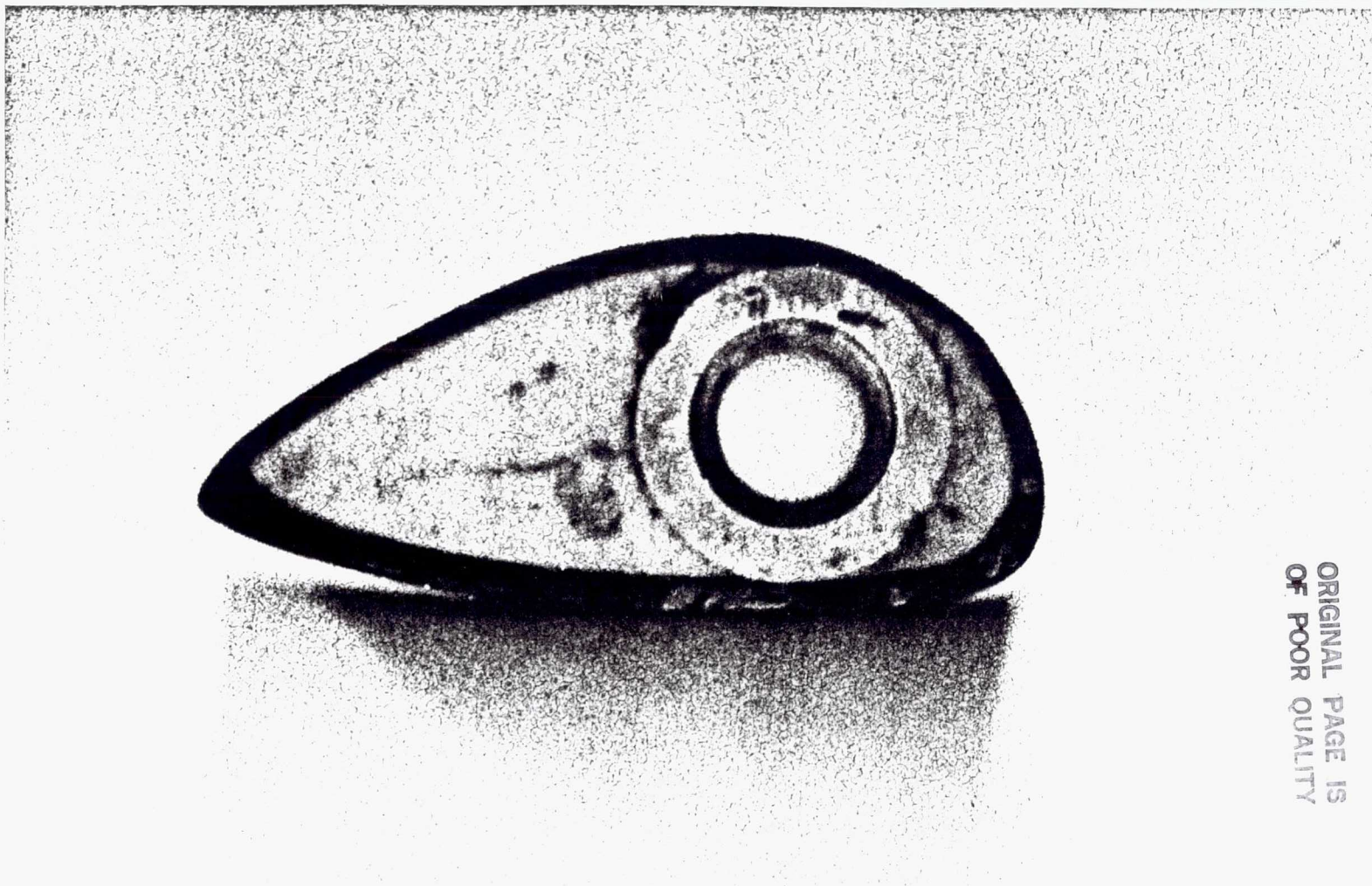


Figure 24. Clark Y airfoil section used on airfoil cuff and transition shank models.

TABLE 2. CLARK Y AIRFOIL COORDINATES

x/c	y_u/t	y_l/t
0.0	0.0	0.0
0.025	0.2766	-0.1383
0.050	0.3787	-0.1915
0.075	0.4553	-0.2234
0.100	0.5106	-0.2447
0.200	0.6702	-0.2766
0.300	0.7128	-0.2872
0.400	0.7085	-0.2809
0.500	0.6681	-0.2660
0.600	0.5957	-0.2404
0.700	0.4936	-0.2021
0.800	0.3723	-0.1638
0.900	0.2340	-0.1170
0.975	0.1596	-0.0957
1.000	0.0	0.0



ORIGINAL PAGE IS
OF POOR QUALITY

Figure 25. Sectional view of modeled Clark Y airfoil shank illustrating foam core, composite layers, and retention shank spar.

ORIGINAL PAGE IS
OF POOR QUALITY

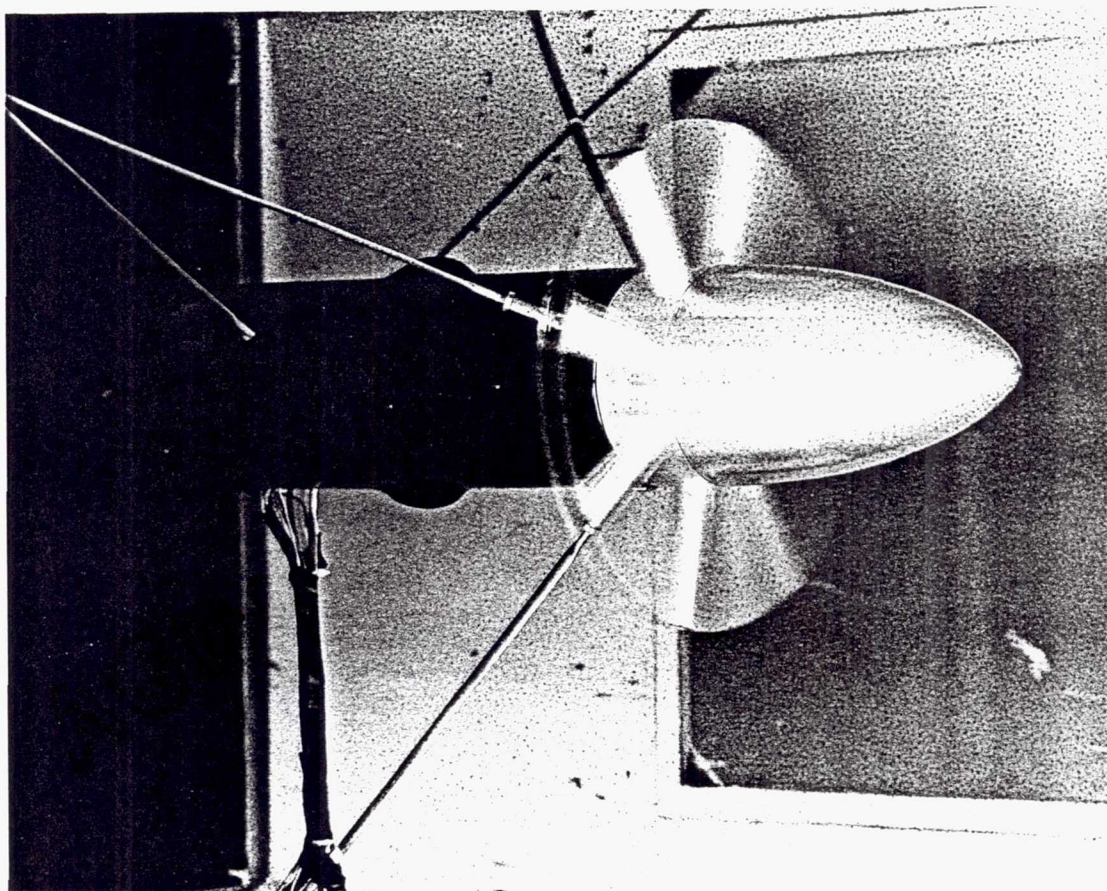


Figure 26. PTR installation in TAMU 2ft. x 3ft. low speed wind tunnel.

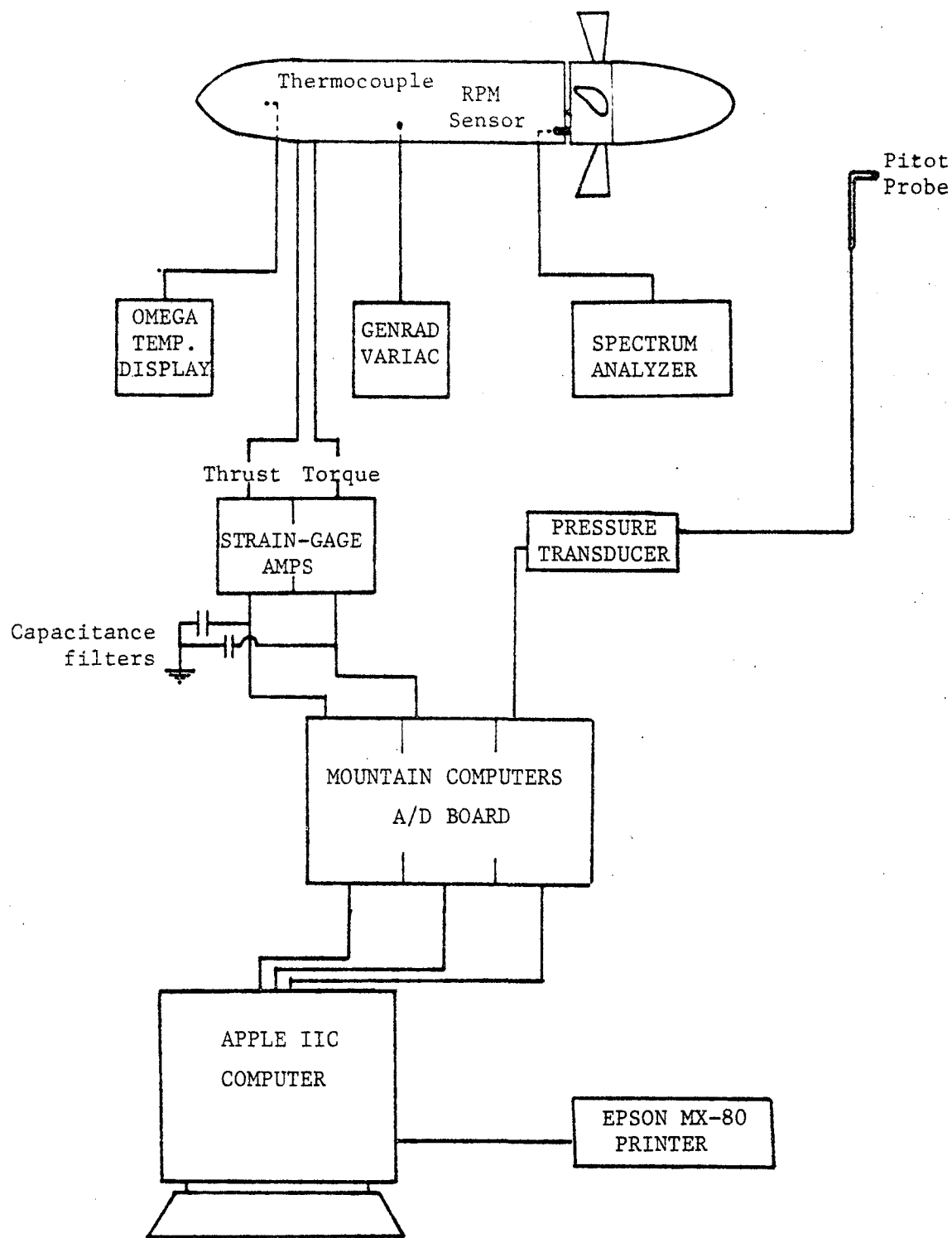


Figure 27. Schematic of instrumentation used in data acquisition.

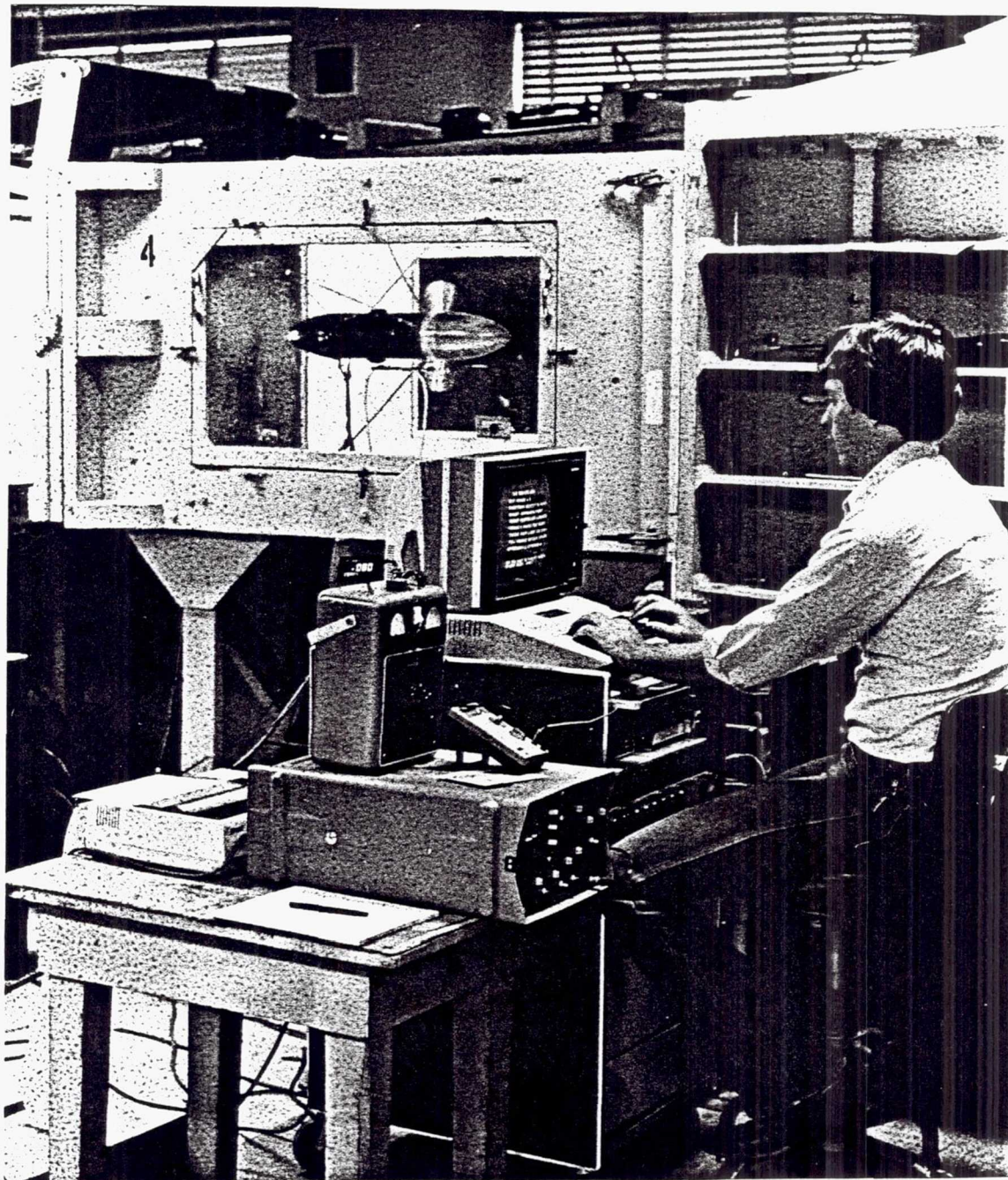


Figure 28. Photo of wind tunnel and data acquisition installation.

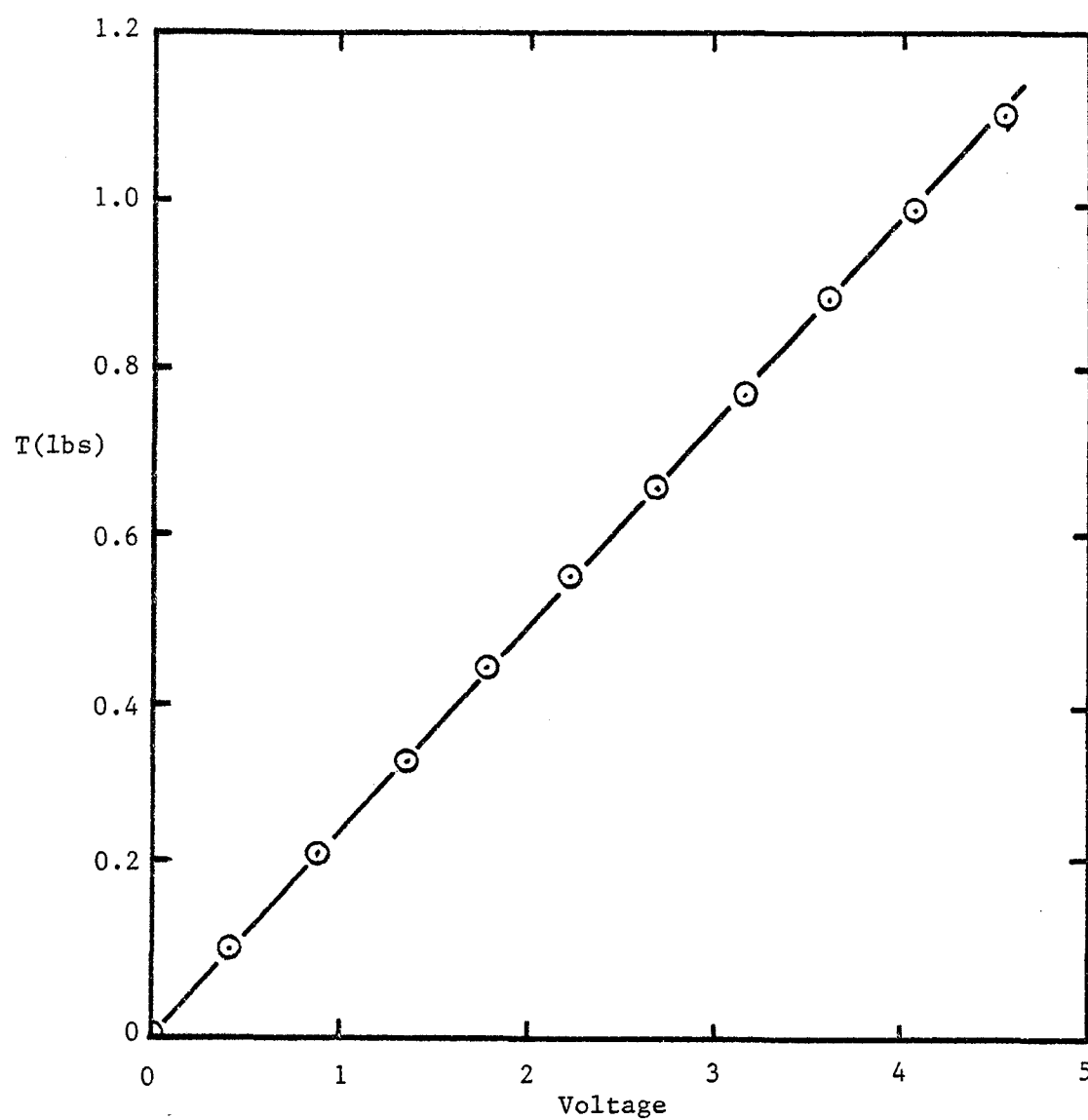


Figure 29. Thrust load cell calibration.

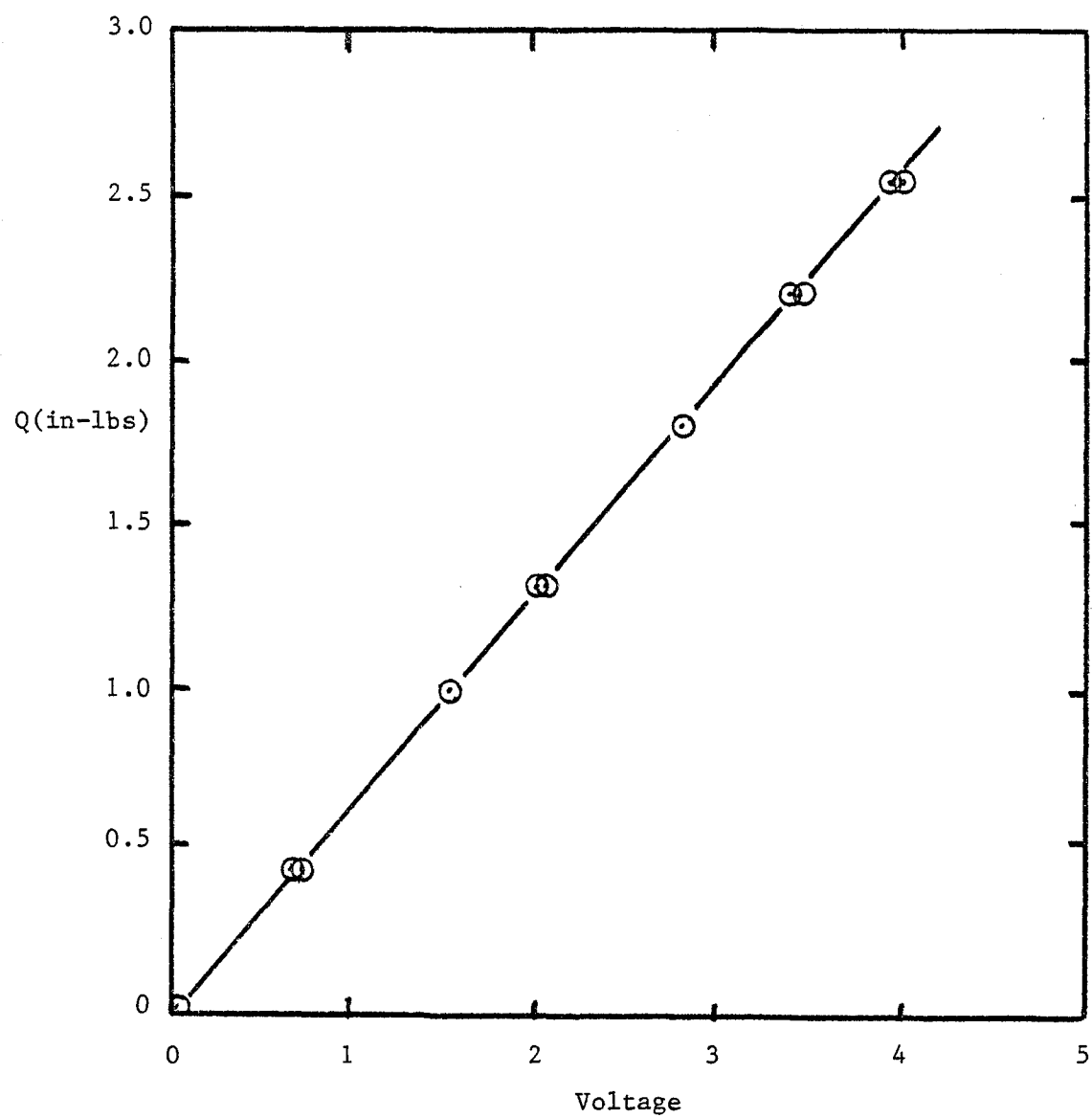


Figure 30. Torque load cell calibration.

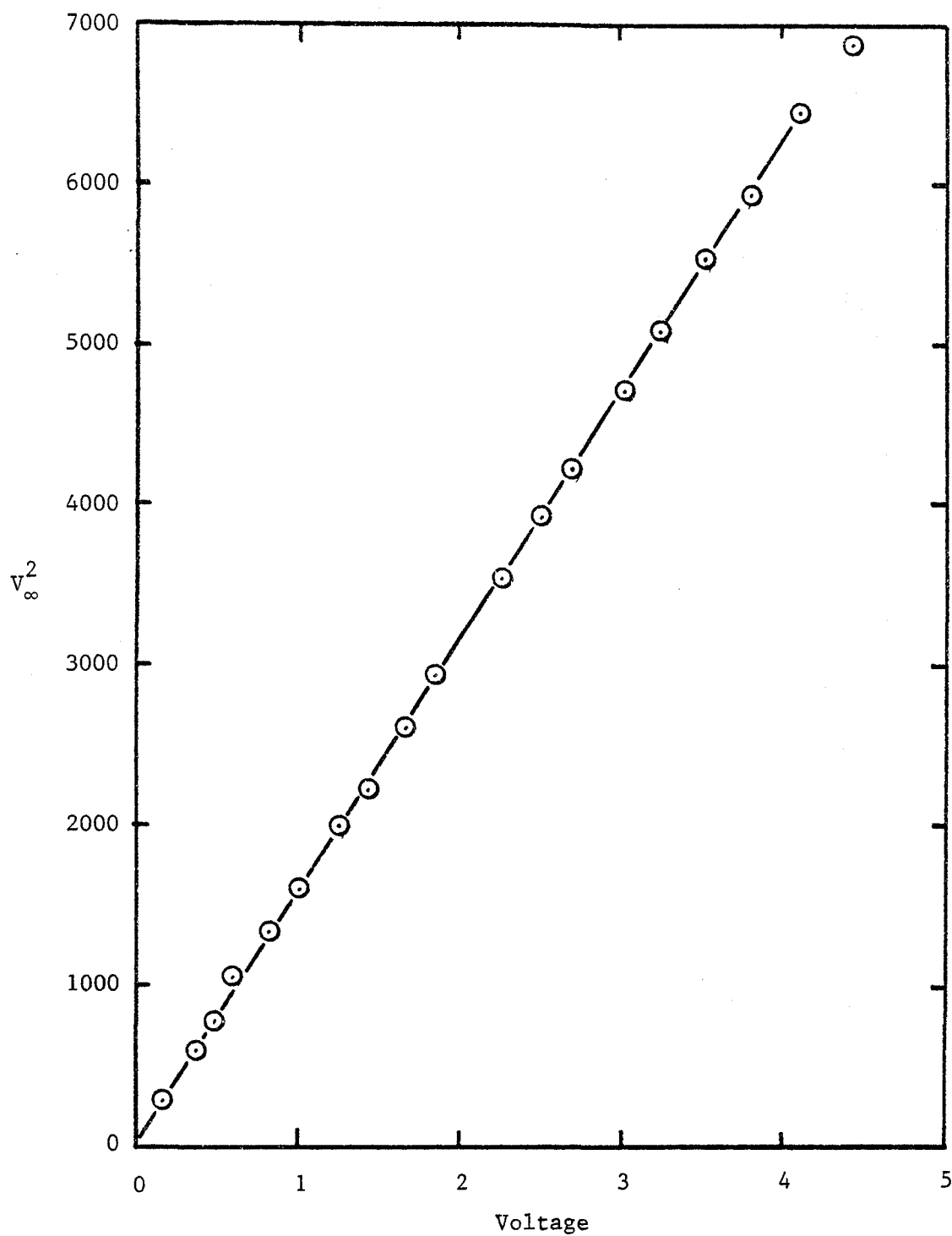


Figure 31. Pressure transducer calibration for tunnel velocity measurement.

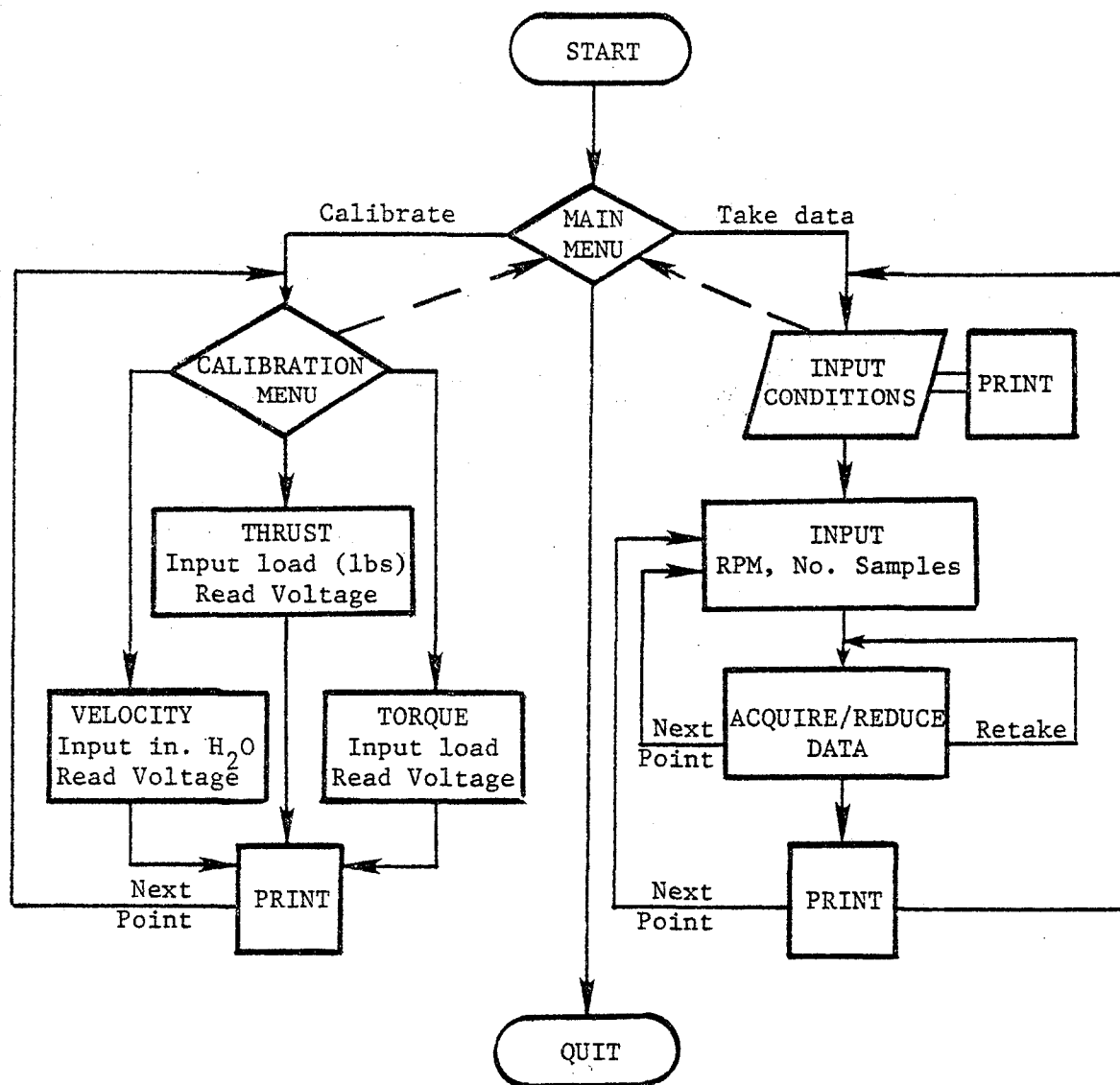


Figure 32. Data acquisition/reduction program flowchart.

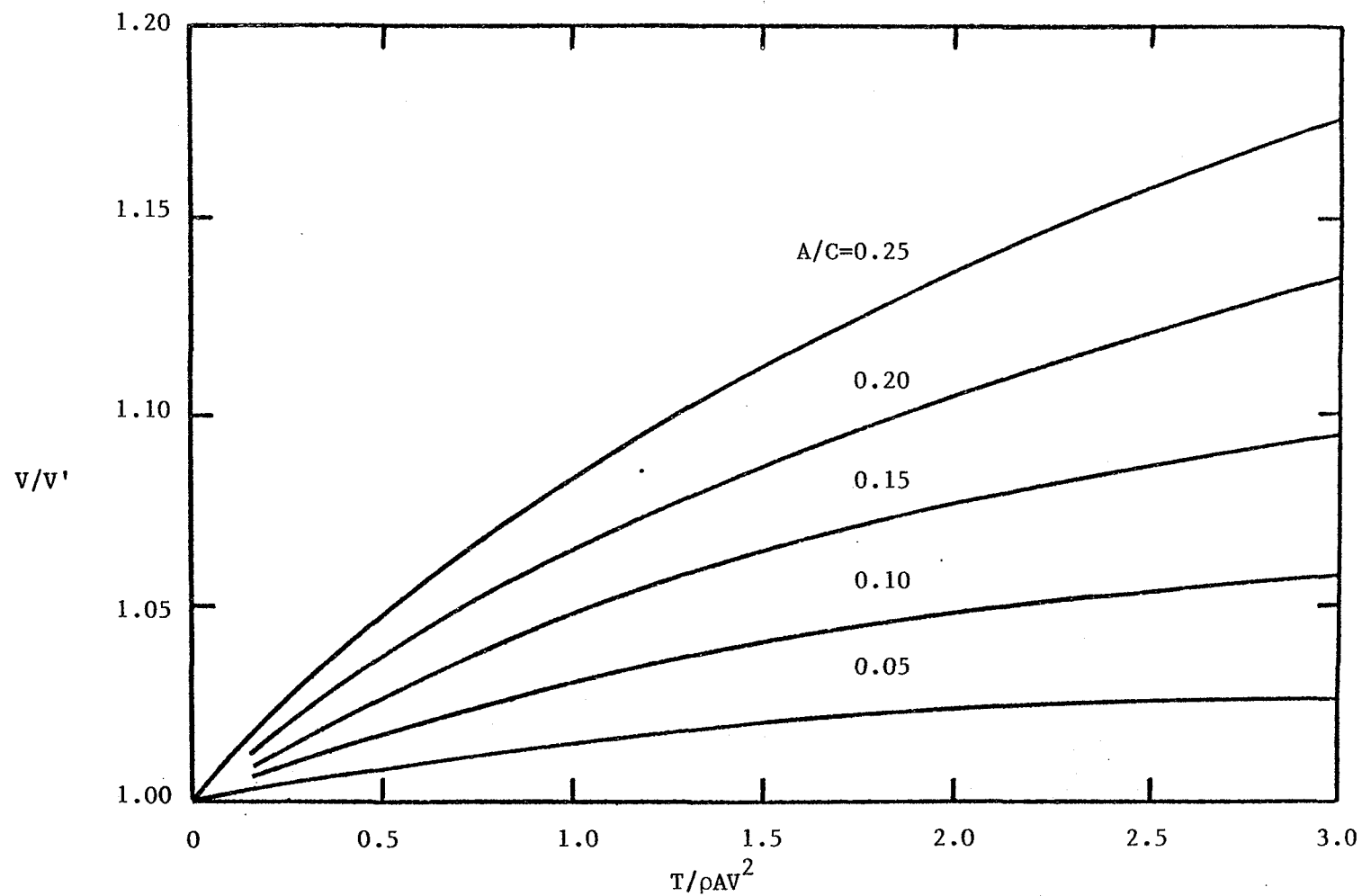
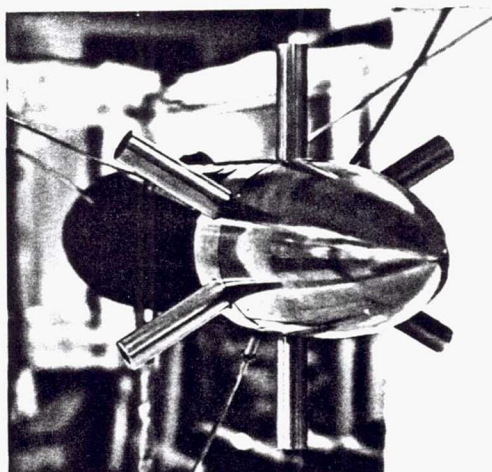
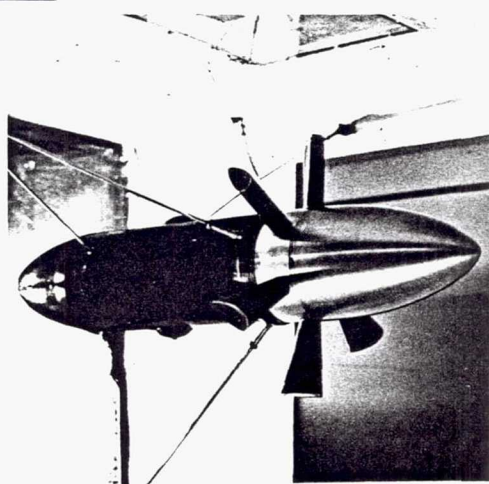


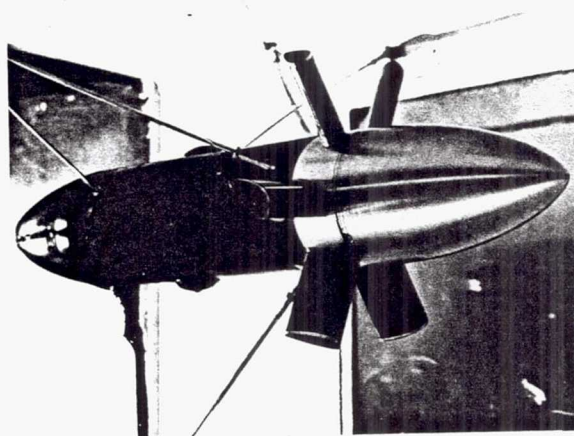
Figure 33. Tunnel constraint corrections to tunnel datum velocity for propeller tests.



(a)



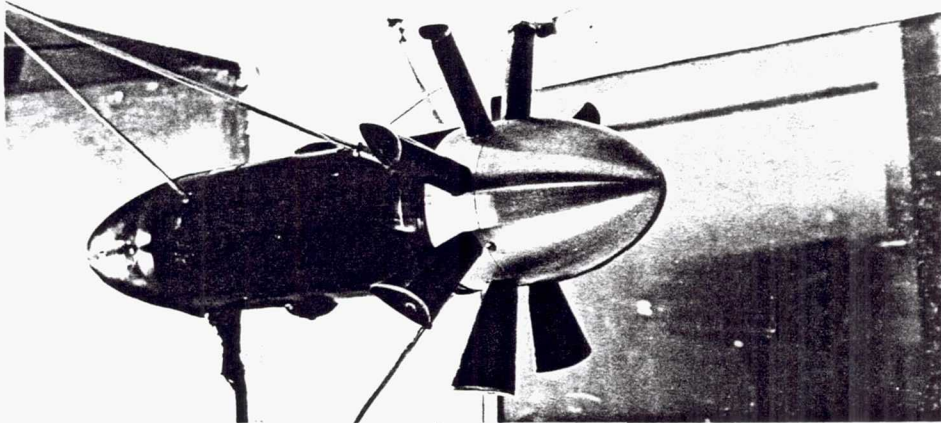
(b)



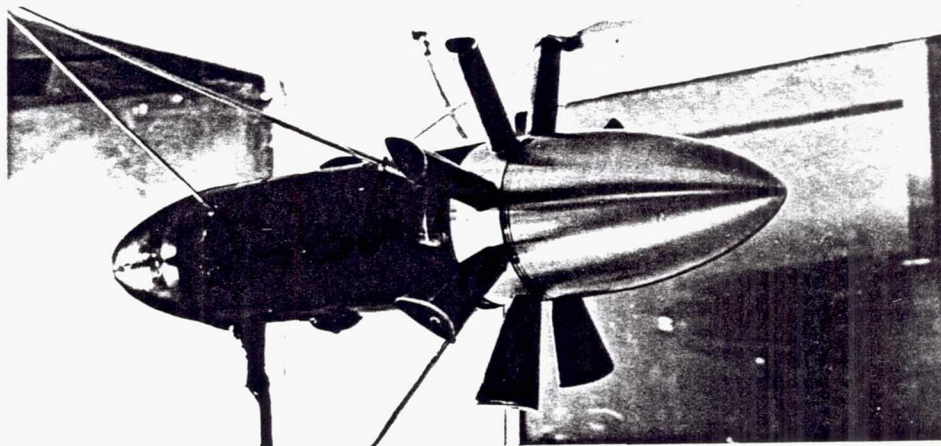
(c)

ORIGINAL PAGE IS
OF POOR QUALITY

Figure 34. (a) Cylindrical shanks installed on PTR for Phase I.
(b) Transition shank installed on PTR for Phase II.
(c) Airfoil cuff models installed on PTR for Phase III.



(a)



(b)

Figure 35. Spinners installed on PTR for: (a) $\lambda=1.0$, (b) $\lambda=1.6$.

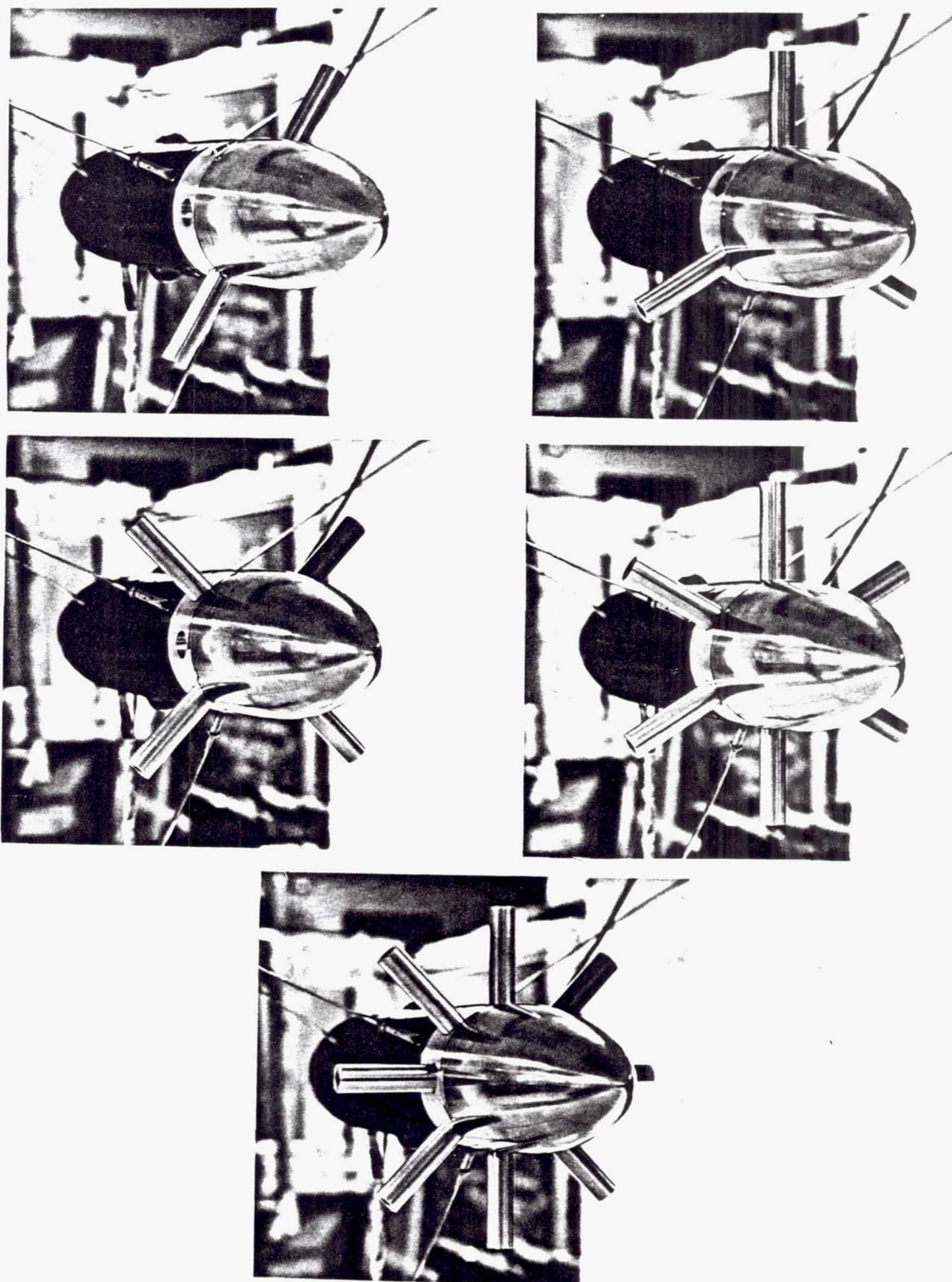


Figure 36. Array of number of blades in installed configuration.

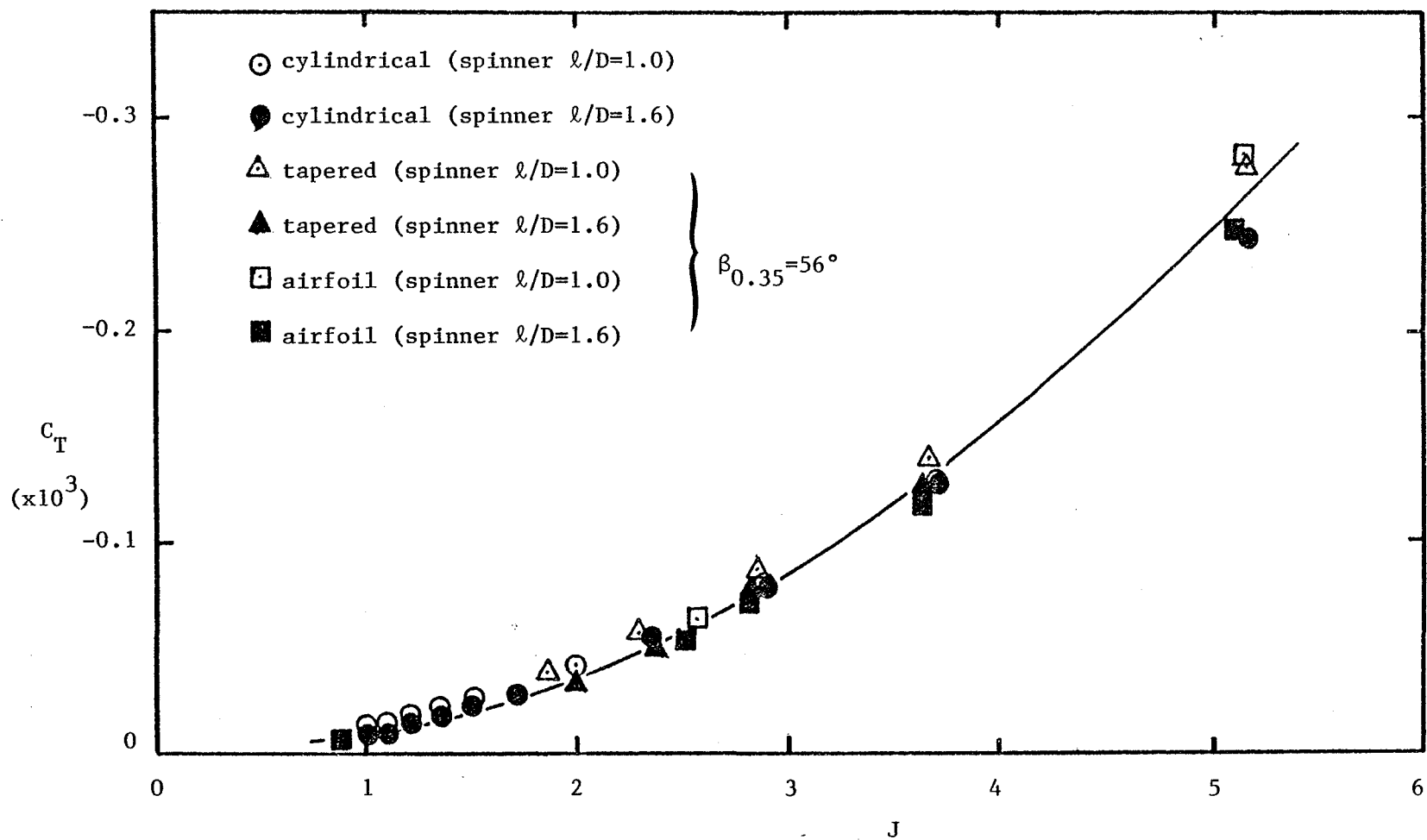


Figure 37. Representative raw thrust data ($B=6$).

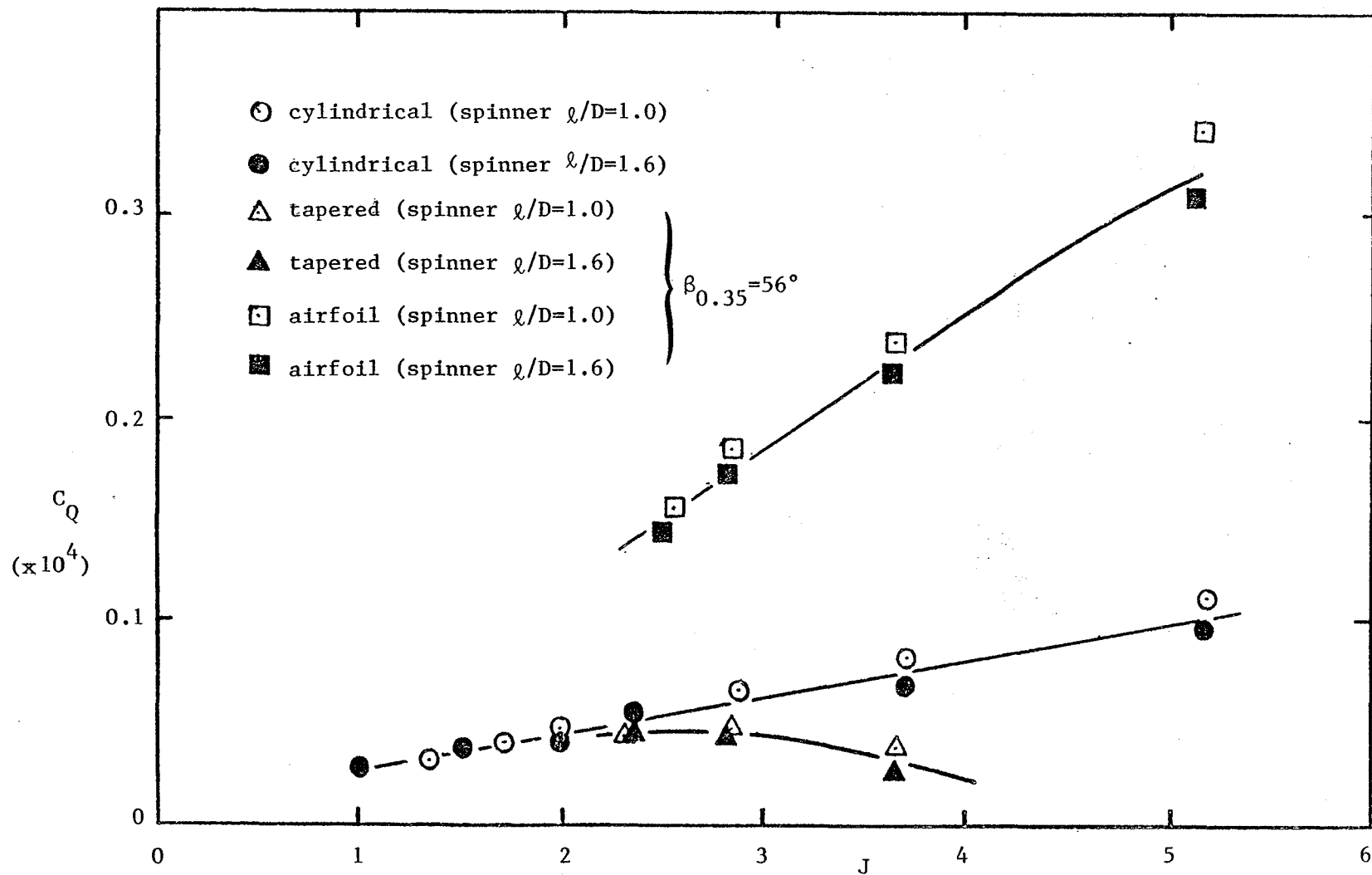


Figure 38. Representative raw torque data ($B=6$).

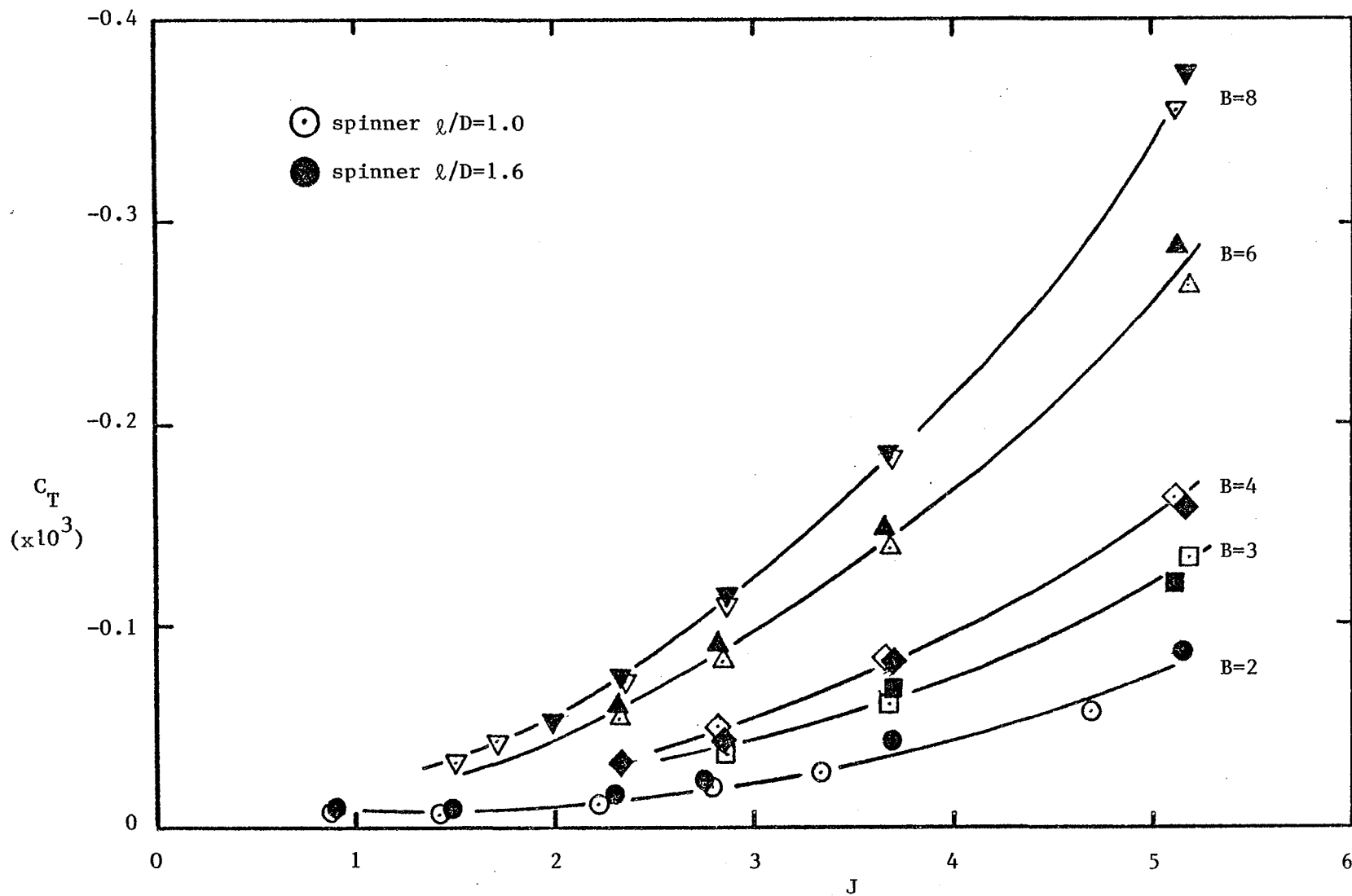


Figure 39. Representative measured effects of number of blades (tapered shanks, $\beta=51^\circ$).

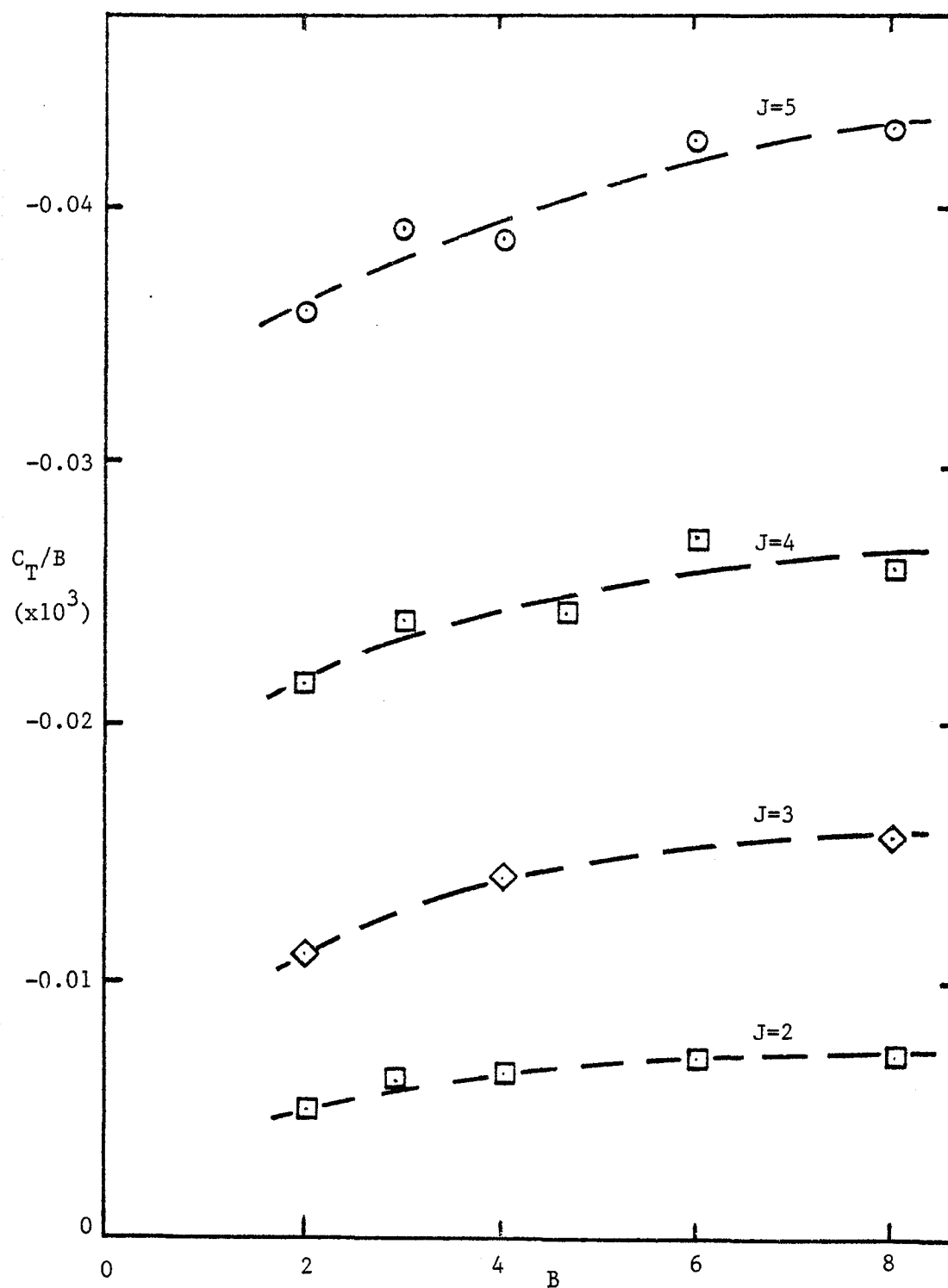


Figure 40. Cursory example of blade interference (tapered shanks, $\beta=51^\circ$).

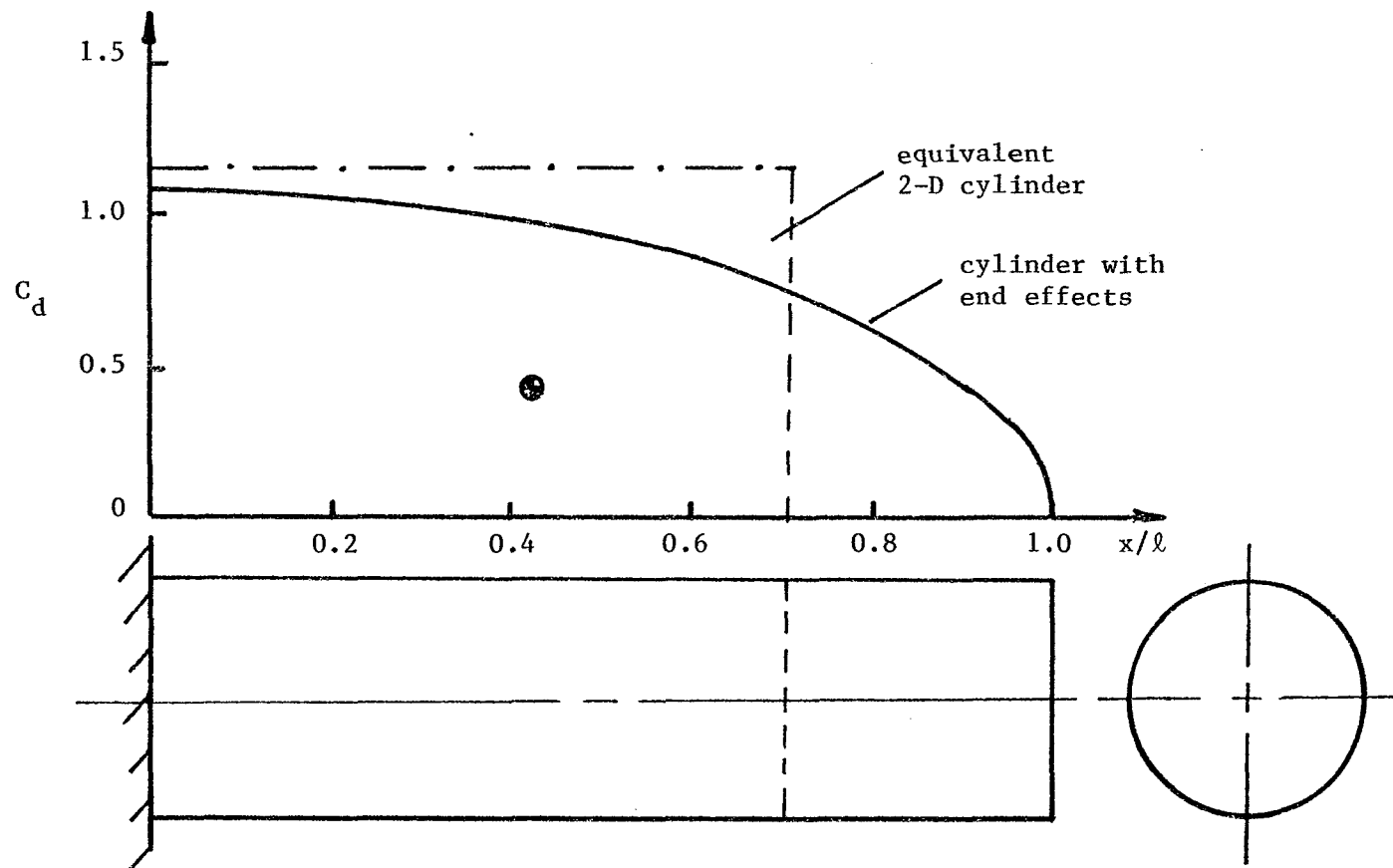


Figure 41. Drag distributions of finite aspect ratio cylinder and two-dimensional equivalent.

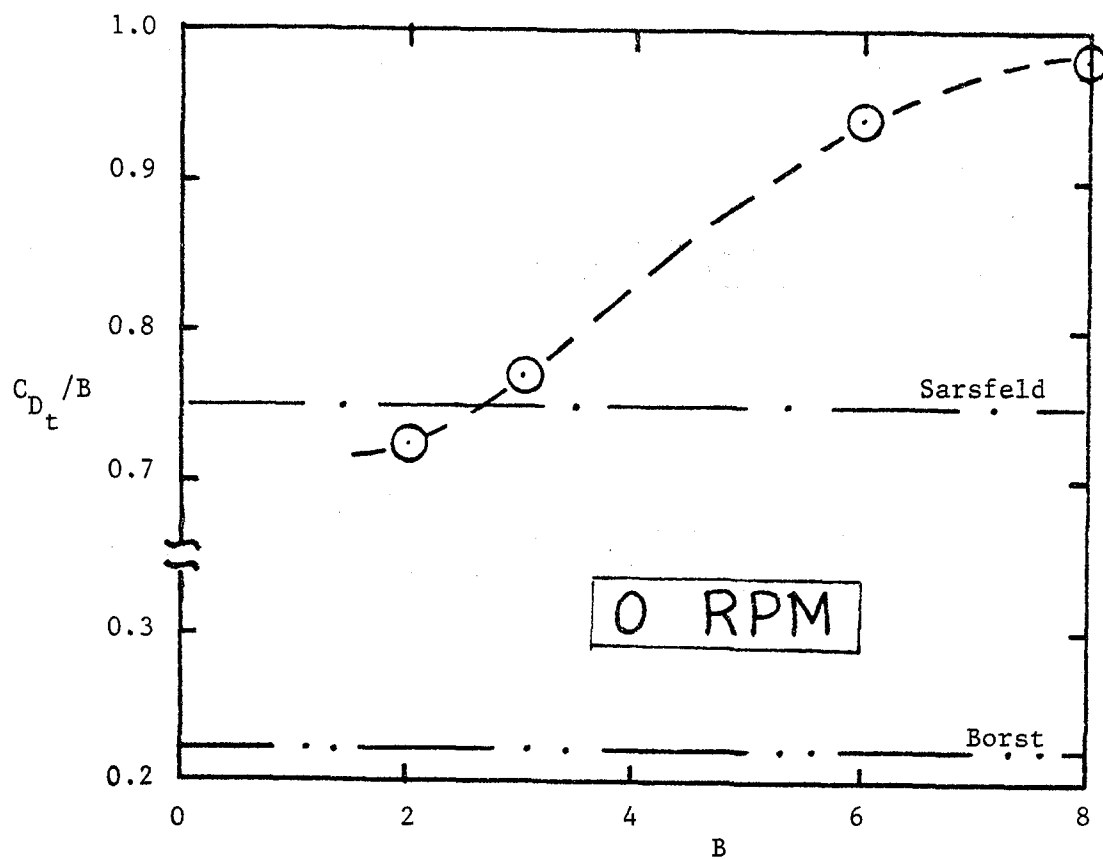


Figure 42. Development of interference C_D with increasing number of cylindrical blade shanks.

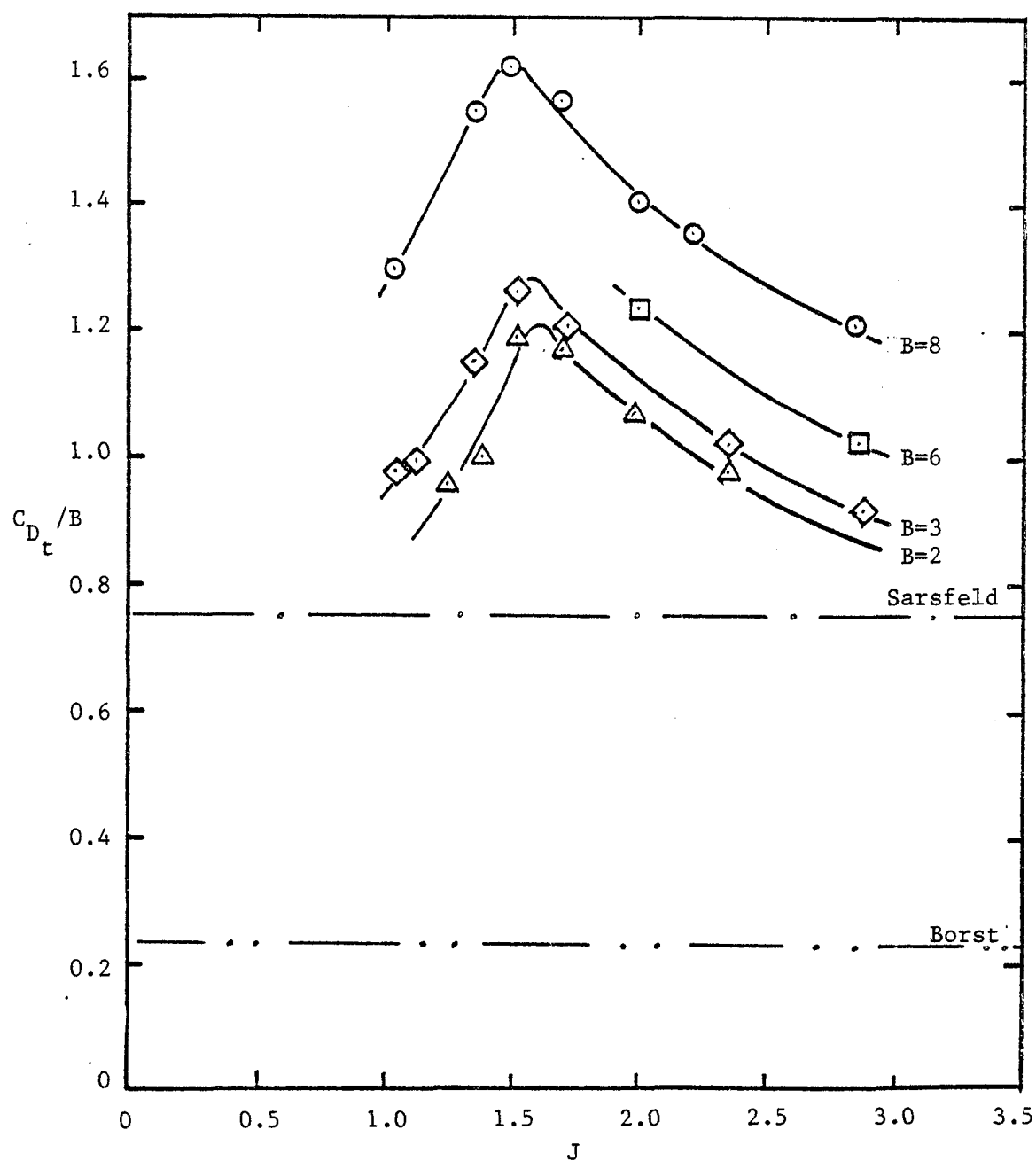


Figure 43. Effect of rotation on interference C_D for cylindrical blade shanks.

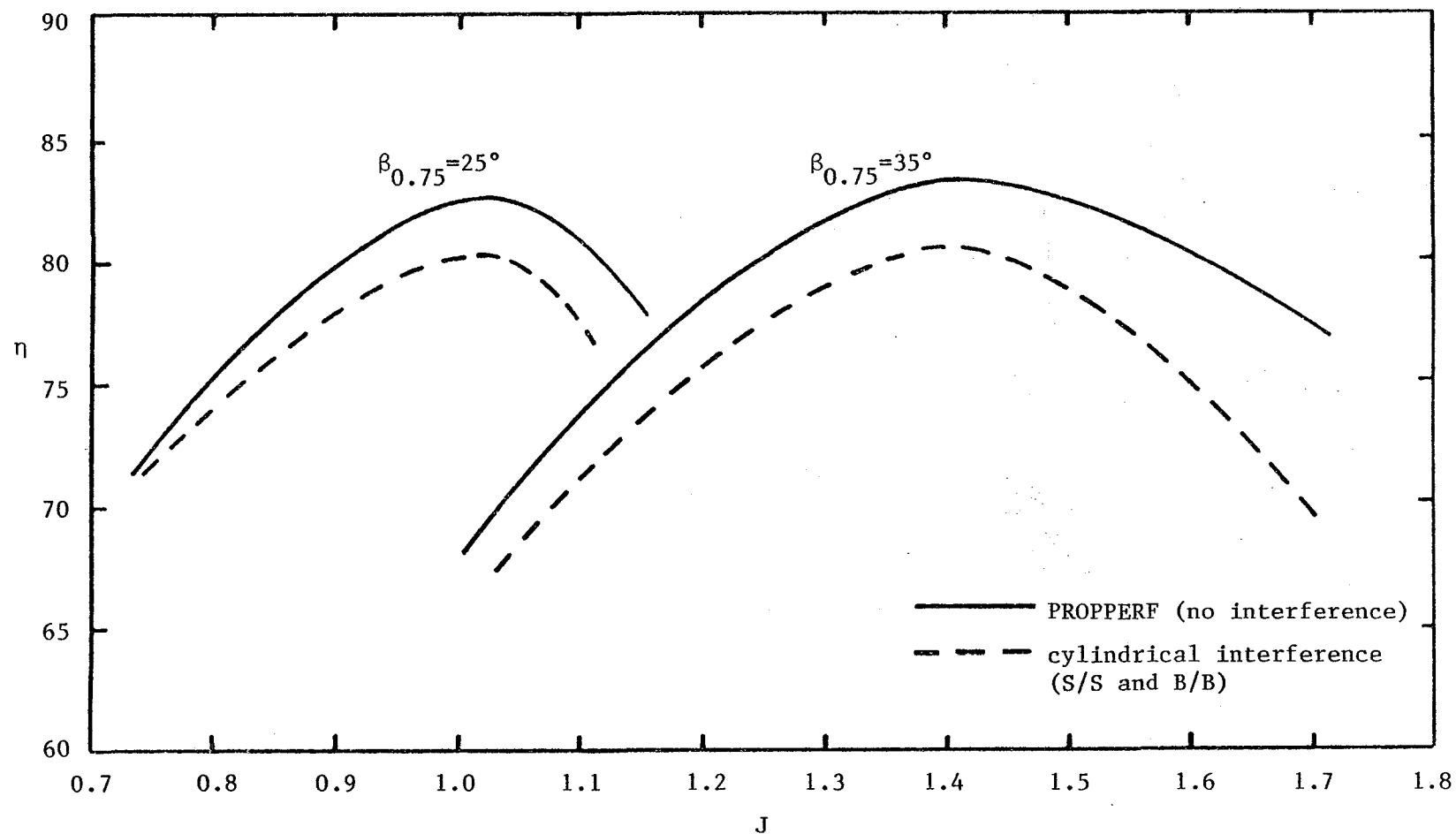


Figure 44. Application of cylindrical shank interference drag values to Reid's baseline propeller efficiency.

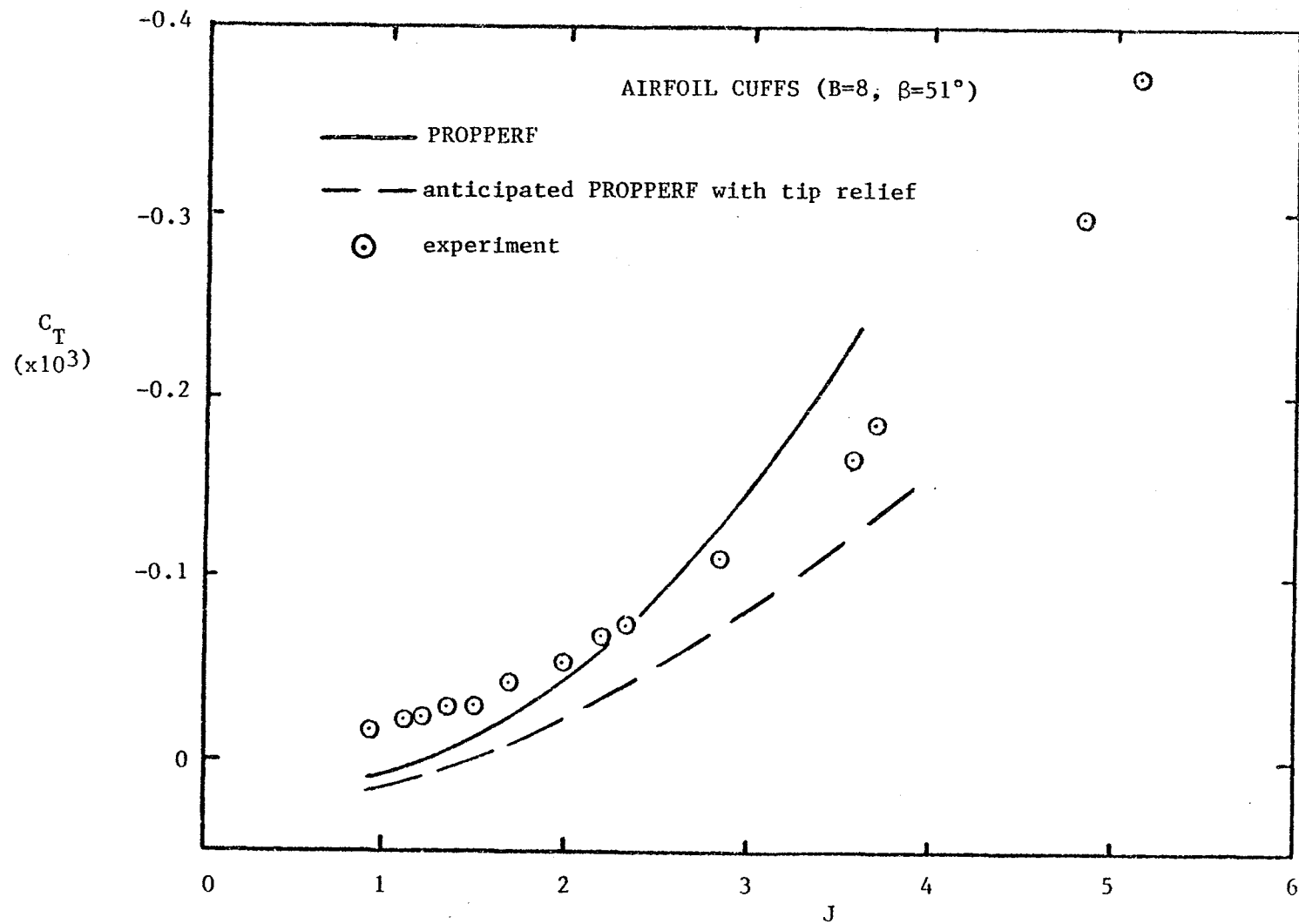


Figure 45. Propeller performance prediction of shank contribution as compared to experimental measurements.

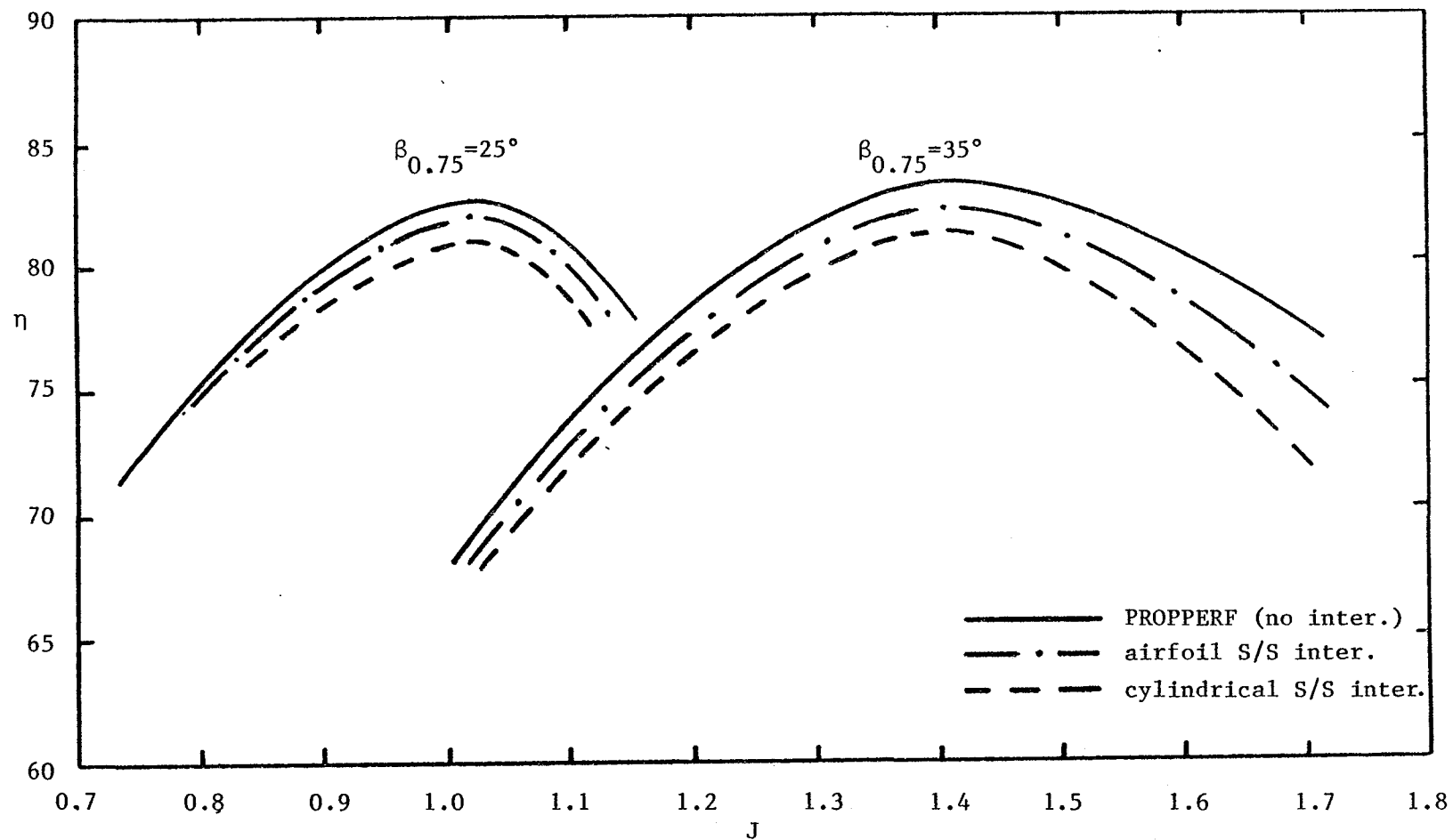


Figure 46. Application of cylindrical shank spinner/shank C_D 's and airfoil cuff C_D 's to efficiency curves of Reid's baseline blade.

APPENDIX II
DATA ACQUISITION/REDUCTION PROGRAM LISTING

JLIST

90 REM -- ADVERTISING

```

97 B$ = CHR$ (7)
98 D$ = CHR$ (4)
99 E$ = CHR$ (12)
100 HOME
101 PRINT D$;"PR#0"
110 INVERSE
115 FLASH
117 SPEED= 32
118 VTAB 12
120 PRINT "          CAMBA ENGINEERI
      NG INC          "
121 PRINT "          ADVANCED VE
      RSION           "
125 PRINT : PRINT : PRINT : PRINT

130 NORMAL
131 DIM PT(22),PQ(22),PN(22),PJ(
    22),PS(22)
132 DIM U(30),PR(30),V(30)
133 DIM TR(20),TZ(20),QR(20),QZ(
    20)
134 DIM QT(20),TQ(20)
135 SPEED= 255
140 HOME
150 REM -- INPUT SECTION

```

1000 REM

- MENU 1

```

1005 PRINT " MENU 1 FOR THE SPIN
      NER SHANK TEST RIG"
1010 VTAB 5: PRINT "          (1) TAK
      E DATA"
1020 VTAB 10: PRINT "          (2) CA
      LIBRATE"
1030 VTAB 15: PRINT "          (3) GO
      CHASE WOMEN !!!!!!"
1040 VTAB 20: PRINT "TYPE NUMBER
      TO EXECUTE ": GET M1$
1050 IF M1$ < > "1" THEN GOTO
      1060
1055 M$ = " TAKE DATA?": GOTO 110
      0
1060 IF M1$ < > "2" THEN GOTO
      1070
1065 M$ = " CALIBRATE?": GOTO 110
      0
1070 IF M1$ < > "3" THEN GOTO
      1080
1075 M$ = " WHOOOOOPPPPP!!!!!!!!!"
      : GOTO 1100
1080 GOTO 140

```

```

1100 PRINT "ARE YOU SURE YOU WAN
      T TO";M$: PRINT "(TYPE Y OR
      N)"
1105 PRINT
1200 GET YN$: IF YN$ = "Y" THEN
      GOTO 1210
1205 GOTO 140
1210 IF M1$ = "1" THEN GOTO 200
      0
1220 IF M1$ = "2" THEN GOTO 700
      0
1230 IF M1$ = "3" THEN GOTO 900
      0
2000 HOME
2010 PRINT " MENU 2 TEST CONDITI
      ON INPUT "
2020 PRINT : INPUT "          (1) TI
      TLE:";T$
2030 PRINT : INPUT "          (2) TE
      ST NUMBER:";TE
2040 PRINT : INPUT "          (3) DA
      TE:";DA$
2050 PRINT : INPUT "          (4) TE
      MPERATURE (F):";T
2060 PRINT : INPUT "          (5) BA
      ROMETRIC PRESS(IN.HG):";P
2070 PRINT : PRINT "          (6) SP
      INNER (1,2,3):"
2072 PRINT "                  1) L/D = 1
      .6"
2074 PRINT "                  2) L/D = 1
      .3"
2076 PRINT "                  3) L/D = 1
      .0 ";SP
2077 IF SP = 1 THEN GOTO 2085
2078 IF SP = 2 THEN GOTO 2085
2079 IF SP = 3 THEN GOTO 2085
2080 VTAB 12: GOTO 2070
2085 PRINT : PRINT "          (7) BL
      ADE TYPE (1,2,3,4):"
2090 PRINT "                  1) BARE HU
      BS"
2100 PRINT "                  2) CYL SHA
      NKS"
2110 PRINT "                  3) AIRFOIL
      SHANKS"
2120 PRINT "                  4) TAPERED
      SHANKS ";ST
2130 IF ST = 1 THEN GOTO 2185
2140 IF ST = 2 THEN GOTO 2185
2160 IF ST = 3 THEN GOTO 2185
2170 IF ST = 4 THEN GOTO 2185
2180 VTAB 17: GOTO 2085
2185 PRINT : INPUT "          (8) #
      OF SHANKS? (0,2,3,4,6,8):";N
      S
2195 HOME
2200 PRINT "THE CONDITONS YOU CH
      OSE WERE"
2210 PRINT : PRINT " 1)TEST TITL
      E:";T$
2220 PRINT : PRINT " 2)TEST NUMB
      ER:";TE
2230 PRINT : PRINT " 3)TODAY'S D
      ATE:";DA$
2240 PRINT : PRINT " 4)TEMPERATU

```

```

RE:";T;" F"
2250 PRINT : PRINT " 5)BAROMETRI
C PRESSURE:";P;" IN.HG"
2260 IF SP = 1 THEN SP$ = " L/D
OF 1.6"
2270 IF SP = 2 THEN SP$ = " L/D
OF 1.3"
2280 IF SP = 3 THEN SP$ = " L/D
OF 1.0"
2290 PRINT : PRINT " 6)SPINNER "
;SP;" HAS A";SP$
2300 IF ST = 1 THEN ST$ = " BARE
HUBS"
2310 IF ST = 2 THEN ST$ = " CYLI
NDRICAL SHANKS"
2320 IF ST = 3 THEN ST$ = " AIRF
OIL SHANKS"
2330 IF ST = 4 THEN ST$ = " TAPE
RED SHANKS"
2340 PRINT : PRINT " 7)BLADE TYP
E ";ST;" ARE";ST$
2350 PRINT : PRINT " 8) NUMBER O
F SHANKS ";NS
2400 PRINT : PRINT " DO YOU WANT
TO CHANGE ANY VALUES ?": PRINT
"(Y,N,OR R-RETURN TO MENU 1)
"
2410 GET YN$: IF YN$ = "N" THEN
GOTO 2600
2415 IF YN$ = "R" THEN GOTO 140
2420 VTAB 19: PRINT "WHICH ONE W
OULD YOU LIKE TO CHANGE ?": PRINT
" (TYPE 1 THROUGH 8)"
2430 GET CH
2440 HOME
2450 IF CH < > 1 THEN GOTO 246
0
2455 VTAB 10: INPUT "NEW TITLE:"
;T$
2458 GOTO 2195
2460 IF CH < > 2 THEN GOTO 247
0
2465 VTAB 10: INPUT "NEW TEST NU
MBER:";TE
2468 GOTO 2195
2470 IF CH < > 3 THEN GOTO 248
0
2475 VTAB 10: INPUT "NEW DATE (W
ITH -----):";DA$
2478 GOTO 2195
2480 IF CH < > 4 THEN GOTO 249
0
2485 VTAB 10: INPUT "NEW TEMPERA
TURE:";T
2488 GOTO 2195
2490 IF CH < > 5 THEN GOTO 250
0
2495 VTAB 10: INPUT "NEW BAROMET
RIC PRESSURE:";P
2498 GOTO 2195
2500 IF CH < > 6 THEN GOTO 251
0
2505 VTAB 10: INPUT "NEW SPINNER
(1,2,3):";SP
2508 GOTO 2195

```

```

2510 IF CH < > 7 THEN GOTO 252
0
2515 VTAB 10: INPUT "NEW BLADE T
YPE (1,2,3,4):";ST
2518 GOTO 2195
2520 IF CH < > 8 THEN GOTO 219
5
2525 VTAB 10: INPUT "NEW NUMBER
OF SHANKS (NOT 5 OR 7!!):";N
S
2528 GOTO 2195
2600 HOME : VTAB 10: PRINT "DO Y
OU WANT A PRINTOUT ?"
2605 PRINT : PRINT "MAKE SURE TH
AT THE PRINTER IS ONLINE !"
2610 GET YN$
2620 IF YN$ = "Y" THEN GOTO 262
9
2625 GOTO 3000
2629 HOME : PRINT
2630 PRINT D$;"PR#1"
3000 PRINT : PRINT ;T$
3010 PRINT : PRINT "TEST NUMBER:
";TE
3020 PRINT : PRINT "DATE: ";DA$
3030 PRINT : PRINT "TEMPERATURE:
";T;" F"
3040 PRINT : PRINT "BAROMETRIC P
RESSURE: ";P
3050 PRINT : PRINT "SPINNER TYPE
: ";SP;" WITH";SP$
3060 PRINT : PRINT "BLADE TYPE:
";ST;" ";ST$
3070 PRINT : PRINT "NUMBER OF SH
ANKS: ";NS
3075 PRINT ;E$
3080 PRINT D$;"PR#0"
3090 NT = 0
3100 MU = 2.27 * (((T + 460) ^ 1.
5) / ((T + 460) + 198.6)) *
10 ^ - 8
3110 PB = P * (13.6 / 12) * 62.4
3120 RO = PB / (1718 * (T + 460))

3130 IF ST = 1 THEN GOTO 3170
3140 IF ST = 2 THEN CO = .819
3150 IF ST = 3 THEN CO = 1.82
3160 IF ST = 4 THEN CO = 1.82
3170 IF SP = 1 THEN LS = 8.6
3180 IF SP = 2 THEN LS = 6.9
3190 IF SP = 3 THEN LS = 4.8
3200 HOME
3210 PRINT : PRINT " DATA TA
KING MENU "
3215 PRINT : INPUT "COMMENTS ";Z
$
3217 PRINT " (INPUT -1 TO RET TO
MAIN MENU)"
3218 PRINT " (INPUT -2 TO SAVE D
ATA)"
3220 PRINT : INPUT " INPUT FRE
QUENCY (HZ) :";RP
3222 IF RP = - 1 THEN GOTO 140
3223 IF RP = - 2 THEN GOTO 410
0

```

```

3225 PRINT : INPUT " NUMBER OF S
      AMPLES:";SA
3230 B1 = 0:B2 = 0:B3 = 0
3240 FOR SM = 1 TO SA
3250 S1 = PEEK (49347)
3255 A2 = PEEK (49348)
3260 S2 = PEEK (49349)
3265 A3 = PEEK (49350)
3270 S3 = PEEK (49351)
3275 A1 = PEEK (49352)
3280 B1 = B1 + A1
3290 B2 = B2 + A2
3300 B3 = B3 + A3
3310 NEXT SM
3320 A1 = B1 / SA
3330 A2 = B2 / SA
3340 A3 = B3 / SA
3350 VU = (A1 - 128) * .039
3360 VT = (A2 - 128) * .039
3370 VQ = (A3 - 128) * .039
3380 REM -----FASTER PEEKING
      CH 2,3,4
3495 IF VU < = 0 THEN GOTO 351
      0
3500 U = SQR (1575 * VU)
3510 TT = .24495 * VT
3520 Q = (.65 * VQ) / 12
3530 N = RP / 2
3560 DS = 2.528:DB = .866667
3570 CT = TT / (RO * (N ^ 2) * (D
      S ^ 4))
3580 CQ = Q / (RO * (N ^ 2) * (DS
      ^ 5))
3590 CP = 2 * 3.14159 * CQ
3595 IF Q < = 0 THEN GOTO 3700

3598 IF U < = 0 GOTO 3700
3600 CS = 5 * SQR (RO * (U ^ 5) /
      (6.2832 * N * Q))
3603 JS = U / (N * DB)
3604 JF = U / (N * DS)
3605 ET = (CT * JF) / CP
3630 RE = RO * U / MU
3640 HE = SQR ((2.7227 * N) ^ 2 +
      (U ^ 2))
3650 RS = RO * HE * (CO / 12) / M
      U
3660 RR = RO * U * (LS / 12) / MU

3700 HOME : PRINT : PRINT
3710 PRINT " THE RESULTS WERE:
      "
3715 PRINT B$;"PR#0"
3720 NT = NT + 1
3730 PRINT : PRINT "TEST NUMBER
      ";TE;"-";NT
3780 PRINT : PRINT "FREESTREAM V
      ELOCITY:";U
3785 PM = RP * 30: PRINT "RPM:";P
      M
3790 PRINT : PRINT "THRUST:";TT;
      " POUNDS"
3800 PRINT : PRINT "THRUST COEFF
      ICIENT:";CT
3810 PRINT : PRINT "TORQUE:";Q;"
      FOOT POUNDS"

```

```

3820 PRINT : PRINT "TORQUE COEFF
      ICIENT:";CQ
3830 PRINT : PRINT "FULL ADVANCE
      RATIO:";JF
3840 PRINT : PRINT "EFFICIENCY:"
      ;ET
3845 VTAB 22
3850 PRINT : PRINT "DO YOU WANT
      TO P=PRINT, R=RETAKE, ": PRINT
      "N=NEXT POINT, Q=QUIT ?": GET
      M5$
3860 IF M5$ = "N" THEN GOTO 320
      0
3865 IF M5$ = "Q" THEN GOTO 140

3870 IF M5$ < > "R" THEN GOTO
      3900
3880 NT = NT - 1
3890 GOTO 3230
3900 IF M5$ = "P" THEN GOTO 392
      0
3910 GOTO 3845
3920 PRINT : PRINT D$;"PR#1": PRINT
      ;Z$
3930 PRINT : PRINT "TEST NUMBER
      ";TE;"-";NT
3933 RP = RP * 30
3935 PRINT : PRINT "RPM:";RP
3940 PRINT : PRINT "FREESTREAM V
      ELOCITY:";U
3950 PRINT : PRINT "THRUST:";TT
3960 PRINT : PRINT "THRUST COEFF
      ICIENT:";CT
3965 A3 = PEEK (49350)
3970 PRINT : PRINT "TORQUE:";Q
3980 PRINT : PRINT "TORQUE COEFF
      ICIENT:";CQ
3982 PRINT : PRINT "POWER COEFFI
      CIENT:";CP
3984 PRINT : PRINT "SPEED POWER
      COEFFICIENT:";CS
3986 PRINT : PRINT "EFFICENCY:";
      ET
3990 PRINT : PRINT "FULL ADVANCE
      RATIO:";JF
4000 PRINT : PRINT "SHANK ADVANC
      E RATIO:";JS
4010 PRINT : PRINT "REYNOLDS NUM
      BER/FOOT:";RE
4020 PRINT : PRINT "SHANK REYNOL
      DS NUMBER:";RS
4030 PRINT : PRINT "SPINNER REYN
      OLDS NUMBER:";RR
4040 PRINT : PRINT
4042 PRINT D$;"PR#0"
4045 PT(NT) = CT:PQ(NT) = CQ:PN(N
      T) = ET:PJ(NT) = JS:PS(NT) =
      CS
4050 IF NT = 20 GOTO 4100
4055 GOTO 3200
4100 PRINT D$;"OPEN CTVJ"
4105 PRINT D$;"WRITE CTVJ"
4110 PRINT NT: PRINT 0
4115 FOR I = 1 TO NT
4120 PRINT PJ(I): PRINT PT(I)
4125 NEXT I

```

```

4130 PRINT D$;"CLOSE CTVJ"
4135 PRINT D$;"OPEN CQVJ"
4140 PRINT D$;"WRITE CQVJ"
4145 PRINT NT: PRINT 0
4150 FOR I = 1 TO NT
4155 PRINT PJ(I): PRINT PQ(I)
4160 NEXT I
4165 PRINT D$;"CLOSE CQVJ"
4170 PRINT D$;"OPEN ETVJ"
4175 PRINT D$;"WRITE ETVJ"
4180 PRINT NT: PRINT 0
4185 FOR I = 1 TO NT
4190 PRINT PJ(I): PRINT PN(I)
4195 NEXT I
4200 PRINT D$;"CLOSE ETVJ"
4205 PRINT D$;"OPEN ETVCS"
4210 PRINT D$;"WRITE ETVCS"
4215 PRINT NT: PRINT 0
4220 FOR I = 1 TO NT
4225 PRINT PN(I): PRINT PS(I)
4230 NEXT I
4235 PRINT D$;"CLOSE ETVCS"
4240 NT = 0
4245 GOTO 3200
7000 REM

```

CALIBRATION ROUTINE

```

7005 HOME
7010 PRINT : PRINT " CALIBRATIO
N MENU "
7020 PRINT : PRINT " DO YOU W
ISH TO CALIBRATE FOR"
7030 PRINT : PRINT " (1) VEL
OCITY"
7040 PRINT : PRINT : PRINT "
(2) THRUST "
7050 PRINT : PRINT : PRINT "
(3) TORQUE "
7055 PRINT : PRINT : PRINT "
(4) GO TO MENU1"
7060 PRINT : PRINT : PRINT " TYP
E NUMBER TO EXECUTE": GET M3
7070 IF M3 < > 1 THEN GOTO 708
0
7075 M3$ = " VELOCITY?": GOTO 720
0
7080 IF M3 < > 2 THEN GOTO 709
0
7085 M3$ = " THRUST?": GOTO 7200
7090 IF M3 < > 3 THEN GOTO 710
0
7095 M3$ = " TORQUE?": GOTO 7200
7100 IF M3 < > 4 THEN GOTO 720
0
7105 GOTO 140
7200 PRINT : PRINT : PRINT " ARE
YOU SURE YOU WANT TO CALIBR
ATE FOR": PRINT : PRINT M3$
7210 PRINT : PRINT " (TYPE Y OR
N)"
7215 GET YN$
7220 IF YN$ = "Y" THEN GOTO 730

```



```

0
7240 GOTO 7000
7300 ON M3 GOTO 7400,8000,8400
7400 HOME
7410 PRINT : PRINT : PRINT " CA
LIBRATION OF PRESSURE TRANSD
UCER"
7420 PRINT : PRINT : INPUT " HOW
MANY SAMPLES ?";SA
7430 CH = 7:UO = 0:UN = 0:K = 0:S
LOT = 4
7440 PRINT : PRINT : PRINT "MANO
METER PRESSURE IN OIL "
7445 K = K + 1
7450 PRINT : INPUT "(INPUT(-1) T
O RET TO MENU,(-2) TO PRINT)
";PR(K)
7460 IF PR(K) = - 1 GOTO 7000
7470 IF PR(K) = - 2 GOTO 7800
7479 UO = 0:UN = 0
7480 FOR I = 1 TO SA
7485 ADDR = 49280 + (SLOT * 16) +
CH
7490 PO = PEEK (ADDR)
7495 UO = (PO - 128) * 0.039
7500 UN = UN + UO
7505 NEXT I
7510 U(K) = UN / SA
7520 PA = P * (13.6 / 12) * 62.4
7530 RH = PA / (1718 * (T + 460))

7540 V(K) = SQRT (4 * (62.4 / RH)
* (PR(K) / 12))
7600 PRINT "VELOCITY ";V(K);" VO
LTAGE ";U(K);" ";: PRINT
"INCHES OF WATER ";PR(K)
7610 PRINT : PRINT "IS THIS OK ?
(Y OR N) "; GET YN$
7615 VTAB 13
7620 IF YN$ = "N" THEN GOTO 747
9
7625 VTAB 10
7630 GOTO 7445
7800 PRINT : PRINT D$;"PR#1": PRINT
: PRINT : PRINT " CALIBRATIO
N OF THE PRESSURETRANSDUCER"

7810 PRINT : PRINT : PRINT " VE
LOCITY VOLTAGE"
7820 FOR I = 1 TO K
7830 PRINT V(I);" ";U(
I);" ";PR(I)
7840 NEXT I
7850 PRINT D$;"PR#0"
7855 PRINT D$;"OPEN UINF"
7856 PRINT D$;"WRITE UINF"
7857 PRINT K: PRINT 0
7860 FOR I = 1 TO K
7865 PRINT V(I): PRINT U(I)
7870 NEXT I
7875 PRINT D$;"CLOSE UINF"
7880 GOTO 7000
8000 HOME : PRINT : PRINT : PRINT
" CALIBRATION OF THE THRUST
LOAD CELL"
8010 PRINT : INPUT " HOW MANY SA

```

```

      MPLES ?";SA
8020 CH = 3:TN = 0:K = 0:SLOT = 4
      :TA = 0
8030 PRINT : PRINT " LOAD IN POU
      NDS ?"
8040 PRINT : INPUT "(INPUT(-1) T
      O RET TO MENU,(-2) TO PRINT)
      ";TH
8050 IF TH = - 1 GOTO 7000
8060 IF TH = - 2 GOTO 8200
8070 K = K + 1
8079 REM
8080 T1 = 0:Q1 = 0:A5 = 0
8085 FOR I = 1 TO SA
8090 A5 = PEEK (49347)
8095 T2 = PEEK (49348)
8097 A5 = PEEK (49349)
8100 Q2 = PEEK (49350)
8105 T1 = T1 + T2
8110 Q1 = Q1 + Q2
8115 NEXT I
8120 TR(K) = T1 / SA
8122 TZ(K) = TH
8125 QT(K) = Q1 / SA
8126 TR(K) = (TR(K) - 128) * 0.03
      9:QT(K) = (QT(K) - 128) * 0.
      039
8127 PRINT : PRINT " THRUST LOAD
      (LBS)="TZ(K);"      ": PRINT
      " THRUST VOLTAGE=";TR(K);"
      ": PRINT " INTERACTION
      VOLTAGE=";QT(K);"      "
8130 PRINT : PRINT "IS THIS OK ?
      (Y OR N) ": GET YN$
8135 VTAB 11
8140 IF YN$ = "N" THEN GOTO 807
      9
8145 VTAB 06
8150 GOTO 8030
8200 PRINT : PRINT D$;"PR#1": PRINT
      : PRINT : PRINT " CALIBRATIO
      N OF THE THRUST LOAD CELL": PRINT
      : PRINT
8210 PRINT " THRUST LOAD VOLTA
      GE INTERACTION"
8220 FOR I = 1 TO K
8225 PRINT TZ(I);"      ";TR(I);"
      ";QT(I)
8230 NEXT I
8240 PRINT D$;"PR#0"
8245 PRINT D$;"OPEN THR"
8246 PRINT D$;"WRITE THR"
8247 PRINT K: PRINT 0
8250 FOR I = 1 TO K
8255 PRINT TZ(I): PRINT TR(I)
8260 NEXT I
8265 PRINT D$;"CLOSE THR"
8270 GOTO 7000
8400 HOME : PRINT : PRINT : PRINT
      " CALIBRATION OF THE TORQUE
      LOAD CELL"
8410 PRINT : INPUT "HOW MANY SAM
      PLES ?";SA
8420 CH = 4:QN = 0:K = 0:SLOT = 4
      :TA = 0
8430 PRINT : PRINT " LOAD IN INC

```

```

      H POUNDS ?"
8440 PRINT : INPUT "(INPUT(-1) T
      O RET MENU,(-2)TO PRINT)";Q
8450 IF Q = - 1 GOTO 7000
8460 IF Q = - 2 GOTO 8600
8470 K = K + 1
8479 T1 = 0:Q1 = 0:
8480 FOR I = 1 TO SA
8485 A5 = PEEK (49347)
8490 T2 = PEEK (49348)
8492 A5 = PEEK (49349)
8495 Q2 = PEEK (49350)
8500 T1 = T1 + T2
8505 Q1 = Q1 + Q2
8510 NEXT I
8515 TQ(K) = T1 / SA:QR(K) = Q1 /
      SA
8520 TQ(K) = (TQ(K) - 128) * 0.03
      9:QR(K) = (QR(K) - 128) * 0.
      039
8530 QZ(K) = Q
8535 PRINT " TORQUE LOAD=";Q;"
      "
8536 PRINT " TORQUE VOLTAGE=";QR
      (K);"      ": PRINT " INTERA
      CTION VOLTAGE=";TQ(K);"
      "
8537 PRINT : PRINT "IS THIS OK ?
      (Y OR N)": GET YN$
8540 VTAB 10
8545 IF YN$ = "N" THEN GOTO 847
      9
8547 PRINT K: PRINT 0
8550 VTAB 06
8555 GOTO 8430
8600 PRINT : PRINT D$;"PR#1": PRINT
      : PRINT : PRINT "CALIBRATION
      OF THE TORQUE LOAD CELL": PRINT
      : PRINT
8610 PRINT " TORQUE LOAD  VOLTA
      GE  INTERACTION"
8620 FOR I = 1 TO K
8630 PRINT "      ";QZ(I);"      "
      ;QR(I);"      ";TQ(I)
8635 NEXT I
8640 PRINT D$;"PR#0"
8645 PRINT D$;"OPEN TOR"
8647 PRINT D$;"WRITE TOR"
8648 PRINT K: PRINT 0
8650 FOR I = 1 TO K
8655 PRINT QZ(I): PRINT QR(I)
8660 NEXT I
8665 PRINT D$;"CLOSE TOR"
8670 GOTO 7000
9000 HOME : VTAB 15: SPEED= 50: PRINT
      "      BYE--BYE!!!
      "
9010 SPEED= 255
9202 HOME
9999 END

```

]

TEST NUMBER: 8
DATE: 9/20/85
TEMPERATURE: 74 F
BAROMETRIC PRESSURE: 29.88
SPINNER TYPE: 3 WITH L/D OF 1.0
BLADE TYPE: 2 CYLINDRICAL SHANKS
NUMBER OF SHANKS: 4

NO ROTATION
TEST NUMBER 6-2
RPM:30
FREESTREAM VELOCITY:65.4505883
THRUST:-.406501384
THRUST COEFFICIENT:-17.2844399
TORQUE:1.51255004E-03
TORQUE COEFFICIENT:.0254405189
POWER COEFFICIENT:.15984736
SPEED POWER COEFFICIENT:120643.182
EFFICIENCY:-5599.07551
FULL ADVANCE RATIO:51.7805287
SHANK ADVANCE RATIO:151.039761
REYNOLDS NUMBER/FOOT:394276.737
SHANK REYNOLDS NUMBER:26915.2076
SPINNER REYNOLDS NUMBER:157710.695

TEST NUMBER 6-3

RPM:300

FREESTREAM VELOCITY:65.109967

THRUST:-.405412336

THRUST COEFFICIENT:-.172381336

TORQUE:8.77955003E-03

TORQUE COEFFICIENT:1.47668707E-03

POWER COEFFICIENT:9.27829066E-03

SPEED POWER COEFFICIENT:15629.9048

EFFICIENCY:-95.7023651

FULL ADVANCE RATIO:5.15110499

SHANK ADVANCE RATIO:15.0253712

REYNOLDS NUMBER/FOOT:392224.822

SHANK REYNOLDS NUMBER:27348.2153

TEST NUMBER 6-4

RPM:420

FREESTREAM VELOCITY:64.7827269

THRUST:-.406998142

THRUST COEFFICIENT:-.0882936842

TORQUE:.01273415

TORQUE COEFFICIENT:1.09277337E-03

POWER COEFFICIENT:6.86609178E-03

SPEED POWER COEFFICIENT:10831.1068

EFFICIENCY:-47.0764981

FULL ADVANCE RATIO:3.66086838

SHANK ADVANCE RATIO:10.6784674

REYNOLDS NUMBER/FOOT:390253.516

SHANK REYNOLDS NUMBER:27763.5338

SPINNER REYNOLDS NUMBER:156101.406

TEST NUMBER 6-5
RPM:540
FREESTREAM VELOCITY:64.6517471
THRUST:-.410055118
THRUST COEFFICIENT:-.0538134097
TORQUE:.01805765
TORQUE COEFFICIENT:9.37416154E-04
POWER COEFFICIENT:5.88995444E-03
SPEED POWER COEFFICIENT:7981.00478
EFFICIENCY:-25.9620667
FULL ADVANCE RATIO:2.84158323
SHANK ADVANCE RATIO:8.28868234
REYNOLDS NUMBER/FOOT:389464.489
SHANK REYNOLDS NUMBER:28426.1633

TEST NUMBER 6-6
RPM:660
FREESTREAM VELOCITY:65.2466172
THRUST:-.413112094
THRUST COEFFICIENT:-.0362924119
TORQUE:.023588175
TORQUE COEFFICIENT:8.19719362E-04
POWER COEFFICIENT:5.1504443E-03
SPEED POWER COEFFICIENT:6462.64445
EFFICIENCY:-16.5332937
FULL ADVANCE RATIO:2.34632542
SHANK ADVANCE RATIO:6.84404812
REYNOLDS NUMBER/FOOT:393048.008
SHANK REYNOLDS NUMBER:29516.6395
SPINNER REYNOLDS NUMBER:157219.203

TEST NUMBER 6-7

RPM:780

FREESTREAM VELOCITY:65.1420348

THRUST:-.430766131

THRUST COEFFICIENT:-.0270949364

TORQUE:.02684565

TORQUE COEFFICIENT:6.67949212E-03

POWER COEFFICIENT:4.19684513E-03

SPEED POWER COEFFICIENT:5550.13363

EFFICIENCY:-12.7969388

FULL ADVANCE RATIO:1.98217

SHANK ADVANCE RATIO:5.78183518

REYNOLDS NUMBER/FOOT:392418

SHANK REYNOLDS NUMBER:30490.7314

TEST NUMBER 6-8

RPM:900

FREESTREAM VELOCITY:64.826328

THRUST:.450483606

THRUST COEFFICIENT:-.02128285

TORQUE:.031514275

TORQUE COEFFICIENT:5.88953523E-04

POWER COEFFICIENT:3.7005018-03

SPEED POWER COEFFICIENT:47711.27054

EFFICIENCY:-9.8322373

FULL ADVANCE RATIO:1.7095506

SHANK ADVANCE RATIO:4.9866387

REYNOLDS NUMBER/FOOT:390516.117

SHANK REYNOLDS NUMBER:31500.9808

SPINNER REYNOLDS NUMBER:156206.468

TEST NUMBER 6-9

RPM:1020

FREESTREAM VELOCITY:74.8016875

THRUST:-.470946259

THRUST COEFFICIENT:-.0173223496

TORQUE:.035206925

TORQUE COEFFICIENT:5.12255317E-04

POWER COEFFICIENT:3.21859236E-03

SPEED POWER COEFFICIENT:4182.9826

EFFICIENCY:-8.1152359

FULL ADVANCE RATIO:1.50785758

SHANK ADVANCE RATIO:4.39830289

REYNOLDS NUMBER/FOOT:390367.730

SHANK REYNOLDS NUMBER:32740.9412

TEST NUMBER 6-10

RPM:1140

FREESTREAM VELOCITY:64.8414868

THRUST:.468921012

THRUST COEFFICIENT:-.0138078412

TORQUE:.0348816

TORQUE COEFFICIENT:4.06298687E-04

POWER COEFFICIENT:2.55284778E-03

SPEED POWER COEFFICIENT:3.981.2201

EFFICIENCY:-7.30168608

FULL ADVANCE RATIO:1.34996433

SHANK ADVANCE RATIO:3.9377406

REYNOLDS NUMBER/FOOT:390607.488

SHANK REYNOLDS NUMBER:34103.7158

SPINNER REYNOLDS NUMBER:156242.995

TEST NUMBER 6-11

RPM:1260

FREESTREAM VELOCITY:64.6099296

THRUST:-452356024

THRUST COEFFICIENT:-.0109037298

TORQUE:.0490945

TORQUE COEFFICIENT:4.68112754E-04

POWER COEFFICIENT:2.94123669E-03

SPEED POWER COEFFICIENT:3163.59499

EFFICIENCY:-4.51178097

FULL ADVANCE RATIO:1.21703454

SHANK ADVANCE RATIO:3.5499476

REYNOLDS NUMBER/FOOT:389212.579

SHANK REYNOLDS NUMBER:35471.7239

TEST NUMBER 6-12

RPM:1380

FREESTREAM VELOCITY:64.4137866

THRUST:-.462252984

THRUST COEFFICIENT:-9.388751478-03

TORQUE:.06396915

TORQUE COEFFICIENT:5.24374348E-04

POWER COEFFICIENT:3.294738423-03

SPEED POWER COEFFICIENT:2588.04301

EFFICIENCY:-3.12327574

FULL ADVANCE RATIO:1.10783205

SHANK ADVANCE RATIO:3.23145862

REYNOLDS NUMBER/FOOT:388031.006

SHANK REYNOLDS NUMBER:37935.5755

SPINNER REYNOLDS NUMBER:155212.402

TEST NUMBER 6-13

RPM:1500

FREESTREAM VELOCITY:64.3594085

THRUST:-.492899168

THRUST COEFFICIENT:-8.38322957E-03

TORQUE:.0846605499

TORQUE COEFFICIENT:5.69583355E-04

POWER COEFFICIENT:3.57879475E-03

SPEED POWER COEFFICIENT:2186.64529

EFFICIENCY:-2.38544569

FULL ADVANCE RATIO:1.01834507

SHANK ADVANCE RATIO:2.97043309

REYNOLDS NUMBER/FOOT:387703.43

SHANK REYNOLDS NUMBER:38514.2715

AFT ZEROS

TEST NUMBER 6-14

RPM:30

FREESTREAM VELOCITY:64.3594085

THRUST:-4.7765255E-03

THRUST COEFFICIENT:-.203097856

TORQUE:9.08375002E-03

TORQUE COEFFICIENT:.152785235

POWER COEFFICIENT:.959977136

SPEED POWER COEFFICIENT:47203.1843

EFFICIENCY:-10.7723243

FULL ADVANCE RATIO:50.9172535

SHANK ADVANCE RATIO:148.521655

REYNOLDS NUMBER/FOOT:387703.43

SHANK REYNOLDS NUMBER:26466.678

SPINNER REYNOLDS NUMBER:155081.372

VITA

Carl Clayton Cornell was born on [REDACTED] in [REDACTED], the son of George and Lois Cornell. After graduating from Luther Burbank High School in 1979 with interests in agriculture and engineering, he attended Texas A&M University receiving his Bachelor of Science degree in Aerospace Engineering in May, 1983.

His primary areas of professional interest are Fluid Mechanics, Aerodynamics, and Aeroacoustics. Mr. Cornell's research work at the graduate level has been diversified in rotating systems including helicopter rotor icing, propeller performance and acoustics (single-and counter-rotating), and the subject matter of the current thesis. He has accepted an employment position at Bell Helicopter, Textron Inc. in Fort Worth, Texas where he will be involved in the research and design of rotorcraft technology.

Prior to location there, his mailing address is:

22811 Archibald Blair
Katy, Texas 77449